U.PORTO
FEUP FACULDADE DE ENGENHARIA
UNIVERSIDADE DO PORTO

OPTIMAL SENSOR PLACEMENT FOR VIBRATION-BASED MONITORING ILLUSTRATED IN A BUILDING MODEL

VÂNIA FERNANDES FERREIRA

Dissertation submitted for partial satisfaction of the requirements for the degree of

MASTER IN CIVIL ENGINEERING — SPECIALIZATION IN STRUCTURES AND GEOTECHNICS

Supervisor: Professor Doctor Filipe Manuel Rodrigues Leite Magalhães

Co-supervisor: Professor Doctor Edwin Reynders

JUNE, 2025

MASTER IN CIVIL ENGINEERING 2024/2025

DEPARTMENT OF CIVIL ENGINEERING

Tel. +351 22 508 1901

m.ec@fe.up.pt

Edited by

FACULTY OF ENGINEERING OF UNIVERSITY OF PORTO

Rua Dr. Roberto Frias

4200-465 PORTO

Portugal

Tel. +351-22-508 1400

feup@fe.up.pt

http://www.fe.up.pt

To my father

The most effective solutions often emerge not from the complexity of systems, but from the precise placement of key observations.

Donald C. Kammer

PREFACE

This dissertation explores the optimal sensor placement for vibration-based monitoring of a steel Vierendeel truss railway bridge. The research was conducted at the Structural Mechanics Section of the Department of Civil Engineering at KU Leuven, under the supervision of Prof. Edwin Reynders and his assistant, Dimitrios Anastasopoulos, and at my home university under the guidance of Prof. Filipe Magalhães.

First of all, I would like to express my gratitude to Prof. Filipe Magalhães for providing me with the opportunity to pursue my dissertation at KU Leuven through the mobility program, for his support at the outset, and for his guidance throughout the research period.

I am also very grateful to Prof. Edwin Reynders for the opportunity and welcoming me to the Structural Mechanics Section and for his valuable insights and suggestions during our meetings, which significantly contributed to the progress and quality of this work.

I would also like to extend my thanks to Dimitrios Anastasopoulos for his availability and assistance throughout the development of this research. His feedback, checks on my work, and suggestions were important in the development of this dissertation.

I extend my gratitude to the members of the Structural Mechanics Section for their reception, their invitations to activities outside working hours, and the socializing during this period, which created a welcoming and motivating work environment. To my office colleague, David Carneiro, I am especially grateful for his practical advice and emotional support. His encouragement helped me grow, both in my technical skills and in preparing for the world of work.

A heartfelt thank you goes to my partner, Dinis Sousa, who encouraged me to embark on this experience, and who provided invaluable emotional support throughout this journey. His belief in me, his daily encouragement, and our shared moments, including our first time living independently, made this period truly unforgettable. Our weekend trips were a source of joy and inspiration, and I am deeply thankful to have shared this experience with him.

I am forever grateful to my family, who have always supported me and believed in me. To my mother, sister, grandmother, uncle and aunt, and their child, my favorite 'Didi,' as well as to Dinis's family (his parents, brother, and grandparents) for encouragement, support, and our daily conversations.

Finally, and most importantly, to my father. Although he is no longer with us, I know he is watching proudly from above. His wish for me to become a civil engineer has been my greatest motivation. This dissertation is for you, Dad.

Vânia Ferreira
July 2025

RESUMO

Foi conduzido um estudo relativo ao tema da otimização da localização de sensores, usando como caso de estudo um modelo estrutural em aço, presente no Laboratório de Mecânica Estrutural do Departamento de Engenharia Civil da KU Leuven.

Este estudo foi desenvolvido na KU Leuven, na Secção de Mecânica Estrutural do Departamento de Engenharia Civil, sob a orientação do Professor Edwin Reynders, com o apoio do assistente Dimitrios Anastasopoulos e do Professor Filipe Magalhães, da FEUP.

O trabalho teve início com o desenvolvimento de um modelo estrutural de elementos finitos, em Stabil, permitindo a familiarização com uma nova linguagem de programação e a implementação dos métodos de otimização.

A estrutura é composta por quatro pisos e contraventamentos dispostos exclusivamente na direção x. Devido à elevada rigidez nessa direção, os primeiros quatro modos de vibração apresentam deslocamento apenas na direção y.

Em seguida, foram realizados ensaios experimentais na estrutura real, com o objetivo de comparar os resultados obtidos com o modelo numérico. Os modos de vibração extraídos do MACEC mostraram elevada similaridade nos primeiros quatro modos de vibração com deslocamentos na direção y, mas divergências nos modos mais complexos, como os torsionais e os que envolvem deslocamentos na direção rígida (x) da estrutura.

Foram implementados três métodos de otimização da localização de sensores: Modal Kinetic Energy (MKE), Effective Independence Method (EFI) e Information Entropy Index Method (IEI). A otimização foi inicialmente realizada em 2D e posteriormente estendida para 3D, considerando graus de liberdade apenas na direção y. Todas as otimizações foram acompanhadas pela métrica MAC, que avalia o grau de dependência dos modos de vibração com os sensores otimizados. A otimização também foi realizada utilizando os sensores implementados nos testes experimentais, permitindo a comparação dos resultados obtidos no modelo e nos testes experimentais.

De modo geral, concluiu-se que o método mais indicado para a otimização foi o EFI, pois, ao contrário do MKE, tem em atenção o erro causado por sensores bastante próximos. Embora o método IEI tenha apresentado resultados semelhantes, mostrou-se mais exigente em termos de esforço computacional.

Posteriormente, foram realizados vários testes com o objetivo de comprovar a validade do número de sensores utilizados, avaliando-se o comportamento da otimização face à redução do número de sensores.

Desenvolveu-se um estudo completo e validado em torno dos três métodos, capaz de ser adaptado a qualquer tipo de estrutura.

PALAVRAS-CHAVE: otimização, sensores, vibrações, ensaios, MAC.

ABSTRACT

A study on the topic of Optimal Sensor Placement (OSP) was conducted, using a steel structural model as a case study, located in the Structural Mechanics Laboratory of the Department of Civil Engineering at KU Leuven was addressed.

This study was carried out at KU Leuven, in the Structural Mechanics Section of the Department of Civil Engineering, under the supervision of Professor Edwin Reynders, with the support of assistant Dimitrios Anastasopoulos and Professor Filipe Magalhães from FEUP.

The work began with the development of a finite element structural model in Stabil, allowing familiarization with a new programming language and the implementation of optimization methods.

The structure consists of four floors with bracing arranged exclusively in the x-direction. Due to the resulting high stiffness along this axis, the first four vibration modes exhibit displacements only in the y-direction.

Experimental tests were then carried out on the actual structure to compare the results with those from the numerical model. The vibration modes extracted using MACEC showed strong agreement with the first four modes involving displacements in the y-direction. However, discrepancies were observed in the more complex modes, such as the torsional modes and those with displacements in the stiffer x-direction of the structure.

Three sensor placement optimization methods were implemented: the Modal Kinetic Energy (MKE) method, the Effective Independence (EFI) method, and the Information Entropy Index (IEI) method. The optimization was initially carried out in 2D and later extended to 3D, considering only the degrees of freedom in the y-direction. Throughout the optimization process, the MAC metric was used to evaluate the correlation between the vibration modes and the optimized sensor positions. Additionally, the optimization was performed using the sensor positions from the experimental tests, enabling a direct comparison between the numerical and experimental results.

In general, it was concluded that the most suitable optimization method was EFI, as it accounts for errors introduced by placing sensors too close to each other, unlike the MKE method. Although the IEI method produced similar results, it proved to be more computationally demanding.

Subsequently, several tests were carried out with the aim of proving the validity of the number of optimized sensors used, evaluating the behavior of the optimization in the face of a reduction in the number of sensors.

A complete and validated study was developed around the three methods, capable of being adapted to any type of structure.

KEYWORDS: optimization, sensors, vibrations, tests, MAC.

CONTENTS

LIST OF FIGURES

LIST OF TABLES

SYMBOLS, ACRONYMS AND ABBREVIATIONS

Symbols

x	Scalar
y	Scalar
b	Width [m]
h	Height [m]
E	Young's Modulus [GPa]
ν	Poisson's ratio [-]
ρ	Volumetric Density [kg/m^3]
u	Displacement Vector
M	Mass Matrix
C	Damping Matrix
K	Stiffness Matrix
F	Force vector
t	Time [s]
ξ	Modal Coordinates Vector
n	Number of Degrees of Freedom
m	Number of Target Sensors
p	Number of Sensor Positions
Λ	Vector
i	Number of Degree of Freedom
ω	Natural Frequency [Hz]
C*	Vector
ζ	Modal Damping Ratio
Φ	Mode Shape Matrix

j	Number of Vibration Mode
L	Positions Matrix
s	Number of Degree of Freedom
Σ	Error Covariance Matrix
S	Modal Shape Matrix
F	Fisher Information Matrix
δ	Spatial Distance [m]
λ	Spatial Correlation Length
θ_0	Number of Degrees of Freedom at each iteration
N_θ	Length of θ_0
Q	Fisher Information Matrix
L_{ref}	Configuration with all Degrees of Freedom
F_s	Sampling Frequency [Hz]
F_{max}	Expected Real Frequency of the Structure [Hz]
F_1	Minimum Frequency Expected to the Structure
i	Hankel block rows
f	Natural Frequencies [Hz]
f_0	Experimental Frequencies [Hz]
x_k	State vector at instant k
u_k	Vector of excitations applied to the structure at instant $k{\cdot}\Delta t$
y_k	Vector of measured responses of the structure at instant $k{\cdot}\Delta t$
A	System transition matrix
B	Input matrix
C	Observation matrix
D	Direct transmissibility matrix

w_k	Process noise
v_k	Measurement noise
E	Statistical mean
δ_{pq}	Kronecker Delta
Q	Process noise covariance matrix w_k
R	Measurement noise covariance matrix v_k
S	Cross-correlation matrix between process noise and measurement noise at the same instant
R_k^{ref}	Cross-correlation function
Y_f	Set of future correlation vectors
Y_p^{ref}	Set of vectors of past correlations
$T_{1\|i}^{ref}$	Toeplitz block matrix
R_i^{ref}	Correlation matrix between the system outputs
G^{ref}	Matrix representing the effect of white noise on the model
O_i	Extended observability matrix
Γ_i^{ref}	Reversed extended stochastic controllability matrix
Ψ	Complex eigenvectors (modal shapes)
Λ_d	Discrete-time eigenvalues u_k
μ_k	Eigenvalue in the discrete domain
λ_k	Eigenvalue of the system in the continuous domain
λ_k^*	Complex conjugate of the eigenvalue
V	Mode shapes Matrix

Acronyms

2D	Two-dimensional
3D	Three-dimensional
ARMA	Autoregressive Moving Average
BSSP	Backward Sequential Sensor Placement
GPT	Generative Pre-trained Transformed
DKT	Discrete Kirchhoff Triangles
DOF	Degrees of Freedom
EFI	Effective Independence Method
EOT	Energy Optimization Technique
FBGs	Fiber Bragg Gratings
FEM	Finite Element Model
FIM	Fisher Information Matrix
FOS	Fiber-Optic Sensors
FEM	Finite Element Model
FOS	Fiber-Optic Sensors
FSSP	Forward Sequential Sensor Placement
IEI	Information Entropy Index Method
MAC	Modal Assurance Criterion
MACEC	Modal Analysis for Civil Engineering Constructions
MI	Mutual Information
MKE	Modal Kinetic Energy Method
MSO	Maximum System Order
NI	National Instrument
OMA	Operational Modal Analysis

OSP	Optimal Sensor Placement
PSD	Power Spectral Density
RLSC	Representative Least Squares Criterion
SHM	Structural Health Monitoring
SSI	Stochastic Subspace Identification
SVDR	Singular Value Decomposition Ratio
VBM	Vibration-Based Monitoring
X60	Specialized Adhesive

Abreviations

det.	Determinant
diag.	Diagonal
Fig.	Figure
graph	Graphic

1
INTRODUCTION

All structures are constantly exposed to both permanent and live loads, including environmental factors such as wind, temperature variations, earthquakes, and more. Their continuous and reliable operation is essential for safe and efficient transportation, trade, and ultimately, for economic stability. Most of the structures currently in use across developed countries were built during the 20th century, and many of them are approaching, or have already exceeded, their original design lifespan (ASCE, 2021). These aging structures are subject to ongoing material degradation, often combined with increased loading conditions that surpass the original design specifications. In this context, structural health monitoring (SHM) techniques have emerged as valuable tools for assessing the current performance of structures and detecting early-stage, otherwise invisible, degradation (An et al., 2019).

Structural Health Monitoring (SHM) helps reduce safety risks, minimize overly conservative design approaches, extend the service life of infrastructure by accounting for actual rather than expected degradation, and optimize the allocation of limited maintenance budgets (Farrar, 2013). While many large and critical infrastructures are already equipped with SHM systems, the broader potential of these technologies remains largely untapped. One particularly promising methodology for SHM in civil infrastructure is vibration-based monitoring (VBM), which provides key dynamic characteristics such as natural frequencies and mode shapes (Wei e Pizhong, 2010).

The primary sensors used for data acquisition in Structural Health Monitoring are accelerometers (Farrar, 2013). However, an alternative approach for accurately measuring modal characteristics and supporting structural maintenance is the use of fiber-optic sensors (FOS), such as fiber Bragg gratings (FBGs). These sensors can simultaneously provide stress data, from which internal forces can be derived, as well as modal parameters, making them an attractive option for long-term monitoring (Glišić e Inaudi, 2007; Zhou et al., 2024). Recent research conducted at KU Leuven has demonstrated the advantages of dynamic strain monitoring for SHM of bridges (Anastasopoulos, De Roeck e Reynders, 2021; Anastasopoulos e Reynders, 2023).

The dynamic responses of a structure can be used for System Identification, which involves developing a mathematical dynamic model that fits the measured data, regardless of whether the excitation is known, partially known, or unknown (Juang, 2002; Reynders, 2009). In laboratory conditions, a common and simple method to generate excitation is by applying an impulse using a hammer or a shaker. However, in large-scale civil structures, applying a controlled excitation is often impractical, but ambient excitation is in many case sufficient.

When both the excitation forces and the structural responses are known, the method used is Experimental Modal Analysis (EMA). When only the structural response is available, the appropriate approach is Operational Modal Analysis (OMA), which is the most commonly used method for large-scale structures (Magalhães e Cunha, 2011). Numerous methods have been developed and implemented for OMA (Magalhães, Cunha e Caetano, 2009; Rainieri e Fabbrocino, 2015; Reynders, Houbrechts e De Roeck, 2012; Ubertini, Gentile e Materazzi, 2013). One example of these methods is the Stochastic Subspace Identification (SSI-Cov) (Reynders, 2009).

There are numerous possible sensor placement configurations, and to obtain accurate data while minimizing costs and computational effort, several methods have been developed and implemented for Optimal Sensor Placement (OSP) (Leyder et al., 2016). In this context, a Finite Element (FE) model plays a crucial role in the optimization process, making it essential to perform computational modal analysis before conducting real experiments.

The main objective of this study is to develop an Optimal Sensor Placement (OSP) method based on accelerometers, as proposed by (Ostachowicz, Soman e Malinowski, 2019; Zhang et al., 2017). A Finite Element (FE) model will be used to conduct numerical simulations and perform the sensor placement optimization, using Stabil, a MATLAB toolbox created by researchers from the Structural Mechanics Section of the Department of Civil Engineering at KU Leuven. Stabil is useful for structural analysis (Section e Department of Civil Engineering, 2020), and it is commonly used in both educational and research projects.

Stabil provides an implementation of a finite element model for beam and truss elements, as well as for plates using shell elements, and for both 2D and 3D elasticity problems. Its primary application is the static analysis of 2D and 3D frame and truss structures, following the definition of nodes, elements, boundary conditions, and applied loads. Dedicated post-processing routines are available for visualizing the deformed structure and internal force distribution, tailored specifically for structural analysis.

Stabil also supports dynamic structural analysis. It enables the computation and visualization of eigenmodes, and the use of modal superposition techniques in both the time and frequency domains. Other dynamic analysis capabilities include response spectrum analysis, frequency domain solutions, and direct time integration.

The next step is to apply the OSP methods, initially considering a 2D analysis. Three techniques will be evaluated: the Modal Kinetic Energy (MKE) method, the Effective Independence (EFI) method, and the Information Entropy Index (IEI) method (Leyder et al., 2018). As an extension, these methods will then be applied in a 3D analysis.

The first significant approach to OSP was the powerful procedure called Effective Independence (EFI) (Kammer, 1991), which is based on measuring the contribution of each potential sensor location to the linear independence of the target mode shapes. Subsequent research has shown that this method is an effective way to achieve optimal sensor placement, especially when combined with system realization techniques (Kammer, 1996; Kammer e Yao, 1994).

Subsequently, a modification to the method was proposed emphasizing the importance of considering triaxial accelerometers instead of uniaxial ones, as used in earlier studies. This means that all degrees of freedom at each sensor location are taken into account (Kammer, 1991). To reduce computational costs, an improved approach was introduced, where the process begins with one sensor placed on the structure, and additional sensors are iteratively added based on their highest contribution, until the desired number of sensors is reached (Kammer, 2005).

(Heo, Wang e Satpathi, 1997) proposed a variation of the EFI method by developing the Energy Optimization Technique (EOT), which focuses on maximizing the Modal Kinetic Energy (MKE) matrix. Later, (Li, Li e Fritzen, 2007) compared the EFI and MKE methods. While the MKE method emphasizes the importance of all degrees of freedom based on their kinetic energy, taking into account the mass distribution associated with each degree of freedom, the EFI method can be seen as an iterative form of MKE that operates independently of mass distribution.

A different approach was proposed by (Papadimitriou, 2004), known as the Information Entropy Index (IEI) method, an iterative technique that quantifies the uncertainty associated with each sensor location. In this work, two heuristic algorithms are introduced for sensor placement: Backward Sequential Sensor Placement (BSSP) and Forward Sequential Sensor Placement (FSSP). The BSSP algorithm starts by considering all degrees of freedom and iteratively removes sensor positions based on their contribution. In contrast, the FSSP begins with a single sensor and progressively adds new ones until the desired number of sensors is reached. Both the EFI and IEI methods utilize the Fisher Information Matrix (FIM) in their formulations to quantify the amount of information contained in the sensor measurements (Kim e Cho, 2024; Leyder et al., 2018).

A common issue with the aforementioned methods is the placement of sensors too close to each other. (Leyder et al., 2015) attributed this problem to the use of a dense mesh in the finite element model. To address this, (Papadimitriou e Lombaert, 2012) proposed a solution based on the prediction error correlation between closely spaced sensors, introducing the Covariance Matrix concept (Kim e Cho, 2024). Another approach, proposed by (Stephan, 2012), aims to minimize redundancy by calculating a proximity metric between elementary information matrices and removing sensors with similar information content.

To evaluate the quality of the results from each method, (Carne e Dohrmann, 1995) proposed the Modal Assurance Criterion (MAC), a metric that measures the correlation between mode shapes. The objective is to obtain a matrix with values close to 1 along the diagonal, indicating high correlation, and values close to zero off the diagonal, indicating low correlation. Additionally, (Meo e Zumpano, 2005) proposed using the squared error, between the mode shape of the finite element model and the mode shape obtained by a cubic spline interpolation of the displacement measured at the selected sensor locations, as a metric to compare the performance of different Optimal Sensor Placement (OSP) methods.

(Yi e Li, 2012) mention several additional metrics used to evaluate Optimal Sensor Placement (OSP) methods, including the Singular Value Decomposition Ratio (SVDR), Probability-Based Damage Detection Criterion, Mean Square Error (MSE), Mutual Information (MI), Representative Least Squares Criterion (RLSC), and finally, Visualization of Mode Shapes.

OSP methods are valuable across various fields, including aerospace, mechanical, and civil engineering. These methods have been applied to different types of structures, such as timber structures (Castro-Triguero et al., 2014; Leyder et al., 2018; Omenzetter et al., 2011), plates (Worden e Burrows, 2001), frame structures (Cherng, 2003; Kang, Li e Xu, 2008), and truss beams (Hemez e Farhat, 1994; Liu et al., 2008). (Meo e Zumpano, 2005) and (Chioccarelli et al., 2024) studied OSP methods for bridges using numerical models, while (Faridi et al., 2024; Pachón et al., 2018; Pachón et al., 2020) applied these methods to complex real-world structures.

Typically, OSP methods consider uni-axial sensors; however, when tri-axial sensors are used, the results of experimental tests can be suboptimal. (Leyder et al., 2016) proposed a solution specifically for the application of tri-axial sensors. Additionally, (Kammer, 2005; Papadimitriou, 2004) addressed the consideration of multi-axial sensor configurations in their work.

Experimental testing is essential to assess whether the numerical model is a good approximation of the real structure. These tests were conducted in the Structural Mechanics Laboratory at KU Leuven, using accelerometers to estimate de modal properties of the physical structure and verify whether they correspond with the results obtained from the Finite Element Model (FEM).

The analysis of the experimental test results is performed using MACEC, a MATLAB toolbox for experimental and operational modal analysis of structures. MACEC allows for the extraction of eigenfrequencies, damping ratios, mode shapes, and modal scaling factors from measurement data. It also provides tools for visualizing the vibration modes in both 2D and 3D perspectives, enabling a clear understanding of how the structure deforms under each mode. MACEC supports experimental, operational, and combined modal testing of structures (Reynders, Schevenels e Roeck, 2021).

Furthermore, the Modal Assurance Criterion (MAC) value evaluates the correlation between vibration modes and will be used to compare the mode shapes obtained from the numerical model with those from the experimental tests on the real structure.

The structure used in this study is a steel frame located in the Structural Mechanics Laboratory (Fig. 2) of the Department of Civil Engineering at KU Leuven. Originally developed for educational and demonstration purposes, the frame is permanently installed in the laboratory and can be manually excited, enabling detailed observation and analysis of its dynamic behavior.

The motivation for this work stems from a research project at the Section of Structural Mechanics at KU Leuven, focused on the Vierendeel truss railway bridge M2.17 (depicted in Fig. 1) (Anastasopoulos e Reynders, 2024). This bridge, located in Mechelen, Belgium, near the central railway station, represents one of the most recent applications of real-time dynamic strain monitoring, utilizing a system of 64 fiber Bragg grating (FBG) strain sensors. Known as the M2.17 bridge, it was designed by Belgian engineer and KU Leuven professor Arthur Vierendeel (Fig. 1), who introduced this novel diagonal-free truss design in 1896. Today, the bridge is classified as an architectural heritage structure and forms a critical link between Brussels and Antwerp, serving exclusively passenger trainsets. Projects at the Structural Mechanics Section of KU Leuven are underway on the optimal positioning of these sensors, aiming to enhance monitoring efficiency.

Fig. 1 – Arthur Vierendeel and M2.17 bridge.

The monitoring system of the FBG strain sensors is located on the tapered zones of the vertical elements of the Vierendeel truss. These sensors measure ambient and operational dynamic strains, with the layout specifically designed to monitor fatigue-prone areas through long-gauge dynamic strain measurements. This approach is particularly important for steel bridges constructed in the 1920s and 1930s, as some types of structural steel from that era have been observed to exhibit a ductile-to-brittle transition at temperatures near 0°C.

As a result, sudden cracks may occur at low temperatures (Espion, 2012; Van Bogaert e De Pauw, 2023), potentially leading to brittle failure of structural elements and partial or total collapse, as was the case with the Hasselt bridge in 1938 (Espion, 2012). The measured dynamic strain time series are used in Operational Modal Analysis (OMA) to identify the bridge's natural frequencies, damping ratios, and strain mode shapes on an hourly basis. These identified modal characteristics are then employed to assess the structural condition of the bridge.

The results of the monitoring campaign reveal a clear influence of temperature on the natural frequencies, especially at temperatures below 0°C, due to the ductile-to-brittle transition of the structural steel. In contrast, the strain mode shapes remain insensitive to temperature variations, which is a crucial advantage for vibration-based monitoring (VBM). Additionally, changes in temperature affect the boundary conditions of the bridge, leading to variations in certain vibration modes.

Despite their promise, the practical application of OSP methods to existing structures remains challenging due to constraints such as accessibility, environmental conditions, and budget limitations (Ostachowicz, Soman e Malinowski, 2019).

Throughout the development of this dissertation, I made use of artificial intelligence tools, particularly ChatGPT, to support various aspects of the work. AI was especially helpful during the programming phase, assisting with the development and refinement of MATLAB code, including the generation of figures and graphs that were essential for interpreting and presenting the results clearly.

In the final stages of the dissertation, artificial intelligence played an important role in enhancing the scientific and linguistic quality of the text. It contributed to improving the clarity, coherence, and formality of the English writing, ensuring that the document would be more accessible and professional for its readers.

While AI was used as a supportive tool, all critical thinking, decision-making, and methodological development were carried out independently, with AI serving only as a means to improve efficiency and communication.

This dissertation is structured as follows:

Section 2 presents the theoretical background, including a detailed explanation of the methods used and the MAC metric for result evaluation.

Section 3 describes the structure under study, the development and properties of the Finite Element structural model, as well as the experimental testing procedures.

Section 4 outlines the steps followed for the dynamic analysis of both numerical and experimental results. It also details the procedures used to process the data with MACEC and interpret the experimental outcomes.

Section 5 presents the results obtained from the optimal sensor placement methods applied to the numerical model, as well as from the experimental tests setup, followed by a discussion and interpretation of these findings. The section concludes with an evaluation of the most suitable method to use.

Section 6 presents final tests aimed at validating the optimal number of sensors by exploring the use of very few sensors.

Finally, Section 6 provides the conclusions of the study and suggests future work, including recommendations and possible improvements.

2
OPTIMAL SENSOR PLACEMENT STRATEGIES

Due to the economic and logistical constraints that are often present in civil engineering applications, the instrumentation used for Structural Health Monitoring (SHM) is typically limited to a small number of sensors. Therefore, it is crucial to determine the Optimal Sensor Placement (OSP) in order to maximize the value of the information gathered while minimizing the overall costs (Kim e Cho, 2024).

OSP aims to ensure that the sensors are placed in locations where they can provide the most informative data for identifying the dynamic behavior of the structure, such as natural frequencies, mode shapes, and damping ratios, with the fewest number of sensors possible. This becomes especially important when working with large or complex structures, where full instrumentation is not feasible.

In this research, three different OSP methods are applied and evaluated:

- Modal Kinetic Energy Method (MKE);
- Effective Independence Method (EFI);
- Information Entropy Index Method (IEI).

Each method uses a different criterion to evaluate sensor placement efficiency. These will be detailed in the following subsections.

2.1. Problem Statement

The dynamics of a linear structural system with *n* degrees of freedom (DOFs) are governed by the following matrix differential Equation (1) (Leyder et al., 2018):

$$M\ddot{\mathrm{u}}(t) + \mathrm{C}\dot{\mathrm{u}}(t) + \mathrm{Ku}(t) = \mathrm{F}(t) \qquad (1)$$

where:

- u(t) [$n \times 1$] is the displacement vector;
- M, C and K [$n \times n$] are the mass, damping, and stiffness matrices, respectively;
- F(t) [$n \times 1$] is the force vector.

Assuming proportional damping, the system can be decoupled into modal coordinates, Equation (2):

$$\ddot{\xi}(t) + C^*\dot{\xi}(t) + \Lambda\xi(t) = \Phi^T F(t) \tag{2}$$

where:

- $\xi(t)$ [$n \times 1$] is the vector of modal coordinates;
- Λ = diag $\{\omega_1^2, \dots, \omega_n^2\}2$ [$n \times n$] contains the *i*th natural frequencies (ω_i);
- C* = diag$\{2\zeta_1\omega_1, \dots, 2\zeta_n\omega_n\}$ [$n \times n$] and ζ_i represents the *i*th modal damping ratio;
- Φ [$n \times n$] or [$m \times m$] (if the target modes *m* are considered) is the mode shape matrix.

The structural response is given by Equation (3):

$$u(t) = \Phi\xi(t) \tag{3}$$

The goal of Optimal Sensor Placement (OSP) is to select $m < n$ sensor locations. These selected sensor locations should enable accurate reconstruction of the dominant mode shapes and other modal parameters of interest.

2.2. Modal Kinetic Energy Method (MKE)

The Modal Kinetic Energy (MKE) method (Equation (4)) (Leyder et al., 2018) aims to identify the optimal sensor placement by evaluating the degrees of freedom (DOFs) that exhibit the highest kinetic energy. This approach considers both the mode shape matrix and the mass associated to each node, allowing the selection of sensor locations that contribute most significantly to the system's dynamic response.

$$\mathrm{MKE}_{ij} = (L\Phi)_{ij} \sum_{s=1}^{n} M_{is} (L\Phi)_{sj} \tag{4}$$

where:

- *i* refers to a DOF;
- *j* refers to a vibration mode;
- L [$n \times n$] is a Boolean matrix indicating sensor locations;
- *s* corresponds also to the DOFs and it's used to distinguish the index *i*;
- M is the mass matrix.

In this formulation, the kinetic energy contribution of each DOF for each vibration mode is computed. Initially, L is the identity matrix, considering all possible sensor positions. After computing MKE_{ij} , the total kinetic energy per DOF is calculated by summing over the selected modes (Equation (5)):

$$\mathrm{MKE}_i = \sum_{j=1}^{p} \mathrm{MKE}_{ij} \tag{5}$$

The DOFs with the lowest total kinetic energy are removed, until the desired number of sensors locations is achieved, without iterations. This method ensures that sensors are placed where the kinetic energy, and thus the vibrational activity, is greatest, maximizing the likelihood of capturing informative measurements.

2.3. Effective Independence Method (EFI)

The Effective Independence (EFI) (Leyder et al., 2018) method evaluates the contribution of each sensor location to the linear independence of the target mode shapes. The main goal is to select sensor positions that provide the most linearly independent information about the vibration modes.

Like the MKE method, the EFI method initially considers all available DOFs as potential sensor locations. EFI proceeds iteratively: at each step, it computes an effectiveness value for each DOF, removes the one with the lowest contribution, and recalculates the metrics until the desired number of sensor positions is achieved.

The EFI value ranges between 0 and 1, where values closer to 1 indicate a higher contribution to mode shape independence.

The EFI is calculated using the following Equation (6) (Kim e Cho, 2024):

$$\mathrm{EFI} = \frac{\mathrm{diag}(\Sigma^{-1} S F^{-1} S^{T} \Sigma^{-1})}{\mathrm{diag}(\Sigma^{-1})} \tag{6}$$

where:

- Σ^{-1} $[n \times n]$ is the inverse of the Error Covariance Matrix;
- $S = \Phi$ $[n \times m]$ is the modal shape matrix;
- S^T is the transpose of the modal shape matrix;
- F^{-1} $[n \times m]$ is the inverse of the Fisher Information Matrix;
- diag(·) extracts the diagonal of a matrix as a vector.

2.3.1. Error Covariance Matrix (Σ)

One common issue in Optimal Sensor Placement (OSP) is the close positioning of sensors, which may lead to correlated measurements and redundant information, ultimately reducing the effectiveness of the modal identification. This spatial correlation between sensors can be accounted for using the Error Covariance Matrix (Σ), which models the uncertainty and correlation between measurements at different sensor locations.

The Covariance Matrix quantifies the estimation error between nodes, where closely spaced nodes tend to exhibit higher correlation and, consequently, larger error. By accounting for this, the algorithm discourages the selection of nearby sensor locations, promoting spatial diversity in sensor placement.

According to (Papadimitriou e Lombaert, 2012), the error covariance matrix Σ is not necessarily diagonal when spatial correlation is considered. The matrix element between degrees of freedom (DOFs) i and j is given by Equation (7):

$$\Sigma_{ij} = \mathrm{R}(\delta_{ij})\sqrt{\Sigma_{ii}\Sigma_{jj}} = \exp\left(-\frac{\delta}{\lambda}\right)\sqrt{\Sigma_{ii}\Sigma_{jj}} \tag{7}$$

where:

- Σ_{ij} is the covariance between the errors at DOFs *i* and *j*;
- δ_{ij} is the spatial distance between sensors *i* and *j*;
- λ is the spatial correlation length, which controls the rate of decay of correlation with distance;
- $\mathrm{R}(\delta_{ij})$ is the correlation coefficient, modeled as an exponential decay function of the distance;
- Σ_{ii} and Σ_{jj} are the variances of the covariance matrix at positions *i* and *j* (assumed equal to 1).

In this study, a value of $\lambda = 0.8$ is used. This was derived based on the shape of the identified fourth vibration mode, which approximately follows a quarter of a sine wave between floors. Therefore, the correlation length was estimated by dividing the distance between floors (0.4m) by 0.5 (Kim e Cho, 2024), resulting in $\lambda = 0.8$. This parameter ensures that sensors placed within a small distance are appropriately penalized in terms of correlation, leading to a better-spaced and more informative sensor configuration.

2.3.2. Fisher Information Matrix (FIM)

The Fisher Information Matrix (FIM) quantifies the amount of information that a set of sensors provides about unknown system parameters and thus reflects the effectiveness of a sensor configuration in accurately estimating these parameters.

In the context of structural dynamics and modal identification, the FIM provides a way to evaluate and compare different sensor placement strategies by measuring how well they capture the essential dynamic behavior of the structure, while accounting for uncertainties and noise.

The FIM is computed as follow Equation (8) (Kim e Cho, 2024):

$$\mathrm{F} = \Phi^{\mathrm{T}}\Sigma^{-1}\Phi \tag{8}$$

where:

- F $[n \times n]$ is the Fisher Information Matrix;
- Φ $[n \times m]$ is the mode shape matrix and Φ^{T} the transpose;
- Σ^{-1} is the inverse of the error covariance matrix (Eq. (7)), representing the confidence or uncertainty in the measurements.

This formulation seeks to maximize the sensitivity of the measured system responses to the modal parameters, while minimizing the influence of noise and uncertainty introduced through the sensor measurements.

2.4. Information Entropy Index Method (IEI)

The Information Entropy Index (IEI) method is based on the concept of information entropy, which quantifies the uncertainty associated with a given configuration of sensors. A lower value of information entropy corresponds to less uncertainty, indicating a more informative and effective sensor configuration. Therefore, the objective of this method is to identify the combination of sensor locations that minimizes the information entropy.

The Information Entropy Index (IEI) method is an iterative approach. The process begins by considering all available degrees of freedom. Then, one sensor is removed at a time, and the Information Entropy value is calculated for each resulting combination. The combination with the lowest entropy, indicating the least uncertainty, is selected, and the corresponding node is excluded. This procedure is repeated iteratively until the desired number of sensor locations is reached. Similar to the EFI method, the Covariance Matrix and the Fisher Information Matrix are also incorporated in the IEI method to account for correlation between sensor locations.

The information entropy (IE) of a given sensor configuration is calculated using the following Equation (9) (Leyder et al., 2018):

$$\mathrm{IE}(\mathrm{L}, \theta_0) = \frac{1}{2} N_\theta \ln(2\pi) - \frac{1}{2} \ln[\det\{\mathrm{Q}(\mathrm{L}, \theta_0)\}] \tag{9}$$

where:

- θ_0 is the vector representing the degrees of freedom (DOFs) considered at each iteration;
- N_θ is the number of elements in θ_0;
- $\mathrm{Q}(\mathrm{L}, \theta_0)$ $[N_\theta, N_\theta]$ is the Fisher Information Matrix (FIM) (Eq. (8)) for the current configuration L.

The sensor selection process in the IEI method was performed using the Backward Sequential Sensor Placement (BSSP) algorithm (Papadimitriou e Lombaert, 2012). This algorithm works as follows:

1. Start with the full set of DOFs (i.e., all possible sensor positions);
2. Compute the IE for every possible configuration obtained by removing one sensor;
3. Remove the sensor that leads to the lowest IE;
4. Repeat the process iteratively until the desired number of sensor locations, corresponding to the target number of modes m, is reached;

This iterative procedure ensures that at each step, the sensor configuration retains the most relevant information while minimizing redundancy and uncertainty.

To enable comparison between different configurations and evaluate the method, a normalized version of the entropy is known (Equation (10)), named as the Information Entropy Index (IEI):

$$\mathrm{IEI}(\mathrm{L}, \theta_0) = \sqrt{\frac{\det \mathrm{Q}(\mathrm{L}_{\mathrm{ref}}, \theta_0)}{\det \mathrm{Q}(\mathrm{L}, \theta_0)}} \tag{10}$$

where:

- $\mathrm{L}_{\mathrm{ref}}$ $[n \times n]$ represents the full configuration using all DOFs (i.e., the reference configuration).

2.5. MODAL ASSURANCE CRITERION (MAC)

To evaluate the quality of the results obtained through the Optimal Sensor Placement (OSP) and to assess the level of correlation between sensors, the Modal Assurance Criterion (MAC) is commonly employed. This criterion quantifies the similarity between two mode shape vectors and is defined by the following Equation (11) (Leyder et al., 2018):

$$\mathrm{MAC}(\Phi_1, \Phi_2) = \frac{|\Phi_1^T \Phi_2|^2}{(\Phi_1^T \Phi_1)(\Phi_2^T \Phi_2)} \tag{11}$$

where:

- Φ_1 and Φ_2 $[n \times 1]$ are mode shape vectors.
- Φ_1^T and Φ_2^T are their respective transposes.

The MAC value ranges between 0 and 1:

- A value close to 1 on the diagonal of the MAC matrix indicates high correlation between corresponding mode shapes, which is desirable.
- Values close to 0 in the off-diagonal elements indicate low correlation between different modes, also considered ideal.

There are two typical uses of the MAC:

- AutoMAC: compares mode shapes within the same dataset (e.g., to evaluate the linear independence of the modes identified by the sensor configuration).
- MAC: compares mode shapes obtained from different sources, such as between the Finite Element Model (FEM) and experimental measurements, to assess how well the selected sensor configuration can reproduce the actual structural dynamic behavior.

The MAC thus serves as a valuable validation tool in sensor placement strategies by indicating both the fidelity and uniqueness of the identified modes.

3
CASE STUDY

3.1. Frame Structure

The structure analyzed in this study is a frame situated in the Structural Mechanics Laboratory (Fig. 2) of the Department of Civil Engineering at KU Leuven. Originally designed for educational use and demonstration purposes, the structure is permanently installed in the lab and allows for manual excitation, making it suitable for observing and studying its dynamic response.

Fig. 2 – Laboratory Frame Structure.

The structure is made of steel and consists of four floors. It is braced in the x-direction and unbraced in the y-direction. Each floor is a rectangular plate measuring 0.6 m × 0.4 m with a thickness of 8 mm, supported by four columns, each 0.4 m in height. Diagonal bracings are asymmetrical and oriented to increase the stiffness of the structure in the x-direction. Both the columns and the bracings have identical cross-sections of 6 mm × 40 mm.

Each floor also includes four L-profiles, with dimensions of 40 mm × 40 mm × 4 mm and a length of 0.385 m, which are bolted to the floor plates to enhance in-plane stiffness. At each corner, a connection element joins the bracing members and columns to the plates. These connections differ in size depending on their position: the top floor connections measure 90 mm × 58 mm × 8 mm, while those on the lower floors measure 90 mm × 108 mm × 8 mm.

3.2. FINITE ELEMENT MODEL

Considering the experimental structure located in the KU Leuven Structural Mechanics Laboratory (Fig. 2), a finite element model (FEM) was developed for this structure.

The modeling was performed using Stabil**,** the MATLAB-based toolbox (Section e Department of Civil Engineering, 2020), which enables modal analysis for implementing Optimal Sensor Placement (OSP) methods.

Geometry

Initially, the cross-sections of the structure were defined. For the plates, columns, and bracing elements, the cross-sectional properties were specified, including the area, geometrical center, and moments of inertia. The moments of inertia were calculated in the x, y, and z directions (I_{xx}, I_{yy}, and I_{zz}).

Since the x-direction aligns with the longitudinal axis of the structural elements, I_{xx} represents the torsional moment of inertia. Given that the cross-section of the elements is rectangular, the following Equation (12) was used:

$$I_{xx} = \frac{1}{3} b h^3 \tag{12}$$

For the other two directions, the standard Equation (13) for rectangular cross-sections were applied to obtain I_{yy}, and I_{zz}:

$$I_{yy/zz} = \frac{1}{12} b h^3 \tag{13}$$

where:

- b [m] is the width of cross-section;
- h [m] is the height.

These calculations follow the guidelines and formulas from (Augustyn e Kozień, 2015).

Material Properties

Subsequently, the material properties were defined. All structural elements were assumed to be made of steel, with a Young's modulus of E = 190 GPa, Poisson's ratio ν = 0.3, and a density of ρ = 7750 kg/m^3. For the small connection elements between the plates, bracing, and columns, a higher stiffness was assigned to simulate rigid connections, which was later defined.

Element types and Meshing

Different element types were used for different structural components:

- Beams were used to model the columns, bracing elements, and connections;
- Floors were modeled using four-node shell elements, which combine a bilinear membrane formulation with Discrete Kirchhoff Triangle (DKT) elements to account for bending stiffness.

Boundary Conditions

The boundary conditions were also defined: the base of the structure was assumed to be fully fixed, restricting all degrees of freedom.

Model

A finite element model (FEM) of the frame structure tested in the laboratory was developed using Stabil, as shown in Fig. 3. The red elements represent the rigid connections between plates, columns, and diagonals.

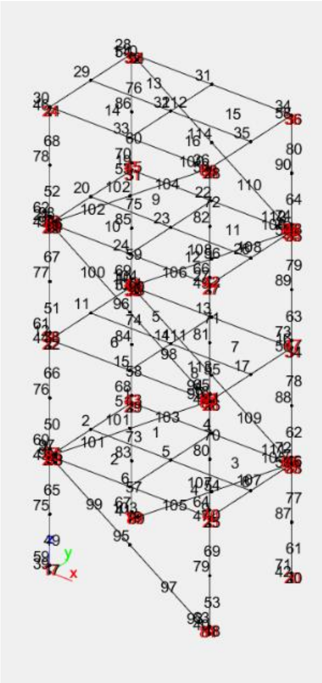

Fig. 3 – Finite Element Model of the structure.

3.3. Experimental Tests

Experimental tests were carried out using twenty-four uniaxial piezoelectric accelerometers to measure the structural response in both the x and y directions at each floor level. The accelerometers are represented as circles in Fig. 7, with twelve installed on each face of the structure (colored blue and red) indicating their orientation and the direction of measurement.

Twenty-four metal mounting plates were first selected and affixed to the structure using a specialized adhesive (Fig. 4). The glue used was “X60 Schnellklebstoff”, a proven cold-curing adhesive widely used in experimental testing and for strain gauge installations. It consists of two components: 1-X60/A-NP, a powder dosed with a measuring spoon, and 1-X60/B-NP, a liquid added drop by drop. The two components are mixed in a dedicated container, allowing the consistency to be adjusted as needed. X60 is suitable for both porous materials (e.g., concrete, cast iron, wood, ceramics) and smooth surfaces (GmbH, 2022). It cures rapidly, within 2 minutes at 35°C, 10 minutes at 20°C, and 60 minutes at 0°C, and remains effective even at cryogenic temperatures down to –200°C.

Fig. 4 – X60 adhesive and metal mounting plates used for sensor installation.

Next, the adhesive was applied to the metal plates, which were then glued to the structure at the twenty-four designated positions. Twenty-four piezoelectric accelerometers were selected for the experiment (Fig. 5). These sensors measure vibrational acceleration and convert it into an electrical signal (France, ES France). Each accelerometer produces an electrical charge proportional to the applied acceleration and was bolted onto its corresponding metal plate, with each location carefully recorded.

Fig. 5 – Piezoelectric accelerometers used to measure structural vibrations.

For the dynamic data acquisition, a National Instruments (NI) CompactDAQ system, model cDAQ-9178 (Fig. 6), was used. This chassis was equipped with data acquisition modules suitable for accelerometer input. The accelerometers were connected to the system via blue and red signal cables, which transmitted the analog signals from the sensors to the chassis. The CompactDAQ system converted the analog signals into digital data and interfaced with a computer for processing and analysis (Instruments, 2025).

Fig. 6 – National Instruments CompactDAQ system, model cDAQ-9178, used for data acquisition.

Two repeated hammer excitations were applied at the top of the structure, in two perpendicular directions (indicated by the green triangle in Fig. 7), in order to identify the modal characteristics of the system. The signals recorded from the accelerometers were processed using MACEC software (Reynders, Schevenels e Roeck, 2021).

The complete experimental setup is illustrated in the Fig. 7.

Fig. 7 – Overview of the experimental setup, including sensor positions and excitation points.

4
DYNAMIC ANALYSIS OF THE FRAME STRUCTURE

4.1. NUMERICAL

The FEM was refined by adjusting mesh density, elements per beam, and rigid element stiffness. A mesh of 2×2 elements, with two elements per beam and a stiffness of $E = 190 \times 10^{12}\ GPa$ for rigid elements, produced highly accurate results.

Natural frequencies were numerically obtained with the new developed model and compared to the numerical values presented in (Zhang, 2019). Four vibration modes were analyzed (Table 1).

Table 1 - Comparison of natural frequencies between numerical results (Zhang, 2019) (f_0) and the FEM (f).

Modes	f_0 [Hz]	f [Hz]	Error (%)
1	4.58	4.60	0.44
2	13.60	13.68	0.59
3	21.86	22.00	0.64
4	27.98	28.06	0.29

The mode shapes are shown in Fig. 8.

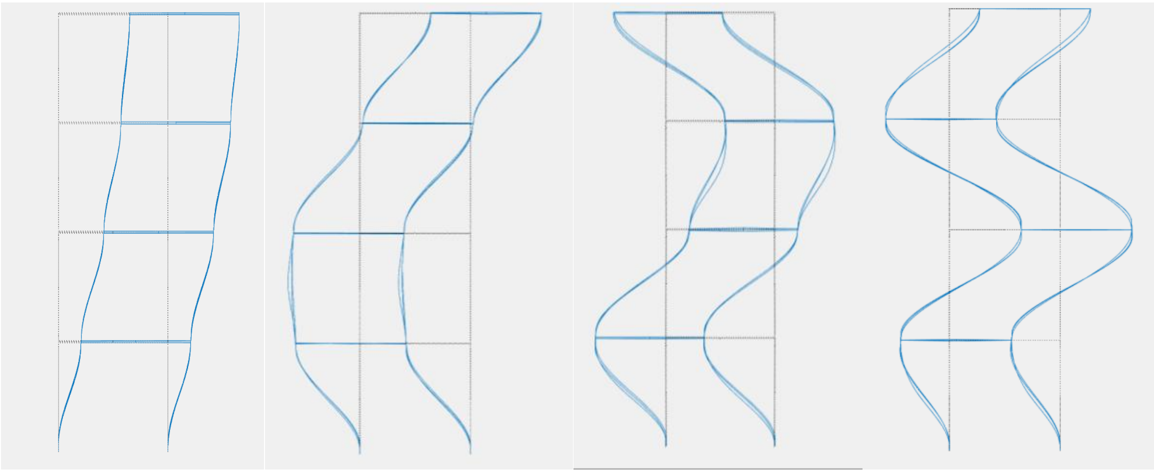

Fig. 8 – First four mode shapes from the FEM.

4.2. Experimental

The MATLAB toolbox MACEC, commonly used for experimental and operational modal analysis, was employed to process and evaluate the results obtained from the finite element model (FEM) and the experimental tests.

4.2.1. Geometry

Initially, the geometry of the structure was defined within MACEC by specifying the locations of the sensor nodes, along with the beams, columns, and bracing elements that comprise the structure, as represented in Fig. 9.

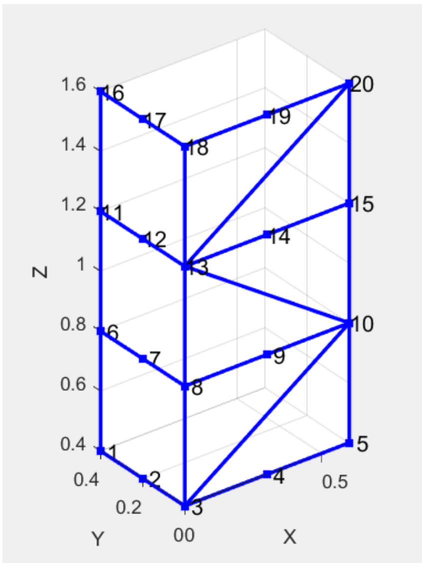

Fig. 9 – Definition of the geometry in MACEC.

4.2.2. SIGNAL PROCESSING

For the signal processing, the raw acceleration data was first converted into a mcsignal, using a sampling frequency of 5120 Hz. When performing modal analysis with MACEC, proper signal sampling is essential during data acquisition, particularly when collecting vibration data from accelerometers. The sampling frequency must be sufficiently high to capture the expected dynamic behavior of the structure, ensuring accurate identification of the modal parameters without aliasing.

The Sampling Frequency must satisfy the Nyquist criterion, expressed by the following Equation (14) (Proakis e Manolakis, 2006):

$$F_s \geq 2F_{max} \tag{14}$$

where:

- F_{max} [Hz] is the maximum expected frequency of the structure.

This ensures that the signal is sampled at a rate sufficient to accurately capture the structural vibrations without introducing aliasing errors.

Then, the signal was processed by removing the static offset from all measurements. Two different excitation setups were performed, resulting in two separate measurement datasets: one corresponding to excitation in the weak direction (y-axis) and the other in the strong direction (x-axis).

The Sampling Frequency (initially set as F_S = 5120 Hz) was decimated to improve the interpretability of the results. For the weak direction (y-axis), a decimation factor of 25 was applied, resulting in a final sampling frequency of 204.8 Hz. For the strong direction (x-axis), a decimation factor of 5 was used, leading to a sampling frequency of 1024 Hz. This approach ensures that the Nyquist criterion is satisfied. The target maximum frequency of interest is estimated as 80% of half the sampling frequency, which provides a sufficiently high resolution for accurately capturing the structure's dynamic response.

The Degrees of Freedom (DOFs) measured by the sensors, along with their corresponding measurement directions, were defined and assigned within the software environment to ensure accurate identification of the structural response.

4.2.3. SYSTEM IDENTIFICATION

System identification involves developing a mathematical dynamic model that fits the measured response, regardless of whether the excitation forces are fully known, partially known, or unknown (Anastasopoulos, 2020). In this study, Stochastic Subspace Identification (SSI-Cov) was employed (Peeters e Roeck, 1999; Reynders, Pintelon e De Roeck, 2008). SSI-Cov is particularly suited for cases in which input parameters are unknown but exhibit a stochastic (e.g., noise-like) behavior.

To characterize the dynamic behavior of a structure, it is essential to define a suitable idealization of the acting loads, have accurate knowledge of the geometric and mechanical properties of the structural elements, and construct a mathematical model capable of predicting the structural response as accurately as possible, based on the nature of the excitation (Magalhães).

Excitations that vary over time can be described in two main ways: deterministic or stochastic. If the temporal evolution of the excitation is fully known, it is treated as deterministic, and the structural response can also be determined deterministically, assuming there is no uncertainty in the structural parameters. In contrast, when the excitation has a random nature, it is modeled stochastically, allowing the structural response to be described in statistical terms using excitation,response relationships based on probability theory.

The chosen mathematical model must be able to simulate the dynamic behavior of the structure. This simulation is never perfect, as practical limitations necessitate simplifications. The model is defined based on the structure's mass, stiffness, and damping properties.

These dynamic models can be either continuous or discrete in time. Continuous models describe the system's response over a continuous time domain, while discrete models describe it at specific time intervals.

Different types of mathematical models exist for describing dynamic behavior:

- The classical formulation, based on second-order differential equations;
- The state-space formulation, which involves first-order differential equations and doubles the dimensionality of the classical model;
- Autoregressive Moving Average (ARMA) models, which are discrete in time.

In the classical modal formulation, the modal analysis of a linear system typically assumes proportional damping, meaning the damping matrix is a linear combination of the mass and stiffness matrices. Under this assumption, the damped mode shapes are identical to those of the undamped system. However, this condition is rarely met in real structures. For instance, the presence of a localized damper can break this proportionality.

The state-space formulation overcomes this limitation and allows for models that incorporate characteristics specific to the experimental data. It also enables the inclusion of noise modeling, an inherent aspect of experimental measurements, and is well suited for the development of discrete-time models based on time series data.

In experimental conditions, collected data includes noise that is not directly measurable but must be considered in the modeling process. To this end, stochastic components are added to the discrete model, yielding the following discrete stochastic state-space Formulations (15) (16):

$$x_{k+1} = A \cdot x_k + B \cdot u_k + w_k \tag{15}$$

$$y_k = C \cdot x_k + D \cdot u_k + v_k \tag{16}$$

where:

- x_k : state vector at instant k; contains the displacements and velocities of the structure at instant $k{\cdot}\Delta t$;
- x_{k+1} : state at the next instant (k+1), that is, it predicts the future behavior of the system;
- u_k : vector of excitations applied to the structure at instant $k{\cdot}\Delta t$; for example, input forces (in the case of tests with measured excitation);
- y_k : vector of measured responses of the structure (e.g. accelerations, velocities, displacements), at instant $k{\cdot}\Delta t$;
- A : system transition matrix, describes how the state evolves from one instant to the next, without external input;
- B : input matrix, relates the excitations u_k to the future state;
- C : observation matrix, transforms the state vector into observable values (what is measured);

- D : direct transmissibility matrix, relates the excitations directly to the output (response), if such a relationship exists;
- w_k : process noise, represents uncertainties in the modeling of the state evolution (such as simplifications or non-linearities);
- v_k : measurement noise, represents errors or noise in the measurement sensors.

Here, w_k and v_k are zero-mean white noise processes of dimension n, representing process and measurement noise, respectively. The correlation between these stochastic processes is defined as Equation (17):

$$E\left(\begin{bmatrix} w_p \\ v_p \end{bmatrix} \cdot \begin{bmatrix} w_q^T & v_q^T \end{bmatrix}\right) = \begin{bmatrix} Q & S \\ S^T & R \end{bmatrix} \cdot \delta_{pq} \tag{17}$$

where:

- w_p, w_q : process noise vectors at instants p and q, come from the Equation (15);
- v_p, v_q : measurement noise vectors at instants p and q, come from the equation (16);
- E : expected value operator, i.e. statistical mean;
- δ_{pq} : kronecker Delta, equals 1 if p=q and 0 otherwise. This means that the noises are uncorrelated between different instants (white noise);
- Q : process noise covariance matrix w_k, quantifies the “strength” or variability of the noise in the evolution of the state;
- R : measurement noise covariance matrix v_k, quantifies measurement errors.
- S : cross-correlation matrix between process noise and measurement noise at the same instant (if w_k and v_k are not independent).

The Kronecker delta δ_{pq} ensures that these noise processes are uncorrelated in time, meaning the processes are ideal white noise. The matrices Q, R, and S describe the auto- and cross-correlations of the noise processes.

In environmental vibration testing, the excitation is not measured, making the input vector u_k unknown. It is generally assumed to be white noise, and all unknown effects are absorbed into w_k and v_k. The model then simplifies to:

$$x_{k+1} = A \cdot x_k + w_k \tag{18}$$

$$y_k = C \cdot x_k + v_k \tag{19}$$

The Stochastic Subspace Identification method based on correlations (SSI-COV) identifies this discrete-time stochastic state-space model using output-only data. It starts by computing the output correlation matrices, arranged into a block Toeplitz matrix (Equation (20)):

$$T_{1|i}^{ref} = Y_f \cdot \left(Y_p^{ref}\right)^T = \begin{bmatrix} R_i^{ref} & R_{i-1}^{ref} & \cdots & R_1^{ref} \\ R_{i+1}^{ref} & R_i^{ref} & \cdots & R_2^{ref} \\ \cdots & \cdots & \cdots & \cdots \\ R_{2i-1}^{ref} & R_{2i-2}^{ref} & \cdots & R_i^{ref} \end{bmatrix} \tag{20}$$

where:

- R_k^{ref} : it is the cross-correlation function of the output (system response) with delay k. It corresponds to the matrix of correlations between output channels separated by k time instants. It is calculated from experimental data;
- Y_f : set of future correlation vectors (future outputs), which refers to the part of the responses with instants ahead of the reference point in time;
- Y_p^{ref} : set of vectors of past correlations (past outputs), that is, responses prior to the reference instant. The exponent "ref" indicates that the reference was a unitary excitation in one of the output channels;
- $T_{1|i}^{ref}$: It is a Toeplitz block matrix, used to extract the observable subspaces. This matrix is essential in the SSI-Cov algorithm to estimate the modes of the structure (frequencies, dampings and mode shapes).

If the correlation matrices can be factorized as Equation (21):

$$R_i^{ref} = C \cdot A^{i-1} \cdot G^{ref} \tag{21}$$

where:

- R_i^{ref} : correlation matrix between the system outputs with delay i−1 (response at time k with the response at time k−i+1, for example). This matrix is what appears in the blocks of the matrix $T_{1|i}^{ref}$;
- A : state transition matrix. Defines how the state of the system evolves over time (from x_k to x_{k+1};
- C : observation matrix. Maps the state x_k to the measured output y_k;
- G^{ref} : matrix representing the effect of white noise on the model, through the Kalman gain solution (or related to the statistical input). It is obtained from the decomposition of the covariance matrix of the process noise w_k and measurement noise v_k, using the Kalman filter gain.

Then the Toeplitz matrix can be decomposed into Equation (22):

$$T_{1|i}^{ref} = \begin{bmatrix} C \\ C \cdot A \\ \cdots \\ C \cdot A^{i-1} \end{bmatrix} \cdot [A^{i-1} \cdot G^{ref} \quad \cdots \quad A \cdot G^{ref} \quad G^{ref}] = O_i \cdot \Gamma_i^{ref} \tag{22}$$

where:

- O_i is the extended observability matrix. Represents how the state influences the outputs over i instants;
- Γ_i^{ref} is the reversed extended stochastic controllability matrix. It represents the influence of noise on the state over the i instants.

A singular value decomposition (SVD) of $T_{1|i}^{ref}$ (Equation (23)) yields:

$$T_{1|i}^{ref} = U \cdot S \cdot V^T = [U_1 \quad U_2] \cdot \begin{bmatrix} S_1 & 0 \\ 0 & 0 \end{bmatrix} \cdot \begin{bmatrix} V_1^T \\ V_2^T \end{bmatrix} = U_1 \cdot S_1 \cdot V_1^T \tag{23}$$

where:

- U, S and V^T are the result of SVD decomposition (Singular Value Decomposition), where:
  - $-$ U contains the singular vectors on the left (orthonormal columns);
  - $-$ S is the diagonal matrix with ordered singular values;
  - $-$ V^T contains the singular vectors on the right.

From this, we can extract Equations (24) (25):

$$O_i = U_1 \cdot S_1^{1/2} \tag{24}$$

$$\Gamma_i^{ref} = S_1^{1/2} \cdot V_1^T \tag{25}$$

This step nearly completes the identification process. The state matrix *A*, which describes the system's dynamics, can now be identified from the observability matrix.

To determine the output matrix *C*, we extract the first *l* rows of O_i. The matrix *A* can then be obtained by Equation (26):

$$A = C^{-1} \cdot (C \cdot A) \tag{26}$$

At this point, the model order *n* (equal to the number of non-zero singular values in Γ_i^{ref} and the matrices *A* and *C* are known. From these, the dynamic properties of the structure can be extracted.

The modal parameters are obtained via eigenvalue decomposition of *A* (Equation (27)):

$$A = \Psi \cdot \Lambda_d \cdot \Psi^{-1} \tag{27}$$

where:

- Ψ contains the complex eigenvectors (modal shapes);
- Λ_d contains the discrete-time eigenvalues u_k.

The continuous-time eigenvalues λ_k, natural frequencies ω_k, and damping ratios ξ_k are then recovered via Equations (28) (29):

$$\mu_k = e^{\lambda_k \Delta t} \tag{28}$$

$$\lambda_k, \lambda_k^* = -\xi_k \omega_k \pm i \cdot \sqrt{1-\xi_k^2} \cdot \omega_k \tag{29}$$

where:

- μ_k : eigenvalue in the discrete domain (system sampled at intervals Δt;
- λ_k : eigenvalue of the system in the continuous domain;
- λ_k^* : the complex conjugate of the eigenvalue, always forming complex conjugate pairs;
- $-\xi_k \omega_k$: represents the damping;
- $\sqrt{1-\xi_k^2} \cdot \omega_k$: represents the oscillatory frequency (damped frequency).

Finally, the observable mode shapes are given by Equation (30):

$$V = C \cdot \Psi \tag{30}$$

The data-driven approach was applied in MACEC, and the half number of Hankel block rows i was defined, without estimating covariances (Peeters e Roeck, 1999; Reynders, Pintelon e De Roeck, 2008). A higher value of i leads to more accurate results, as it allows the algorithm to better capture the system dynamics. The value of i was determined based on the following Equation (31)(Reynders & De Roeck, 2008):

$$i = \frac{F_s}{2 \times F_1} \tag{31}$$

where:

- F_1 [Hz] represents the minimum frequency expected in the structure. A value of i = 25 was assumed for both excitation directions.

The Maximum System Order (MSO) was also defined, and this parameter must be greater than or equal to twice the number of expected modes identified in the FEM model. The MSO is applied incrementally, starting from 2 and increasing in steps of 2 (i.e., 2:2: MSO). In this study, a value of MSO = 80 was adopted.

4.2.4. Modal Analysis

Before performing modal analysis and stabilizing the diagrams, Power Spectral Density (PSD) plots were visualized using 16 data blocks. Mode shapes were then extracted manually from the stabilization diagrams.

Subsequently, the modal analysis was carried out to generate stabilization diagrams, from which the modal parameters were manually selected. Prior to selection, the display was configured to show Power Spectral Density (PSD) plots using 16 data blocks, a number commonly used to enhance the quality and clarity of the spectral representation of the data, thereby facilitating the accurate and reliable identification of the system's vibration modes.

As previously mentioned, two experimental tests were conducted to validate the numerical results. The first test involved excitation using an impact hammer in the *y*-direction (the weak direction of the structure), and the second test in the *x*-direction (the strong direction). These tests aimed to assess the dynamic response of the structure in both principal directions and to compare the measured data with the optimal sensor placements obtained through the numerical analysis.

Firstly, the vibration modes captured from the experimental tests under excitation in the weak direction were identified using the MATLAB toolbox MACEC (Fig. 10).

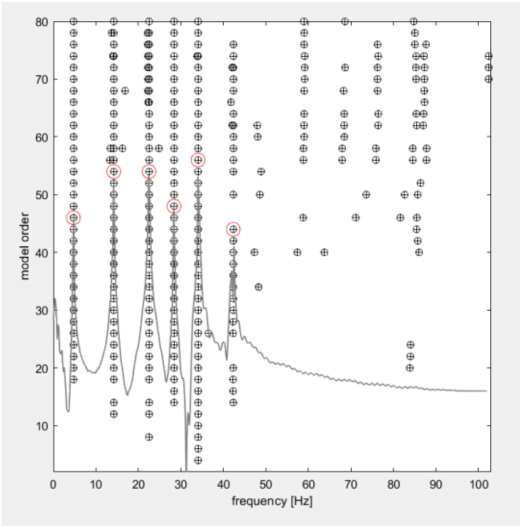

Fig. 10 – Stabilization Diagram (*y*-direction) in MACEC.

The diagram represents the stabilization of the vibration modes relating model order versus frequency. Each peak in the diagram corresponds to a vibration mode, and a total of six vibration modes were identified. The selection of poles for capturing the vibration mode can be done in the vertical alignment of the peak. Among these, four were identified as bending modes in the *y*-direction, and two as torsional modes.

Then, the vibration modes captured from the experimental tests under excitation in the strong direction were identified using the MATLAB toolbox MACEC (Fig. 11).

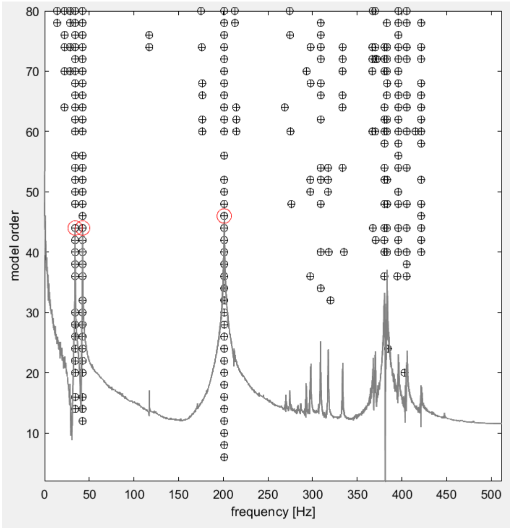

Fig. 11 – Stabilization Diagram (*x*-direction) in MACEC.

From the excitation in the strong direction, three vibration modes were extracted: the same two torsional modes observed previously, and one bending mode in the *x*-direction.

The identified mode shapes were plotted, and the results are shown in Fig. 12, along with their corresponding natural frequencies.

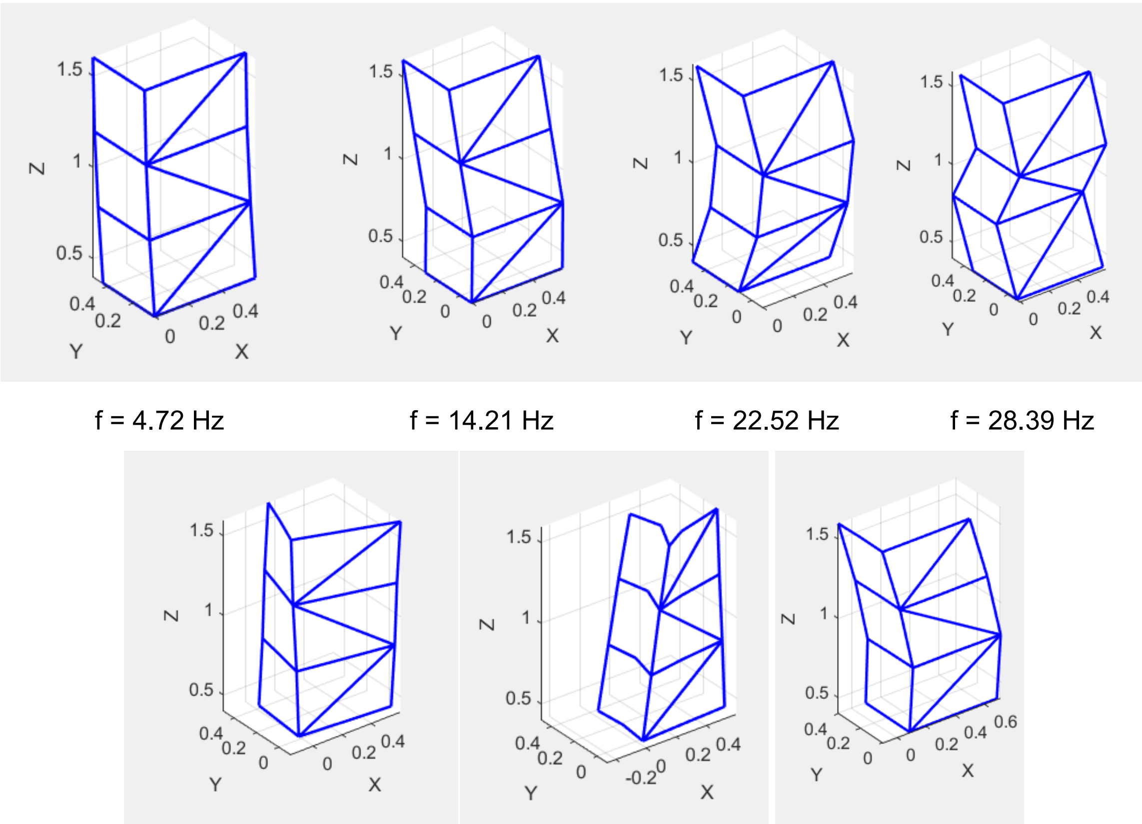

f = 4.72 Hz f = 14.21 Hz f = 22.52 Hz f = 28.39 Hz

f = 34.14 Hz f = 42.46 Hz f = 201.04 Hz

Fig. 12 – Mode shapes extracted using MACEC.

The extracted modes include four bending modes in the *y*-direction, two torsional modes (with displacements in both *x* and *y* directions), and one bending mode in the *x*-direction.

4.3. Comparison between Numerical and Experimental Results

Comparing the vibration modes extracted using MACEC with those obtained from the numerical model, a strong correlation can be observed in the first four modes, all involving displacement in the y-direction (the unbraced direction). This correlation, however, does not extend to the remaining modes. In the numerical model, there are no vibration modes corresponding to the experimental frequencies around f = 34.14 Hz and f = 42.46 Hz, and there is a significant gap between the fourth mode at f = 28.06 Hz and the fifth mode at f = 62.19 Hz. Additionally, only one torsional vibration mode in the model resembles the experimentally identified mode, but with a substantial difference in frequency. Regarding the vibration mode characterized by displacement in the x-direction (the braced direction), the model captures a mode with a visually similar shape, yet again there is a large frequency discrepancy.

All these observations are illustrated in Fig. 13, where the images showing four floors correspond to the vibration modes of the numerical model, and the images with three floors correspond to the vibration modes extracted using MACEC. This difference occurs because only the positions where sensors were placed are represented in the experimental data.

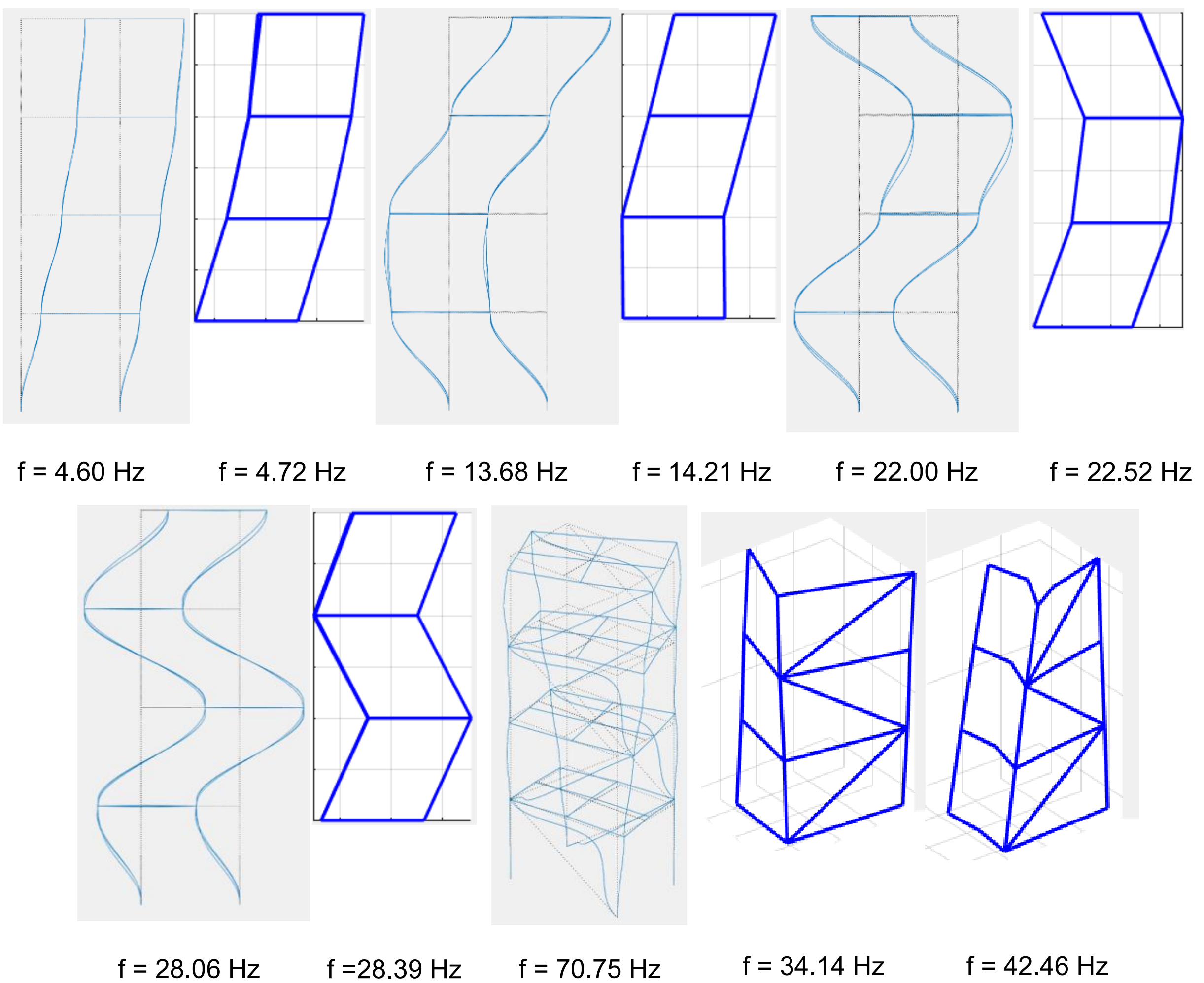

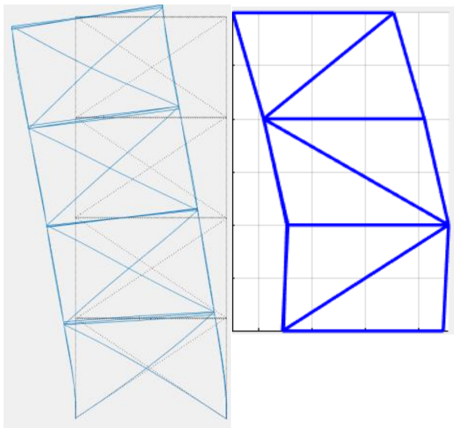

f = 81.48 Hz f = 201.04 Hz

Fig. 13 – Comparison between the vibration modes in numerical and experimental tests.

The vibration modes will now be evaluated using the MAC matrix, which is the most effective method for assessing the correlation between mode shapes. A total of 40 vibration modes were extracted from the original Finite Element Model (FEM) to enable the comparison with experimental results. This extended set of modes allowed for the identification of torsional modes and bending modes in the x-direction, which could not be observed when considering only the first four FEM modes, as these were predominantly associated with displacements in the y-direction.

The Degrees of Freedom (DOFs) corresponding to the locations used in the experimental tests were correctly selected from the mode shape matrix of the Finite Element Model. A MAC matrix (Fig. 14) was then computed to compare the selected vibration modes. In the matrix, the columns represent the experimental vibration modes, ordered as previously described (Fig. 12), while the rows correspond to the 40 vibration modes obtained from the FEM.

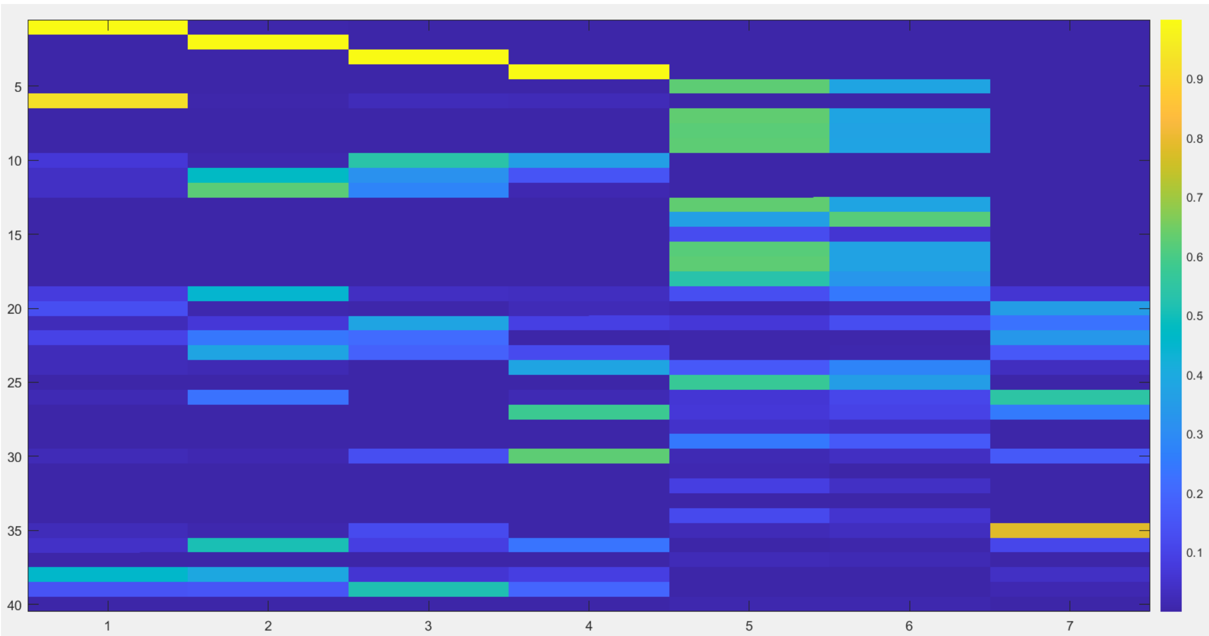

Fig. 14 – MAC matrix comparing experimental and FEM modes.

The first four vibration modes from both the experimental tests and the Finite Element Model showed perfect correlation, confirming the accuracy of the numerical model in predicting the bending modes in the weak direction. The torsional modes identified in the experimental tests did not correlate with any vibration modes of the FEM, as the model does not present modes with frequencies near 34.14 Hz or 42.46 Hz. This discrepancy indicates that the Finite Element Model does not fully capture the dynamic behavior of the real structure, particularly in torsional response, and therefore requires further refinement to improve its accuracy. Furthermore, the last experimental mode, corresponding to a bending mode in the *x*-direction, also showed a low correlation (around 0.8) with the 35th mode of the FEM (as illustrated in Fig. 14). Therefore, for the purposes of this study, only the first four vibration modes with displacement in the *y*-direction (unbraced direction) were considered.

Since the results for the torsional and bending modes in the *x*-direction (modes 5, 6, and 7) were not satisfactory, a reduced MAC matrix was generated considering only the bending modes in the *y*-direction (the first four modes). These were then compared with the corresponding FEM modes (modes 1, 2, 3, and 4), which showed the highest correlation with the experimental data (Fig. 15).

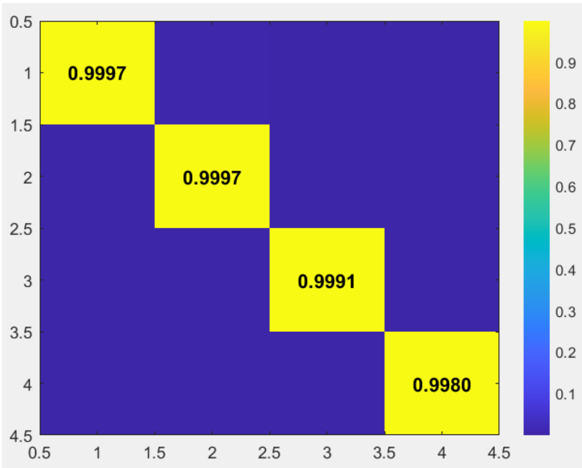

Fig. 15 – MAC matrix showing best-correlated bending mode shapes.

5
RESULTS OF THE OPTIMAL SENSOR PLACEMENT

5.1. NUMERICAL

5.1.1. 2D ANALYSIS

To validate the proposed sensor placement strategies, a preliminary optimization was carried out in a two-dimensional plane defined by x = 0.6 m. Given that the vibration modes of interest exhibit displacement exclusively in the *y*-direction, only the corresponding degrees of freedom (DOFs) were considered in the analysis.

Sensor optimization was conducted using three distinct methods, with the number of sensors limited to four. This constraint aligns with the number of relevant vibration modes identified for this configuration, ensuring that each mode could, in principle, be observed and distinguished.

5.1.1.1. MODAL KINETIC ENERGY METHOD (MKE)

The results of the sensor placement optimization using the Modal Kinetic Energy (MKE) method are shown in Fig. 16.

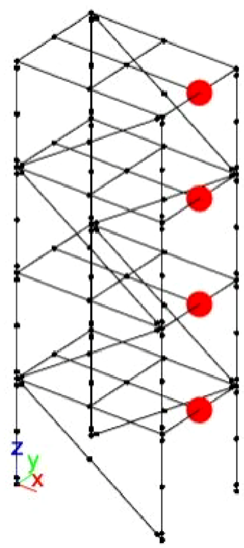

Fig. 16 – Optimal sensor placement using MKE (2D analysis).

The four sensors selected by the MKE method are located at the midpoints of each floor. This distribution reflects the goal of the method: maximizing the modal kinetic energy, as proposed by (Leyder et al., 2018). Because the MKE criterion is based on the mass associated with each node, the selected positions are physically meaningful. Nodes located at the center of the floors support mass contributions from both the left and right structural elements, resulting in higher concentrated mass at these points. As such, placing sensors at these locations ensures maximum sensitivity to modal activity.

The graph in Fig. 17 illustrates the evolution of the MKE values over the course of the sensor removal iterations.

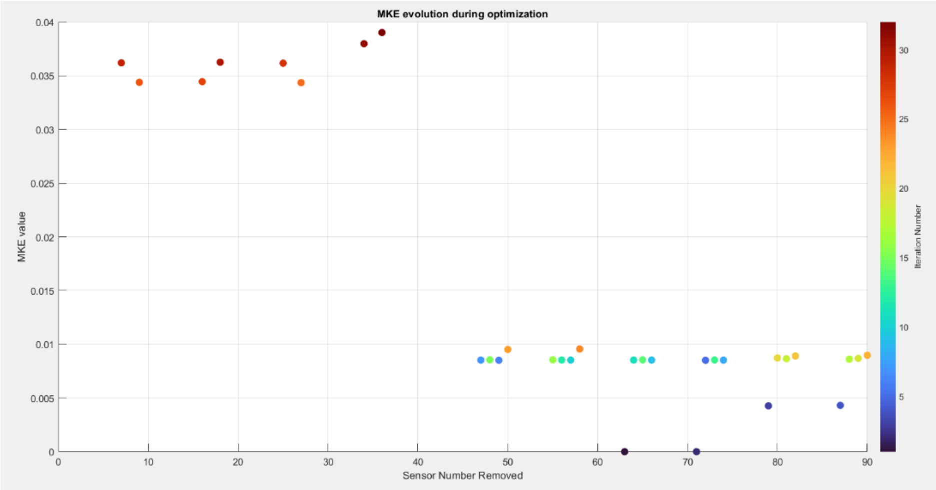

Fig. 17 – Evolution of MKE values throughout the iterations of sensor removal (2D analysis).

Fig. 18 represents the removal of sensors by iteration with MKE method in a 2D analysis.

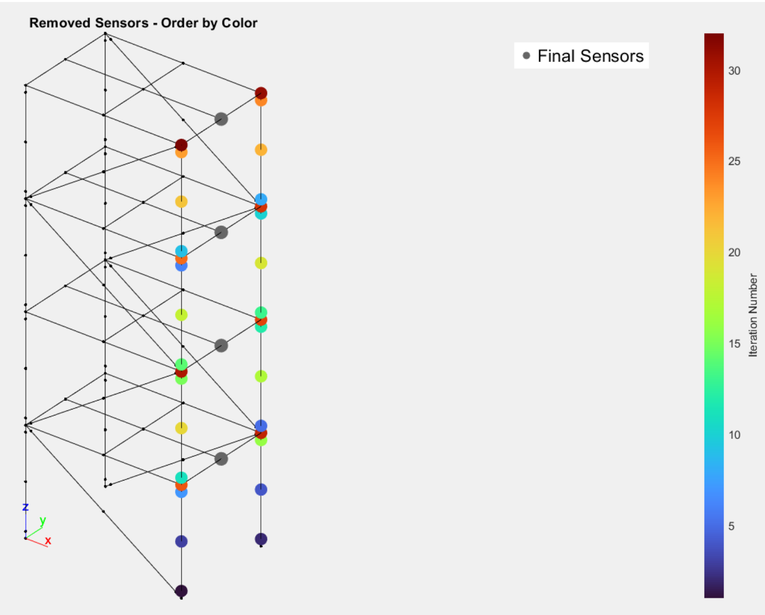

Fig. 18 – Removal of sensors by iteration with MKE method in a 2D analysis.

To better understand the optimization process, visualizations were generated in the form of animations, showing which nodes were removed at each iteration and the corresponding MKE value. The graph in Fig. 17 and the Fig. 18 serves as a representative summary of those animations, where it is possible to locate the removed sensor following the iteration color and evaluate the process. From the analysis, it is evident that the sensor selection process using the MKE method leads to a diversified spatial distribution. Sensors located on rigid structural elements and at the corners were the first to be excluded, as they contributed the least to the overall modal kinetic energy. Although the difference in MKE values between corner nodes and those on rigid elements is minimal, the distinction becomes significantly more pronounced when comparing these with nodes located at the center of the plates, which consistently showed the highest MKE contributions.

To evaluate the effectiveness of the optimization and assess the level of correlation between the selected sensors, the AutoMAC matrix was computed and is presented in Fig. 19.

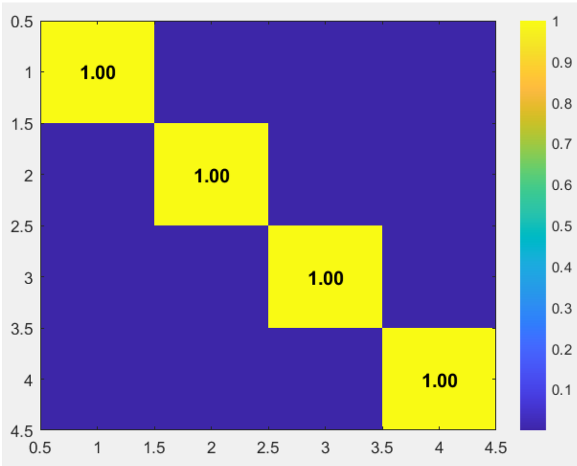

Fig. 19 – AutoMAC matrix for MKE method in 2D.

The AutoMAC matrix shows ideal results: diagonal values are equal to 1, indicating perfect correlation of each mode with itself, while all off-diagonal elements are close to 0, demonstrating a high degree of independence between the measured modes. This confirms that the selected sensor set is well distributed and effectively captures distinct vibration modes. Therefore, it can be concluded that the sensor optimization using the MKE method was successfully implemented for this structure.

5.1.1.2. Effective Independence Method (EFI)

In the EFI method, sensor placement aims to maximize modal independence (Kim e Cho, 2024), using the Fisher Information Matrix and the Error Covariance Matrix to evaluate the contribution of each node to the estimation of modal parameters.

The optimized sensor locations obtained through the EFI method are shown in Fig. 20.

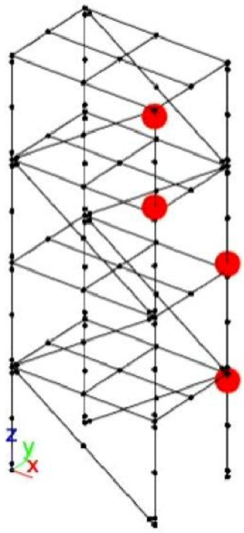

Fig. 20 – Optimal sensor placement using EFI (2D analysis).

The results appear satisfactory, as the selected sensors are well spaced, indicating that the method effectively avoids placing sensors too close to one another. This demonstrates the efficacy of the error covariance matrix in promoting spatial independence. All four optimized sensors are positioned on nodes belonging to rigid elements, which exhibit higher energy.

The graph in Fig. 21 shows the evolution of EFI values throughout the iterations of sensor removal.

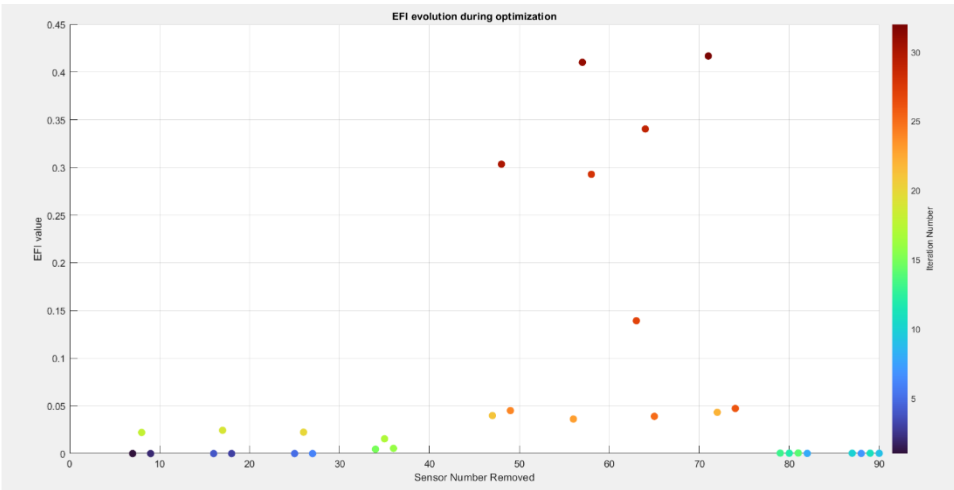

Fig. 21 – Evolution of EFI values throughout the iterations of sensor removal (2D analysis).

Fig. 22 represents the removal of sensors by iteration with EFI method in a 2D analysis.

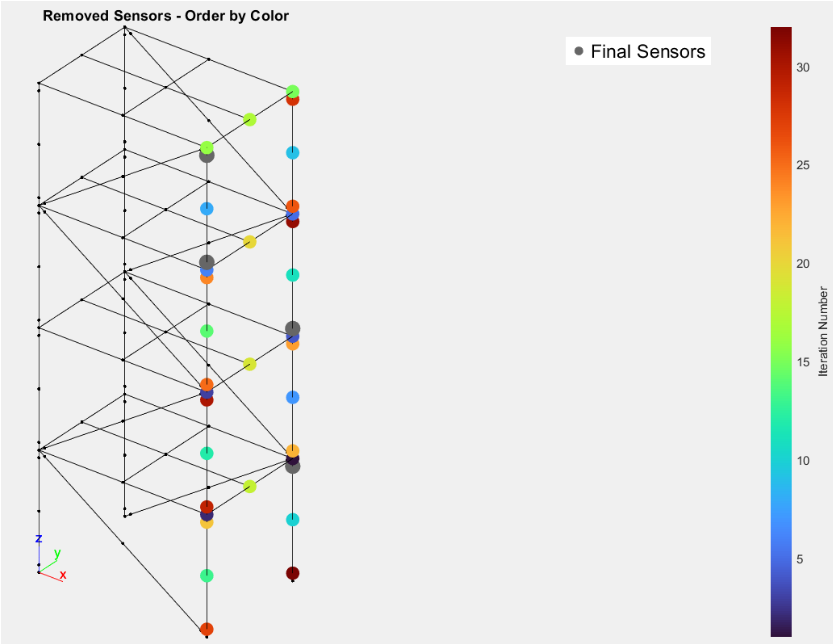

Fig. 22 – Removal of sensors by iteration with EFI method in a 2D analysis.

By analyzing the graph in Fig. 21 and the visual representation of the sensor removal process in Fig. 22, it is evident that the nodes are removed in a dispersed manner. The first nodes to be excluded are typically those located at the corners of the structure and in the middle of the plates. These locations contribute less to the modal independence of the system, justifying their early elimination in the optimization process. The last sensors to be excluded are those located at the rigid elements.

Analyzing the EFI values at each node, it is observed that the values are nearly symmetric across the structure, then placing the sensors on the opposite side would yield similar results. However, a significant contrast is seen when comparing the EFI values between the rigid elements and the corner nodes, with the former clearly showing higher values. This is due to their higher stiffness and natural frequencies, which make them more informative locations.

Additionally, the EFI values increase with node elevation: nodes located at higher levels of the structure tend to have larger EFI values. These locations are more active in the dynamic response and therefore provide better insight into the structure's behavior, making them optimal candidates for sensor placement.

The AutoMAC matrix was plotted to evaluate the effectiveness of the EFI-based optimization and to assess the degree of correlation between selected sensor locations (Fig. 23).

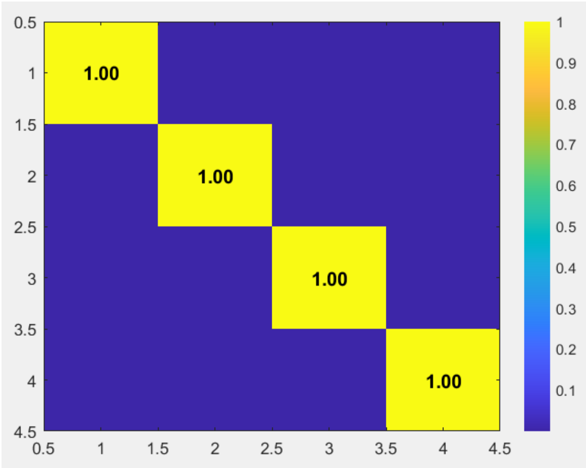

Fig. 23 – AutoMAC matrix for EFI method in 2D.

The AutoMAC matrix once again demonstrates excellent results from the sensor optimization. The diagonal elements display values equal to 1, indicating perfect correlation of each sensor with itself, while the off-diagonal elements are close to zero, confirming minimal correlation between different sensor locations. This reflects a high level of modal independence and validates the effectiveness of the EFI method in selecting well-distributed and informative sensor positions.

5.1.1.3. Information Entropy Index Method (IEI)

The sensor configuration resulting from the optimization using the Information Entropy Index (IEI) method is shown in Fig. 24.

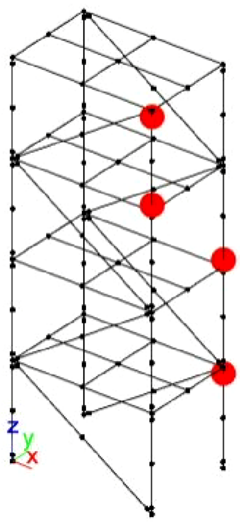

Fig. 24 – Optimal sensor placement using IEI (2D analysis).

The four optimal sensor locations obtained with the IEI method are identical to those derived using the EFI method, i.e., positioned on the nodes belonging to the rigid elements and located on the same side of the structure. This outcome is expected, as both methods are based on the Fisher Information Matrix and utilize the error covariance matrix in their formulations. While the EFI method iteratively maximizes modal independence, the IEI method iteratively refines the sensor configuration by minimizing the uncertainty associated with the identified modal parameters (Leyder et al., 2018). Despite the differing implementation approaches, both methods converge to the same sensor distribution, reinforcing the robustness of the selected configuration.

Fig. 25 illustrates the evolution of Information Entropy Index (IE) values throughout the sensor removal iterations.

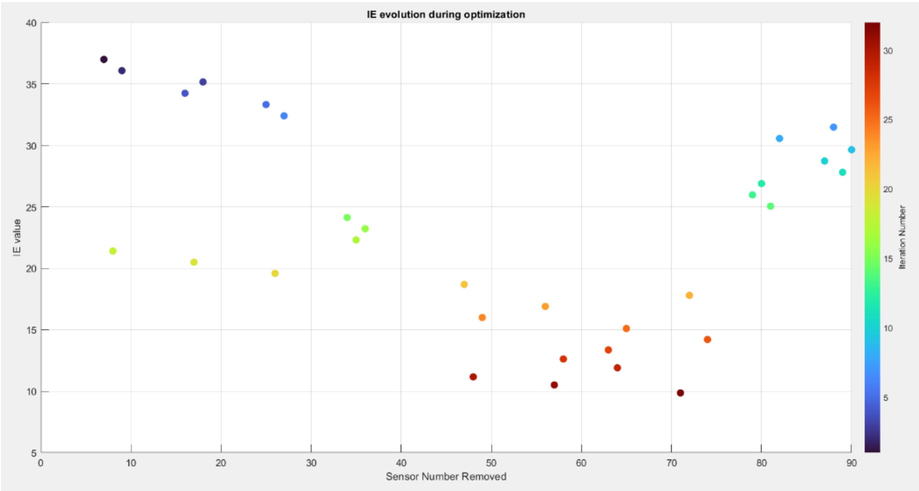

Fig. 25 – Evolution of IE values throughout the iterations of sensor removal (2D analysis).

Fig. 26 represents the removal of sensors by iteration with EFI method in a 2D analysis.

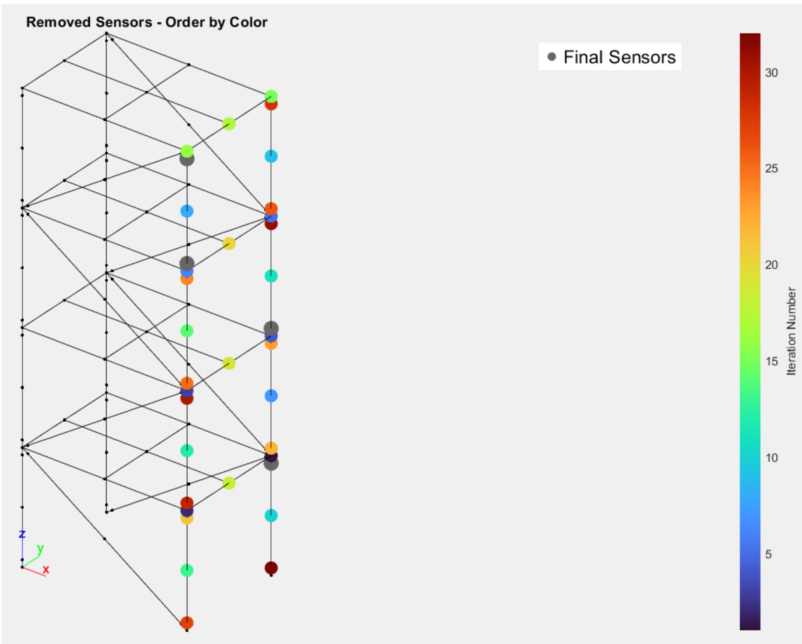

Fig. 26 – Removal of sensors by iteration with IEI method in a 2D analysis.

When comparing the sequence of sensor removal between the IEI and EFI methods, the selection process is found to be identical. This indicates that the two methods are proportional in their behavior, both prioritizing the removal of sensors based on the same informational criteria. Such consistency reinforces the equivalence of the approaches in terms of the underlying optimization strategy and further validates the robustness of the sensor placement configuration.

The AutoMAC matrix was plotted to evaluate the sensor configuration resulting from the IEI method and to assess the level of correlation between the selected sensors (Fig. 27).

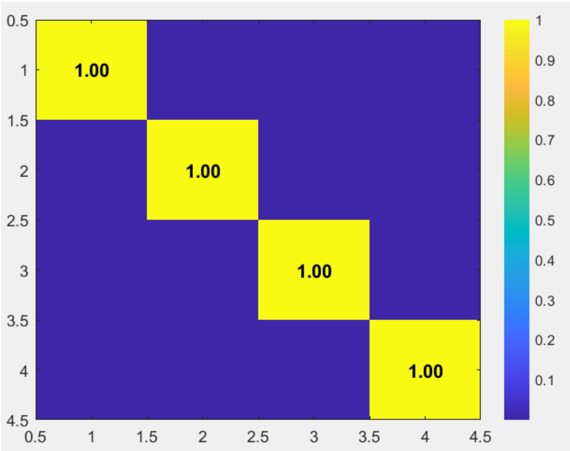

Fig. 27 – AutoMAC matrix for IEI method in 2D.

The AutoMAC matrix shows results identical to those obtained with the EFI method, confirming excellent sensor placement. The diagonal elements are equal to 1, indicating perfect self-correlation, while the off-diagonal elements are close to zero, demonstrating low correlation between different sensors. This reflects a well-optimized sensor configuration capable of capturing independent modal information.

A comparison of the AutoMAC after each optimization, considering only the final selected sensors, with the AutoMAC prior to optimization, where all possible sensor locations were initially included, revealed no significant differences in a 2D analysis, as shown in Fig. 28.

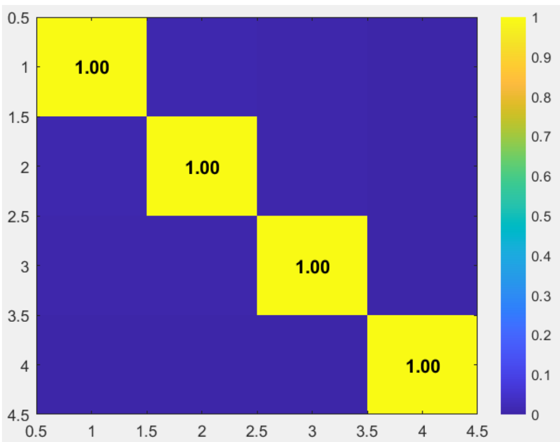

Fig. 28 – AutoMAC matrix without optimization of sensor placements (2D analysis).

5.1.2. 3D Analysis

Following the 2D analysis, the sensor placement optimization was extended to a full 3D model, considering all nodes of the structure and including the degrees of freedom (DOFs) in the *y*-direction and the first four vibration modes.

.

5.1.2.1. Modal Kinetic Energy Method (MKE)

The results of the sensor placement optimization using the Modal Kinetic Energy (MKE) method, considering only the degrees of freedom (DOFs) in the *y*-direction, are presented in the Fig. 29:

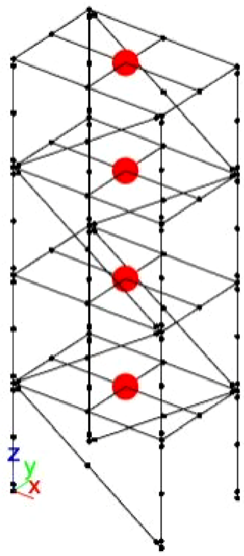

Fig. 29 – MKE sensor placement (*y*-direction, 3D).

The four optimized sensors are positioned at the midpoint of each floor, which corresponds to locations of higher mass concentration in the structure. This outcome is consistent with the objective of the MKE method, which prioritizes sensor placement at locations that contribute most to the modal kinetic energy.

In the 3D model, the midpoints of the floors provide a balanced representation of the structure's mass distribution in the *y*-direction, since these nodes are shared by all four surrounding finite elements on each floor.

The graph in Fig. 30 shows the evolution of MKE values during the sensor removal process in the *y*-direction.

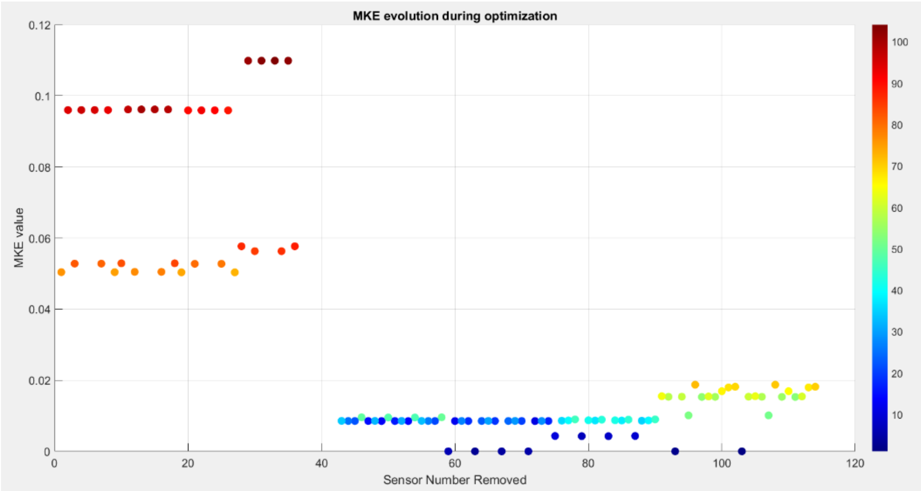

Fig. 30 – Evolution of MKE values throughout the iterations of sensor removal (3D, *y*-direction).

Fig. 31 represents the removal of sensors by iteration with MKE method in a 3D analysis in the *y*-direction.

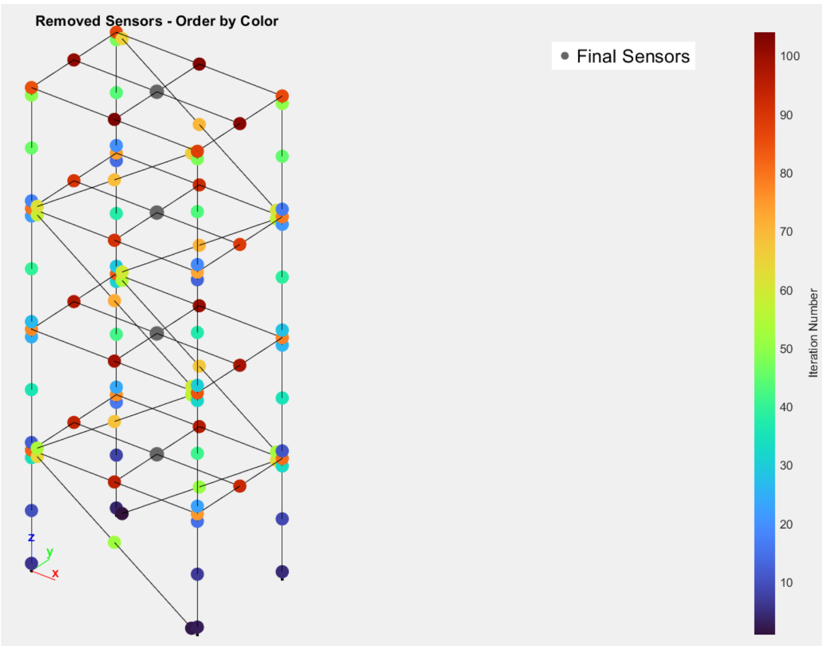

Fig. 31 – Removal of sensors by iteration with MKE method in a 3D analysis (*y*-direction).

By analyzing both the accompanying animation and the graph, it is observed that the first nodes removed during the optimization process are located at the base of the structure on rigid elements, diagonals, and at the corners of the structure, regions that contribute minimally to the modal kinetic energy. In contrast, the last sensors to be removed are those located at the midpoints of each floor, where the kinetic energy is most concentrated. Among them, the sensor at the fourth floor consistently shows the highest MKE value, highlighting it as the most significant measurement location in the *y*-direction.

The AutoMAC matrix was plotted to assess the quality of the sensor placement and evaluate the level of correlation between the measured vibration modes (Fig. 32).

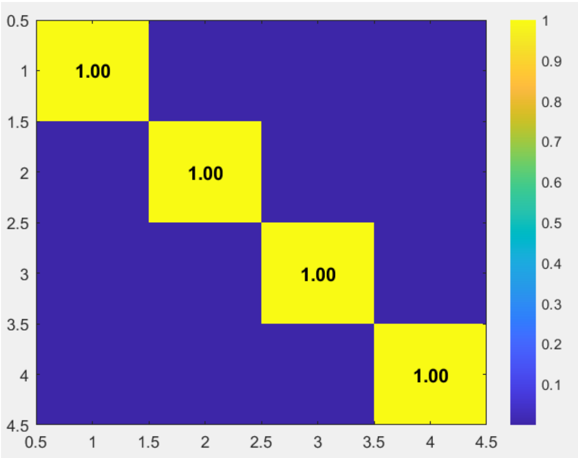

Fig. 32 – AutoMAC matrix (MKE, *y*-direction, 3D).

The AutoMAC matrix confirms the effectiveness of the optimization, showing no significant correlation between different modes, with diagonal values equal to 1 and off-diagonal values close to 0. This indicates that the selected sensor locations provide good modal independence, ensuring a robust and informative sensor configuration.

5.1.2.2. Effective Independence Method (EFI)

The resultant sensor layout from the optimization using the EFI method, considering degrees of freedom in the *y*-direction, is presented in Fig. 33.

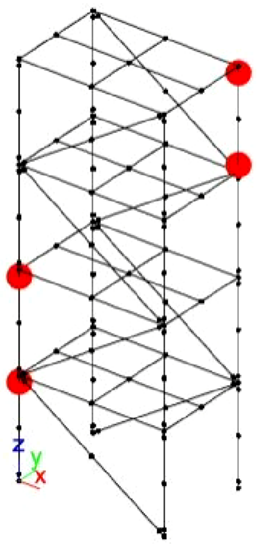

Fig. 33 – EFI sensor placement (*y*-direction, 3D).

The optimization was conducted using the first four vibration modes in the y-direction and the three vibration modes previously selected for the 3D y-direction analysis. The results demonstrate a well-distributed sensor placement.

The optimized sensors are located on nodes belonging to the rigid elements, with two of them positioned on opposite sides of the structure. The spatial distribution ensures effective coverage and good modal observability. This configuration is consistent with the results obtained in the 2D analysis, confirming the robustness of the method.

The graph in Fig. 34 shows the evolution of EFI values throughout the iterations of sensor removal in the y-direction.

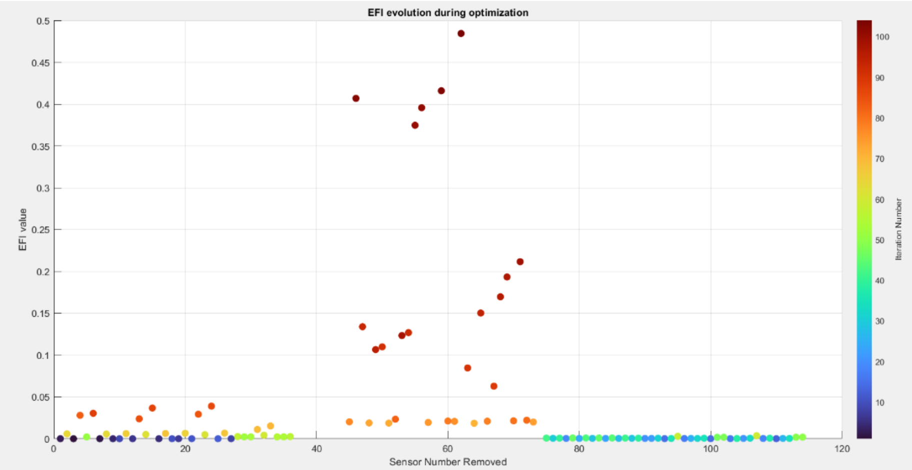

Fig. 34 – Evolution of EFI values throughout the iterations of sensor removal (3D, y-direction).

Fig. 35 represents the removal of sensors by iteration with EFI method in a 3D analysis in the y-direction.

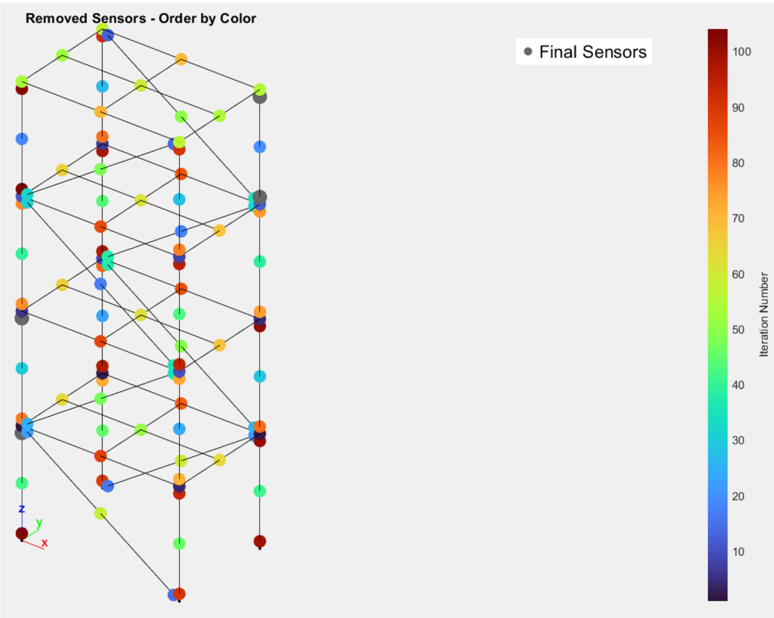

Fig. 35 – Removal of sensors by iteration with EFI method in a 3D analysis (y-direction).

During the deselection process of sensors in the 3D EFI optimization along the *y*-direction, the sensors located in the corners of the plates were the first to be removed, followed by those on the diagonals. As the iterations progressed, the last remaining sensors were those placed on rigid structural elements, indicating their higher informational contribution to the mode shapes.

The AutoMAC matrix was plotted to evaluate the effectiveness of the optimization and to assess the level of correlation between the selected sensors (Fig. 36).

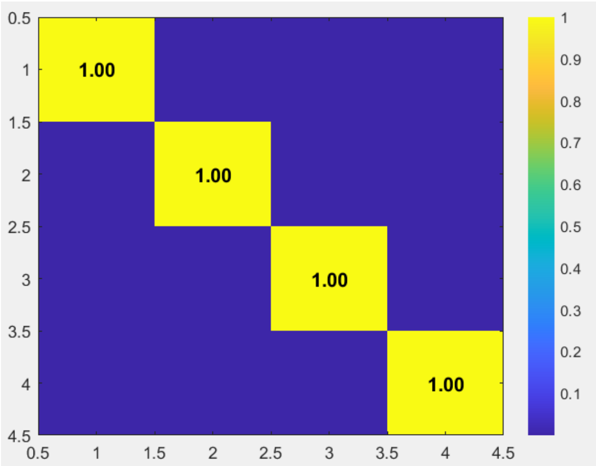

Fig. 36 – AutoMAC matrix (EFI, *y*-direction, 3D).

The AutoMAC results demonstrate excellent sensor independence, with values of 1.0 along the diagonal and values close to zero in the off-diagonal elements. This indicates that the selected sensors are highly uncorrelated and individually contribute to the accurate identification of the structural vibration modes. These results confirm the robustness and effectiveness of the EFI optimization in the *y*-direction of the 3D model.

5.1.2.3. Information Entropy Index Method (IEI)

The resultant sensor placements from the optimization using the IEI method, considering the degrees of freedom in the *y*-direction, are presented in Fig. 37.

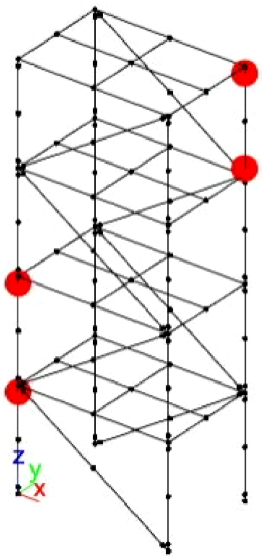

Fig. 37 – IEI sensor placement (*y*-direction, 3D).

The four optimized sensors obtained with the IEI method in the *y*-direction are exactly the same as those obtained with the EFI method in both 2D and 3D analyses. This result is expected, as both methods are based on the Fisher Information Matrix (FIM) and the Covariance Matrix, which explains the identical sensor configurations.

The graph in Fig. 38 shows the evolution of IE values throughout the iterations of sensor removal in the *y*-direction.

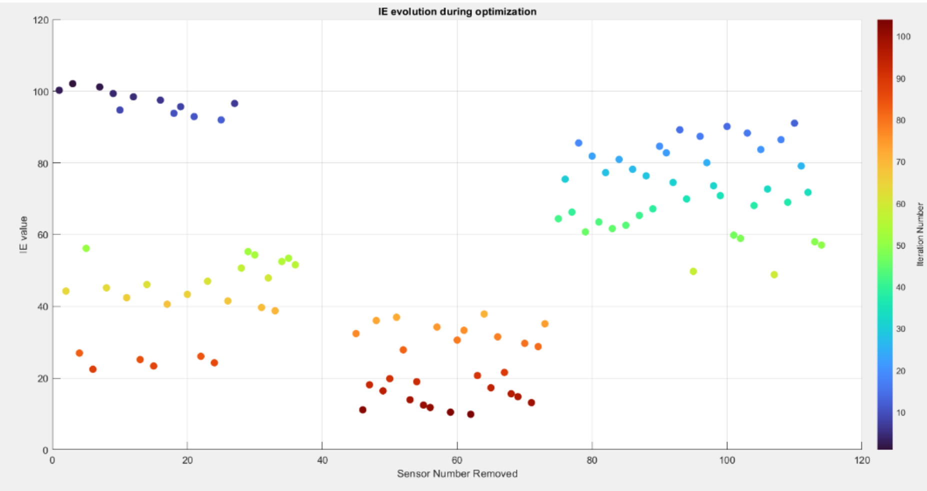

Fig. 38 – Evolution of IE values throughout the iterations of sensor removal (3D, *y*-direction).

Fig. 39 represents the removal of sensors by iteration with IE method in a 3D analysis in the *y*-direction.

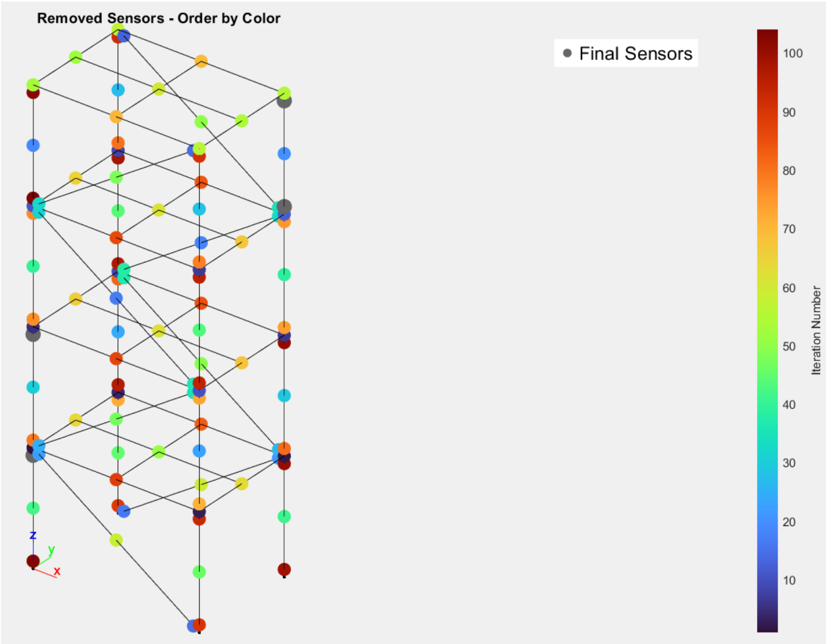

Fig. 39 – Removal of sensors by iteration with IE method in a 3D analysis (*y*-direction).

When comparing the deselection of sensors in the Fig. 38 and Fig. 39, the process is not exactly the same in the initial iterations, occasionally differing by the removal of sensors on the opposite side of the structure, with only minor variations. However, from approximately one-third of the optimization process onward, the deselection sequence becomes identical, leading to exactly the same final results.

The AutoMAC matrix was plotted to evaluate the optimization and to assess the level of correlation between the selected sensors (Fig. 40).

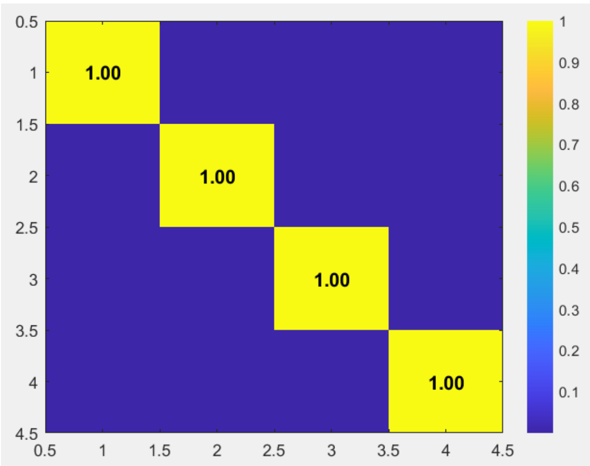

Fig. 40 – AutoMAC matrix (IEI, *y*-direction, 3D).

The AutoMAC matrix results are also exactly the same as those obtained with the EFI method, confirming that the selected sensors exhibit good independence from each other.

A comparison of the AutoMAC after each optimization, considering only the final selected sensors, with the AutoMAC prior to optimization, where all possible sensor locations were initially included, revealed no significant differences in a 3D analysis, as shown in Fig. 41.

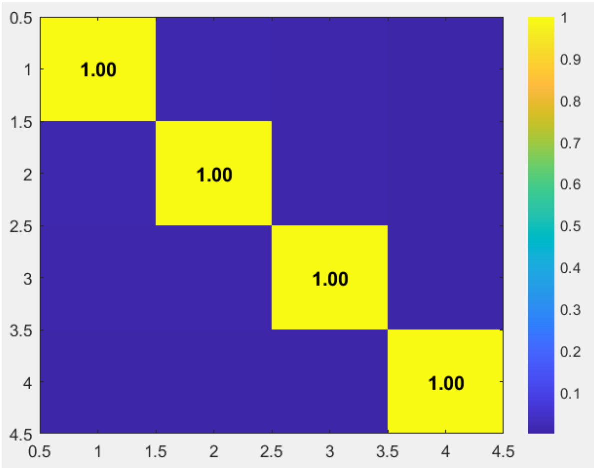

Fig. 41 – AutoMAC matrix without optimization of sensor placements (3D analysis).

5.2. Experimental

5.2.1. Modal Kinetic Energy Method (MKE)

The sensor configuration used in the experimental tests was optimized using the same three methods applied previously, now considering both the Finite Element Model (FEM) and the experimental setup.

The optimization in the *y*-direction was first applied to the sensors present in the FEM, using the Modal Kinetic Energy (MKE) method. The resulting optimal sensor locations are shown in Fig. 42.

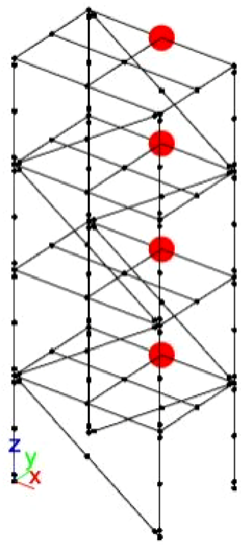

Fig. 42 – Optimal sensor placement using MKE in the *y*-direction (FEM).

The sensor set was reduced to four locations, based on the number of vibration modes identified in the *y*-direction from the experimental data.

The four optimized sensors selected by the MKE method are all located at the midpoint of each floor, on the plane defined by y = 0.4 m. This distribution reflects the concentration of modal energy in this area for the bending modes in the *y*-direction.

The graph in Fig. 43 shows the evolution of MKE values during the iterative sensor removal process, applied to the FEM-based degrees of freedom (DOFs) in the *y*-direction.

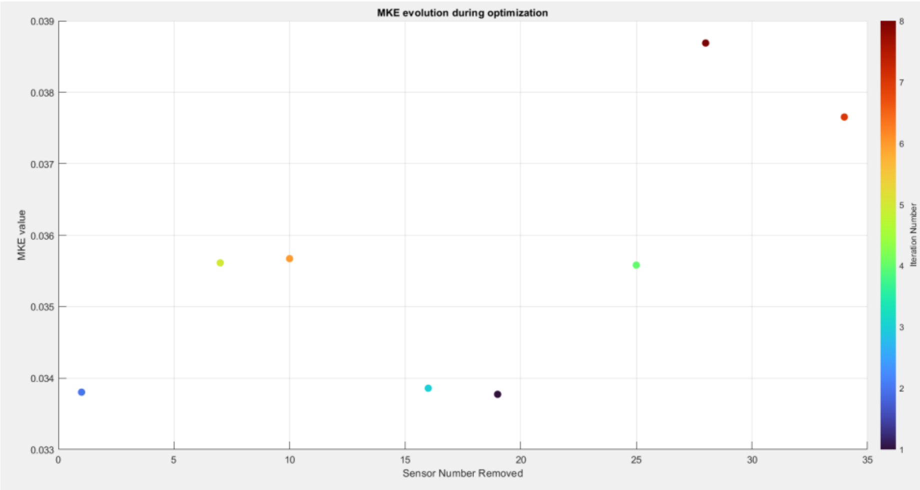

Fig. 43 – Evolution of MKE values throughout the iterations of sensor removal (3D, *y*-direction, FEM).

Fig. 44 represents the removal of sensors by iteration with MKE method in a 3D analysis applied to the FEM-based degrees of freedom (DOFs) in the *y*-direction.

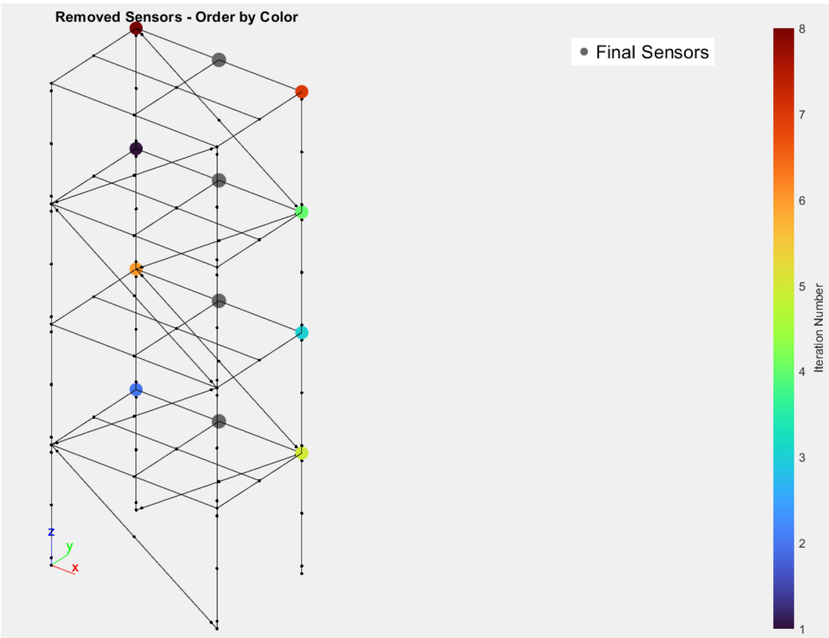

Fig. 44 – Removal of sensors by iteration with MKE method in a 3D analysis (*y*-direction, FEM).

The optimization procedure was applied in the same way to the sensors corresponding to the experimental test configuration. The resulting sensor layout from the MKE-based optimization, considering the degrees of freedom in the y-direction from the experimental setup, is presented in Fig. 45.

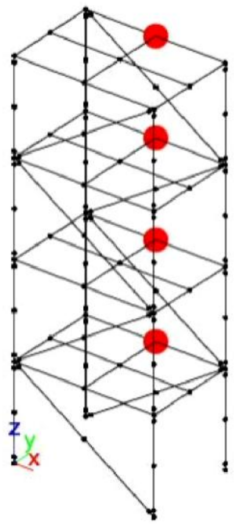

Fig. 45 – Optimal sensor placement using MKE in the y-direction (experimental tests).

The four optimized sensors obtained through the MKE method coincided with those identified in the FEM-based optimization and with the actual sensor positions used in the experimental campaign. The number of sensors was reduced to four to match the number of identified vibration modes in the y-direction. All selected sensors were located at the center of each floor, along the plane y = 0.4 m, demonstrating strong agreement between the model-based and experimental-based optimization outcomes.

The graph in Fig. 46 shows the evolution of MKE values throughout the iterations of sensor removal for the experimental setup in the y-direction.

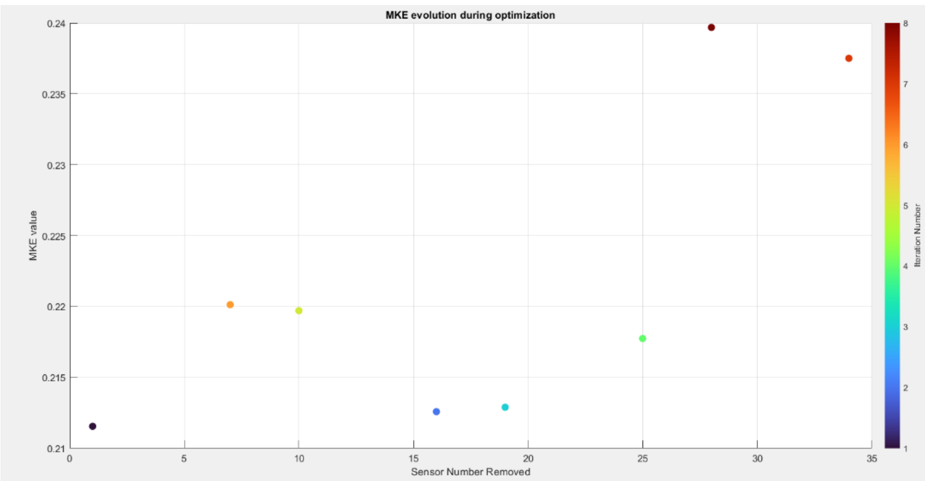

Fig. 46 – Evolution of MKE values throughout the iterations of sensor removal (3D, y-direction, experimental tests).

Fig. 47 represents the removal of sensors by iteration with MKE method in a 3D analysis applied to the experimental setup in the *y*-direction.

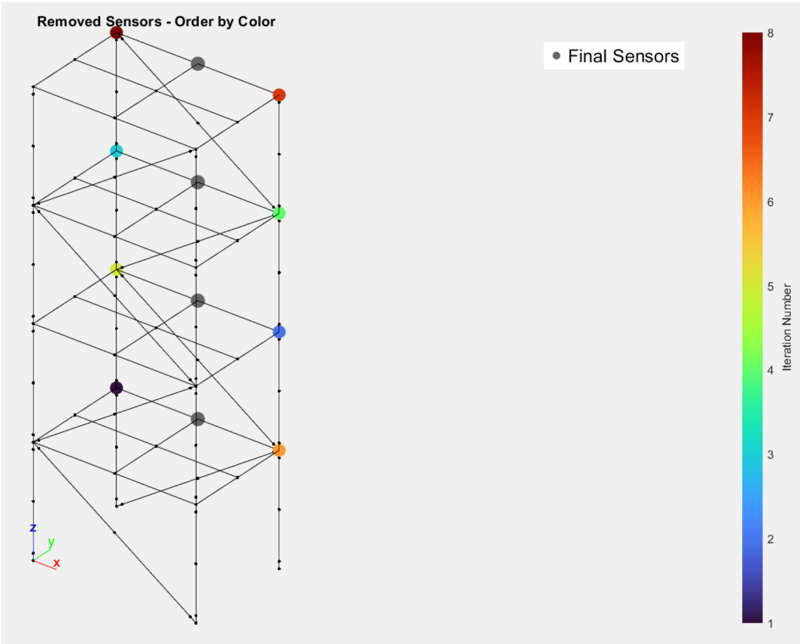

Fig. 47 – Removal of sensors by iteration with MKE method in a 3D analysis (*y*-direction, experimental tests).

Comparing the two optimization in Fig. 46 and Fig. 47, the sequence of sensor removal differs slightly between the FEM and the experimental setup. However, the final optimal sensor configurations are the same in both cases. This highlights the inherent differences between numerical and experimental models, yet also confirms the robustness of the optimization method.

The MAC matrix was computed to evaluate the correlation between the optimized sensor configurations obtained from the FEM and from the experimental setup in the *y*-direction using the MKE method (Fig. 48).

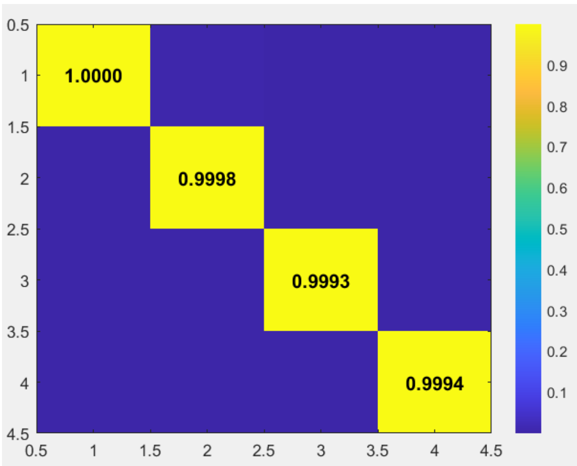

Fig. 48 – MAC matrix comparing MKE sensor configurations (model vs. experiment) – *y*-direction.

The results demonstrate a perfect correlation between the two configurations, confirming that the optimization performed on the numerical model is highly representative of the real structure for the first four vibration modes.

5.2.2. Effective Independence Method (EFI)

The sensors used in the experimental tests were optimized using the EFI method. The first optimization was carried out for the *y*-direction based on the sensors represented in the finite element model. The resulting sensor configuration obtained from the EFI method with degrees of freedom in the *y*-direction is shown in Fig. 49.

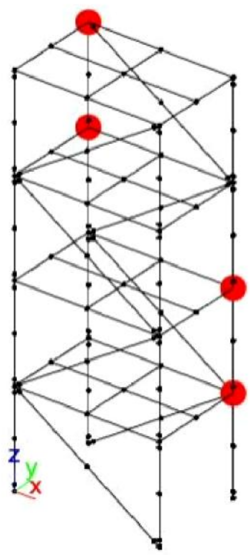

Fig. 49 – Optimal sensor placement using EFI in the *y*-direction (FEM).

The four optimized sensor locations are distributed at the corners of the structure: two on the first and second floors, and the remaining two on the third and fourth floors, placed on the opposite side of the plan at coordinate $y = 0.4$ m.

The graph in Fig. 50 illustrates the evolution of EFI values throughout the sensor removal process for the degrees of freedom defined in the finite element model in the *y*-direction.

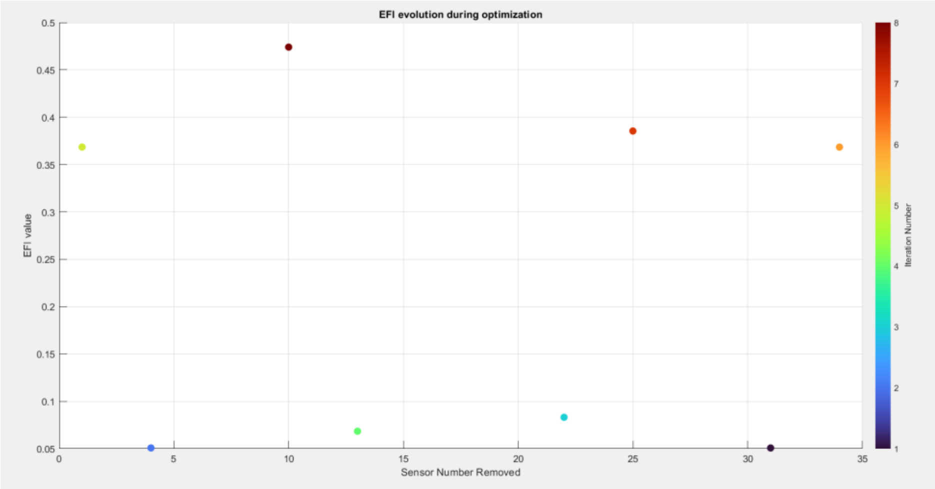

Fig. 50 – Evolution of EFI values throughout the iterations of sensor removal (3D, *y*-direction, FEM).

Fig. 51 represents the removal of sensors by iteration with EFI method in a 3D analysis applied to the FEM-based degrees of freedom (DOFs) in the *y*-direction.

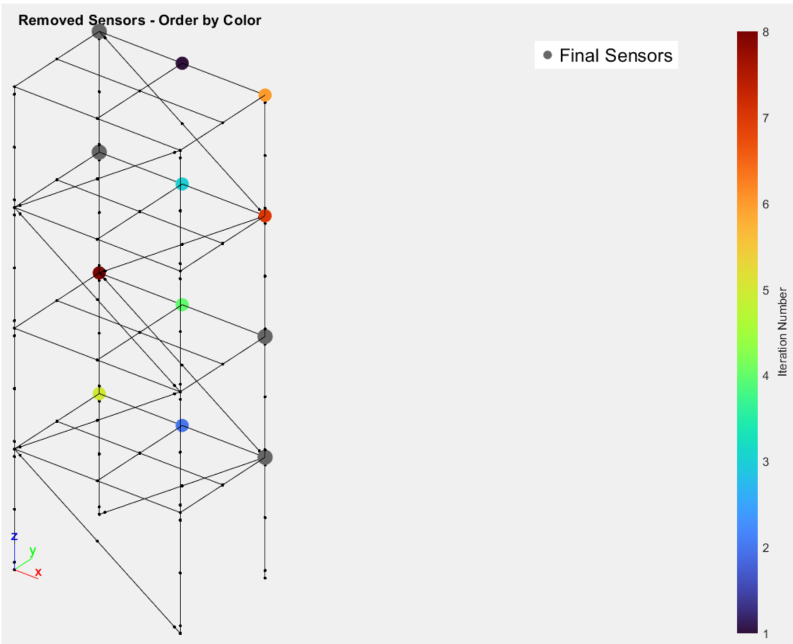

Fig. 51 – Removal of sensors by iteration with EFI method in a 3D analysis (*y*-direction, FEM).

The optimization was also applied to the sensors with the characteristics of the experimental setup. The sensors optimized using the EFI method, based on the degrees of freedom in the *y*-direction from the experimental tests, are shown in Fig. 52.

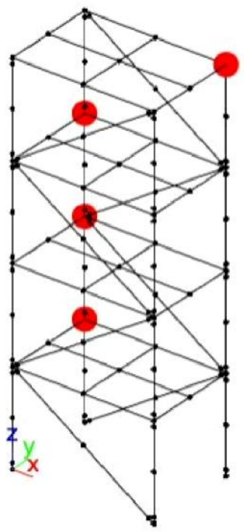

Fig. 52 – Optimal sensor placement using EFI in the *y*-direction (experimental tests).

The four optimized sensors obtained from the EFI method in the experimental setup are located at the corners of the floors, three on one side and one on the opposite side, on the plane with coordinate y = 0.4 m.

The graph in Fig. 53 shows the evolution of EFI values throughout the sensor removal iterations for the experimental setup in the *y*-direction.

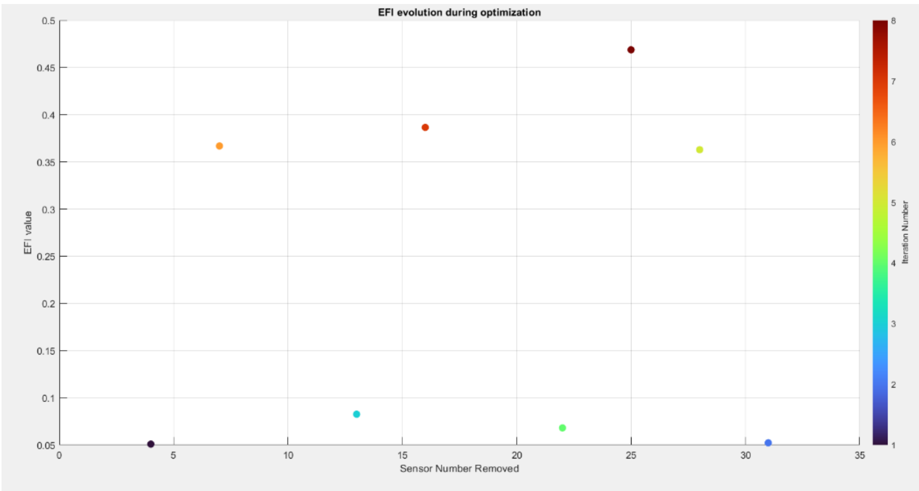

Fig. 53 – Evolution of EFI values throughout the iterations of sensor removal (3D, *y*-direction, experimental tests).

Fig. 54 represents the removal of sensors by iteration with EFI method in a 3D analysis applied to the experimental setup in the *y*-direction.

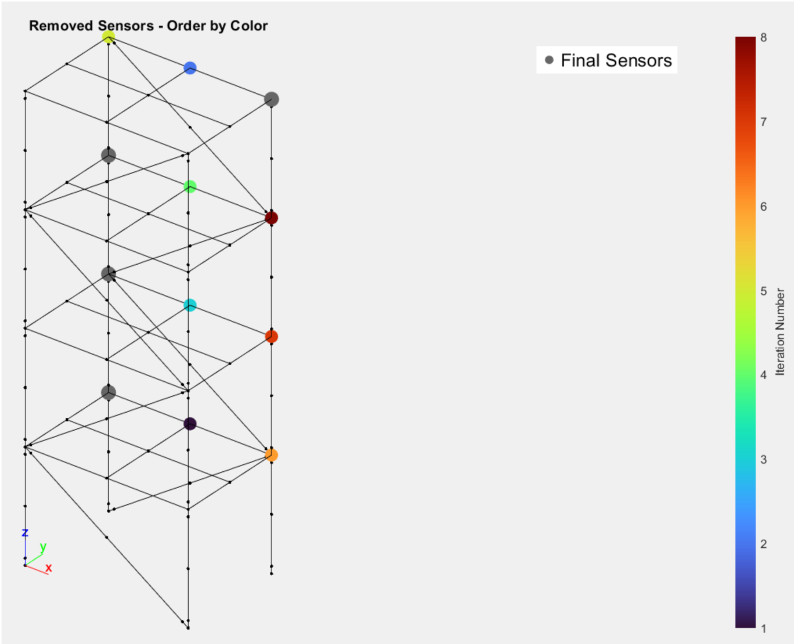

Fig. 54 – Removal of sensors by iteration with EFI method in a 3D analysis (*y*-direction, experimental tests).

For the EFI method in the *y*-direction, the resulting sensor configurations differ between the FEM and experimental setups, as does the sensor removal sequence observed in the optimization animation in Fig. 54. In the FEM setup, the four sensors were placed at the floor corners, two on the first and second floors, and two on the third and fourth floors on the opposite side, along the plane at $y = 0.4$ m. In the experimental setup, three sensors were positioned on one side of the structure and the fourth on the opposite side, also along the $y = 0.4$ m plane.

The MAC matrix was generated to compare the correlation between the optimized sensor configurations in the FEM and experimental setups. The results are presented in Fig. 55.

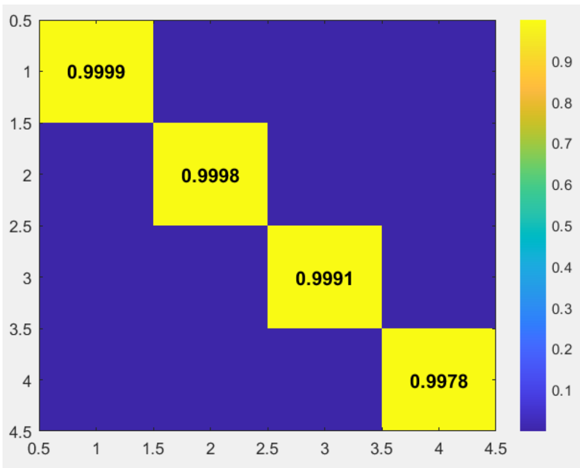

Fig. 55 – MAC matrix comparing EFI sensor configurations (model vs. experiment) – *y*-direction.

The MAC matrix reveals good correlation between the vibration modes obtained from the model and those from the experimental test setup, indicating that the sensor placement strategy was effective across both domains.

5.2.3. Information Entropy Method (IEI)

The sensors used in the experimental tests were optimized using the IEI method. First, the optimization was carried out in the *y*-direction for the sensors represented in the finite element model. The resulting sensor configuration from the optimization using the IEI method with degrees of freedom in the *y*-direction is shown in Fig. 56.

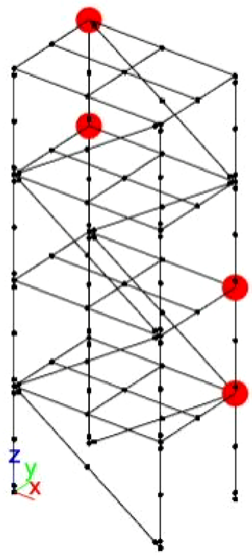

Fig. 56 – Optimal sensor placement using IEI in the *y*-direction (FEM).

The four optimized sensors obtained using the IEI method in the FEM model are positioned at the corners, two on the first and second floors, and the other two on the third and fourth floors but on the opposite side of the plan, at coordinate $y = 0.4$ m.

The graph in Fig. 57 shows the evolution of Information Entropy (IE) values throughout the iterations of sensor removal for the FEM-based degrees of freedom in the *y*-direction.

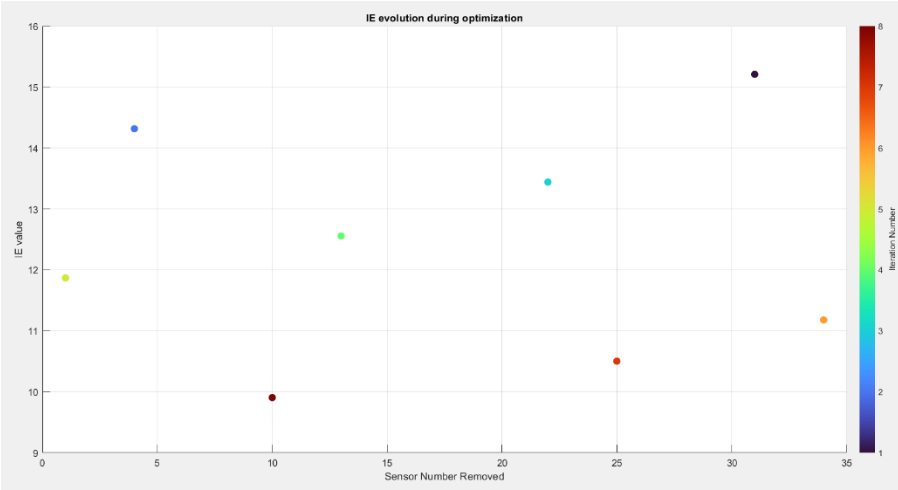

Fig. 57 – Evolution of IE values throughout the iterations of sensor removal (3D, *y*-direction, FEM).

Fig. 58 represents the removal of sensors by iteration with IE method in a 3D analysis applied to the FEM-based degrees of freedom (DOFs) in the *y*-direction.

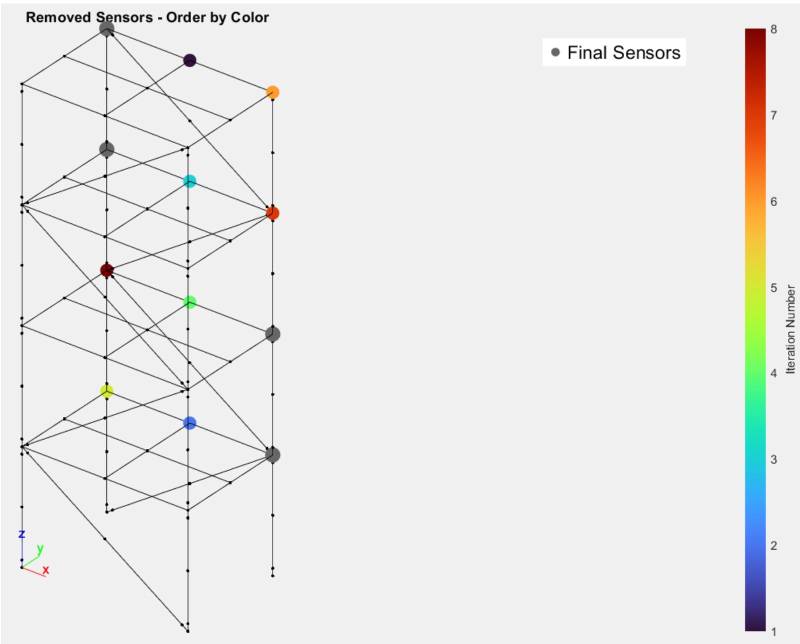

Fig. 58 – Removal of sensors by iteration with IE method in a 3D analysis (*y*-direction, FEM).

The optimization was performed in the same way for the sensors used in the experimental tests. The resulting sensors from the optimization using the IEI method with degrees of freedom in the *y*-direction for the experimental setup are presented in the Fig. 59:

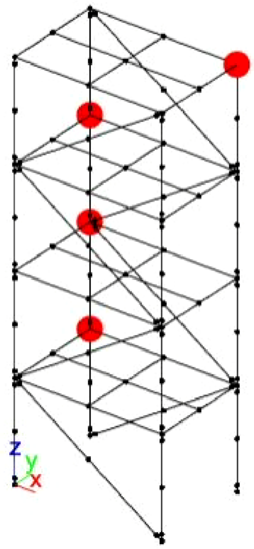

Fig. 59 – Optimal sensor placement using IEI in the *y*-direction (experimental tests).

The four optimized sensors obtained through the IEI method in the experimental setup are located at the corners of the structure, three on one side and the remaining one on the opposite side, along the plane with coordinate $y = 0.4$ m.

The graph in Fig. 60 shows the evolution of IEI values throughout the iterations of sensor removal for the experimental setup in the *y*-direction.

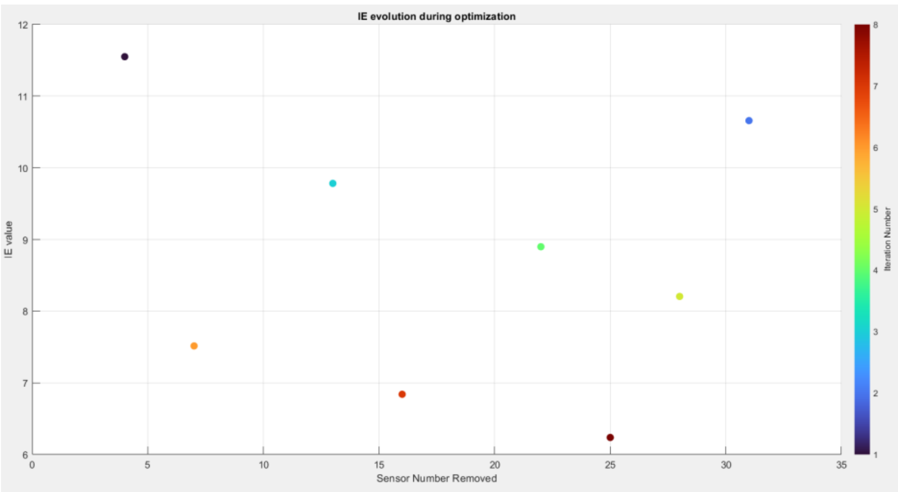

Fig. 60 – Evolution of IE values throughout the iterations of sensor removal (3D, *y*-direction, experimental tests).

Fig. 61 represents the removal of sensors by iteration with IE method in a 3D analysis applied to the experimental setup in the *y*-direction.

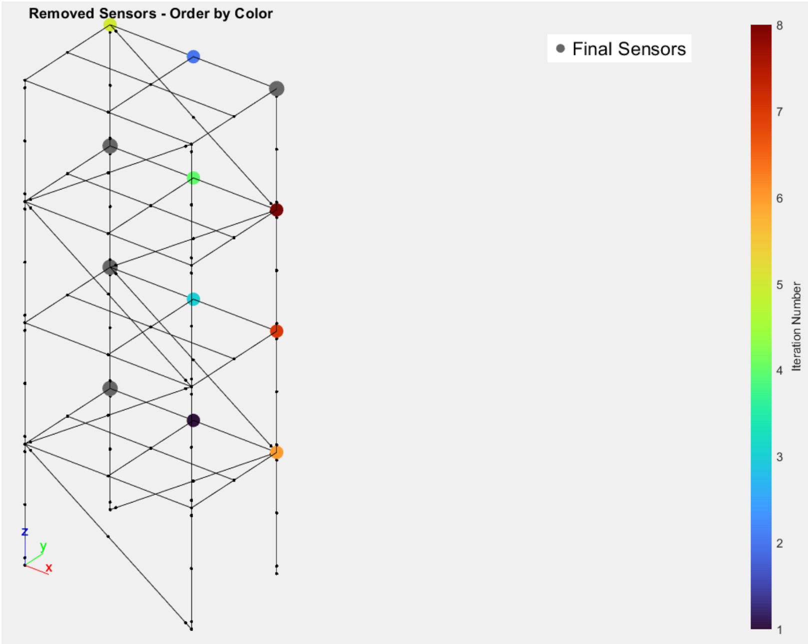

Fig. 61 – Removal of sensors by iteration with IE method in a 3D analysis (*y*-direction, experimental tests).

The MAC matrix was computed to evaluate the correlation between the two optimizations, and the result is shown in Fig. 62.

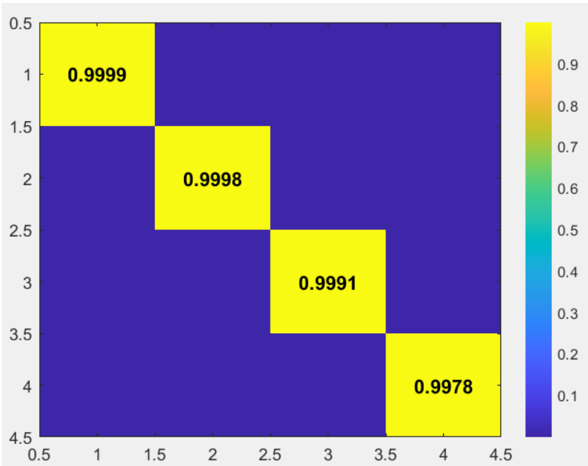

Fig. 62 – MAC matrix comparing IEI sensor configurations (model vs. experiment) – *y*-direction.

The results demonstrate a good correlation between the optimized sensor placements in both setups.

For the IEI method, the optimal sensor placement results, for both the FEM and experimental setups, are identical, as confirmed by the MAC matrix. Given the limited number of optimized sensors, a comparison of the optimization animations for EFI and IEI methods reveals that the deselection sequence is exactly the same. This indicates that both methods exhibit identical behavior, despite differences in the values throughout the iterations. In this context, the methods can be considered proportional to each other.

A comparison of the MAC matrix after each optimization, considering only the final selected sensors, with the MAC matrix prior to optimization, where all possible sensor locations were initially included, revealed no significant differences, as shown in Fig. 63.

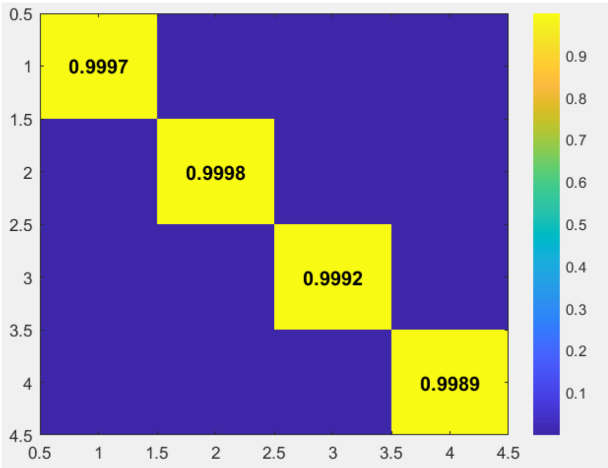

Fig. 63 – MAC matrix without optimization of sensor placements (model vs. experiment).

5.3. Comparison of the methods

The optimization of sensor location for each method was coherently evaluated. The sensor placements obtained by the MKE method consistently differ from those of the EFI and IEI methods because MKE considers the modal kinetic energy (related to the mass of the nodes) but does not take into account the Fisher Information Matrix or the Covariance Matrix, which are fundamental in EFI and IEI approaches.

Between the other two methods, EFI and IEI, although the optimization results are often identical and both are based on the Fisher Information Matrix and the Covariance Matrix, there are instances, especially when more degrees of freedom (DOFs) are considered, where the methods do not behave exactly the same. This indicates a subtle difference between them that is sometimes not easily noticeable.

It is important to note that the IEI method requires significantly more computational capacity because it removes sensors one by one, evaluating the performance after each removal to select the best option, and repeats this process until reaching the target number of sensors. In contrast, the EFI method simply calculates sensor importance and removes the sensor with the lowest value (i.e., the least important) at each iteration, making it computationally more efficient.

From this, it can be concluded that for large-scale structures with more complex vibration modes, the EFI method is the most practical choice for optimal sensor placement due to its computational efficiency. The IEI method, despite its higher computational cost, can be used as a benchmark to compare and validate the results obtained by EFI.

For small structures with simple vibration modes, the MKE method can be used since it is much simpler, does not require iterations, and is not based on the Fisher Information Matrix or Covariance Matrix. Consequently, it delivers different results but demands significantly less computational capacity.

6
IMPACT OF SENSOR QUANTITY

To demonstrate the necessity of using an optimized number of sensors at least equal to the number of vibration modes considered, several evaluations and tests were conducted. These analyses reveal the errors and inconsistencies that arise when this condition is not met.

For this study, the analysis was carried out in the 2D plane at $x = 0.6$ m, considering degrees of freedom in the y-direction, using each of the three previously studied methods (MKE, EFI, and IEI).

Firstly, the optimization was performed down to a single sensor to identify the most informative one, analyzing the sensor removal process while considering all four vibration modes.

The Fig. 64 presents the optimal sensor location identified by each method when limited to a single sensor, considering four vibration modes.

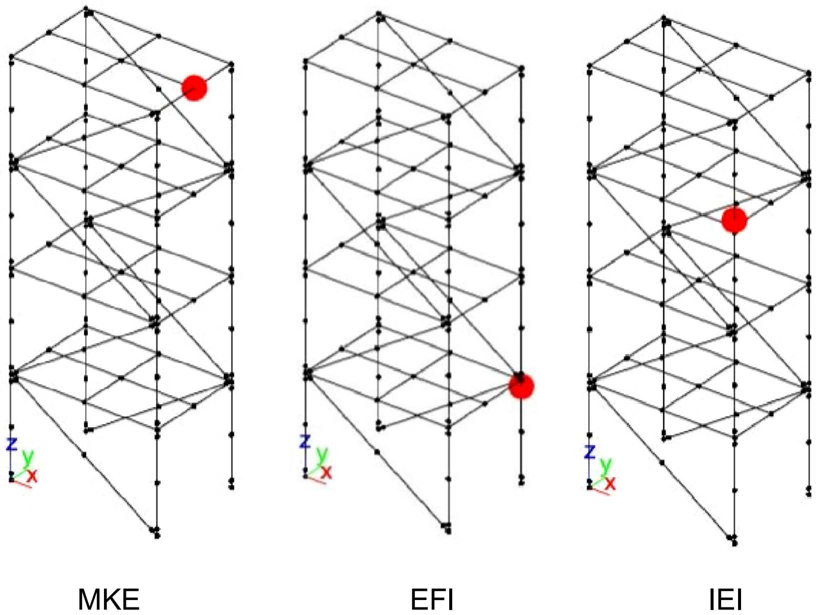

Fig. 64 – Optimal sensor placement using a single sensor for each method (MKE, EFI, and IEI) based on four vibration modes.

As shown in the Fig. 64, the optimal sensor location for the MKE method is positioned on the top floor. In contrast, for the EFI and IEI methods, the optimal sensor is not placed in the same location, which differs from previous analyses where both methods consistently selected the same positions. This highlights that, despite the strong correlation between EFI and IEI, both relying on the Fisher Information Matrix and the Covariance Matrix, differences may still arise when only a single sensor is considered.

Next, the sensor removal process was analyzed. The Fig. 65 presents the graph showing the sensor removed at each iteration for all methods.

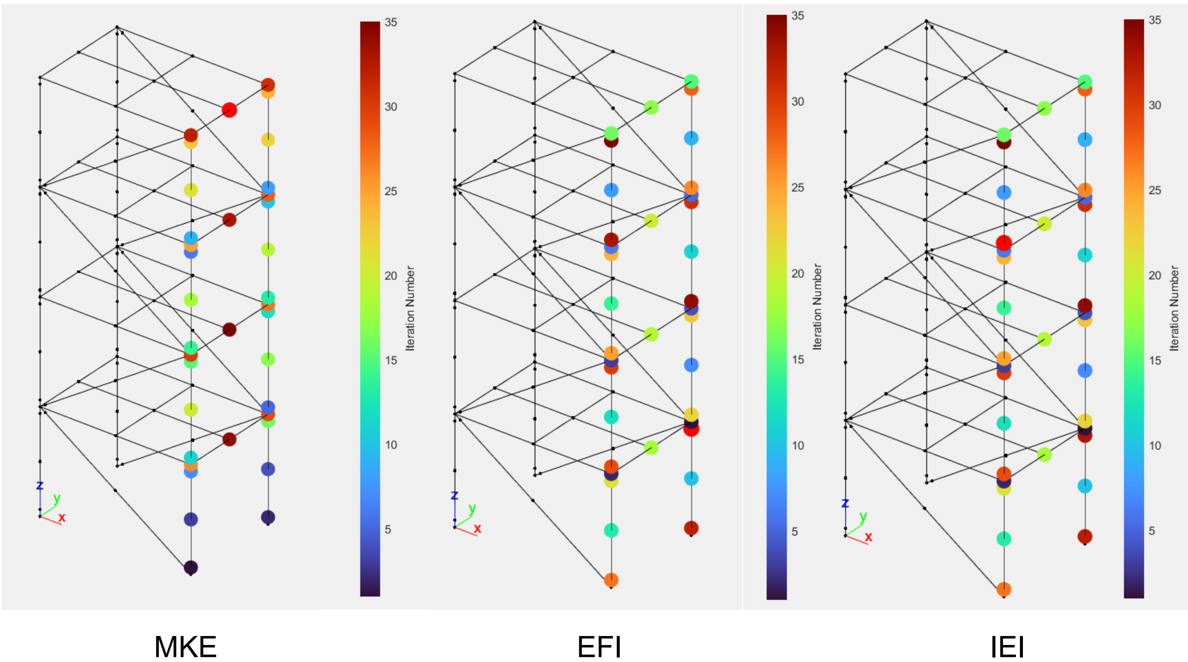

Fig. 65 – Sensor removal per iteration for the MKE, EFI, and IEI methods.

In the Fig. 65, it is possible to analyze the removal sequence of the last four sensors. To MKE method the sensor located on the second floor appears to be the second most influential, just before the final optimized sensor on the top floor. For the EFI and IEI methods, the differences in the selection of the last four sensors can be clearly observed, indicated by the different colors at the same positions, for example, on the upper rigid element of the third floor (left side) and on the lower rigid element of the first floor (right side). This behavior contrasts with the cases where the number of sensors is at least equal to the number of vibration modes, which leads to more consistent and coherent placement.

Next, the graphs showing the sensor removal values at each iteration were extracted for the three methods (Fig. 66).

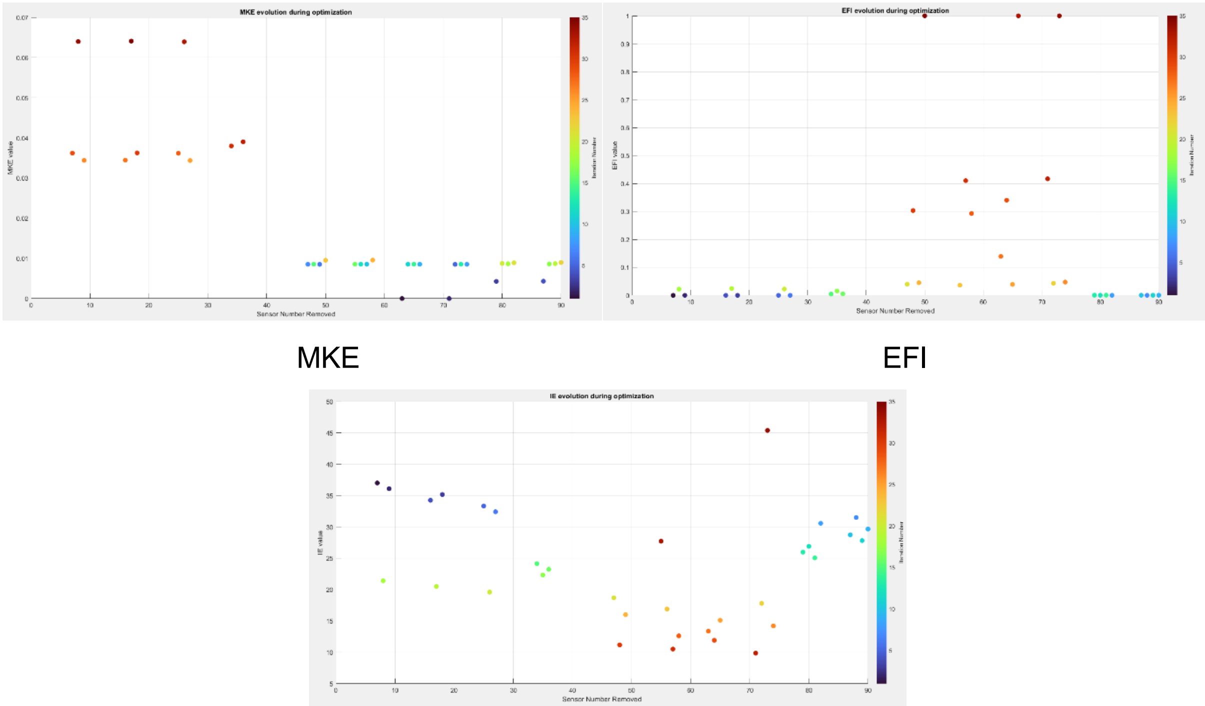

MKE EFI

IEI

Fig. 66 – Evolution of optimization values throughout the iterations for the MKE, EFI, and IEI methods.

From the graphs shown in Fig. 66, it is possible to observe the significance of the three sensors removed in each setup. The optimization values associated with these sensors vary considerably between methods, higher for the EFI and IEI methods, and lower for the MKE method. Notably, significant changes in the optimization metric only occur after the removal of the last four sensors, reinforcing the importance of maintaining at least as many sensors as vibration modes being analyzed.

Next, the AutoMAC results for each optimization were plotted, as shown in Fig. 67.

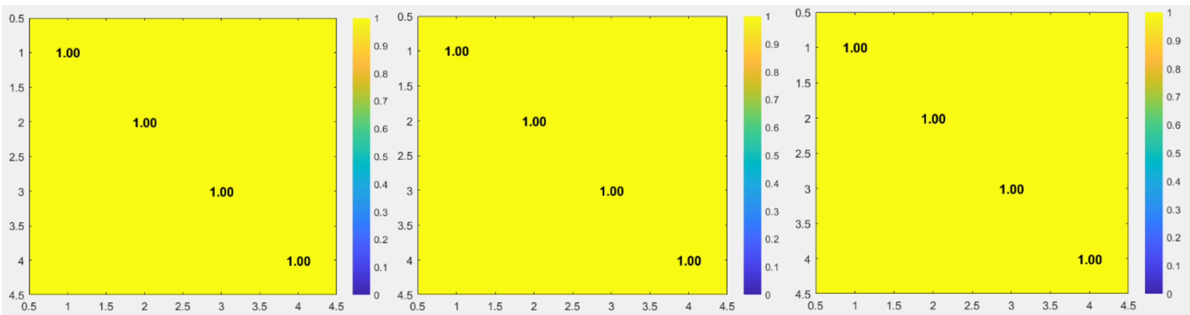

MKE EFI IEI

Fig. 67 – AutoMAC results for the MKE, EFI, and IEI methods using only one sensor.

As shown in Fig. 67, with only one sensor, the AutoMAC indicates that the vibration modes become highly correlated with each other, meaning that this number of sensors is insufficient to properly capture the structure's vibration modes.

Next, the AutoMAC was evaluated when selecting two and three sensors as the optimal number. Fig. 68 shows the AutoMAC results for each method with optimization up to two sensors.

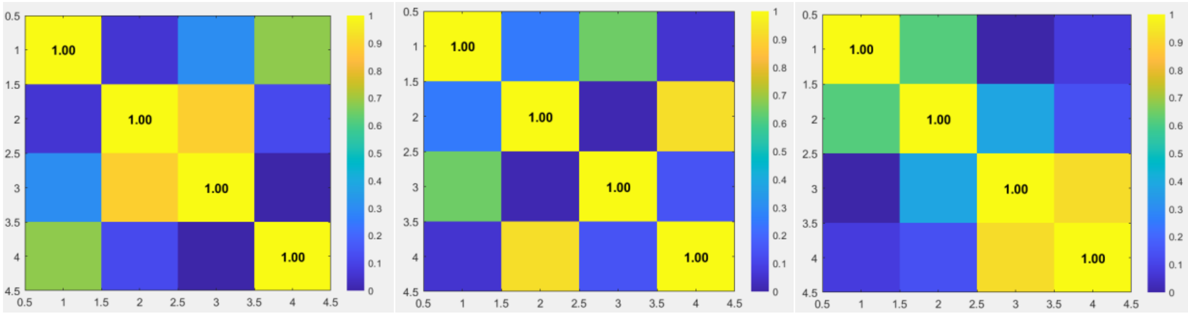

MKE EFI IEI

Fig. 68 – AutoMAC of the MKE, EFI, and IEI methods using two sensors.

As can be seen, the correlation between the vibration modes improves with two sensors but is still not as accurate or complete as with four sensors.

Fig. 69 shows the AutoMAC results for each method after optimizing with up to three sensors.

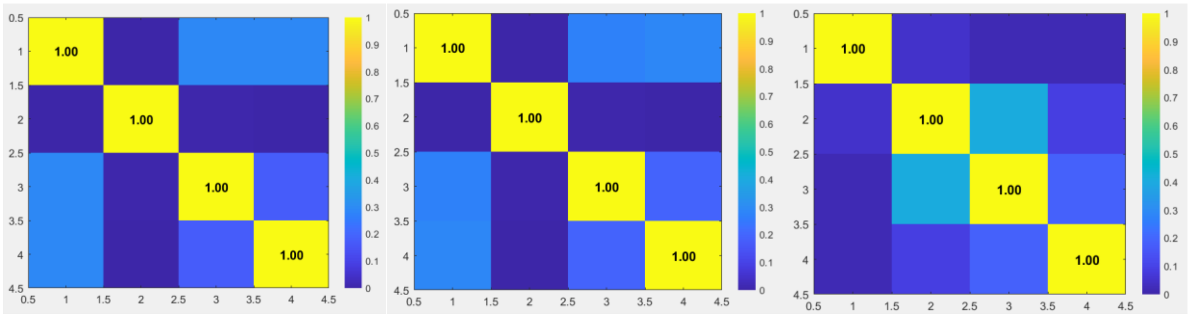

MKE EFI IEI

Fig. 69 – AutoMAC of the MKE, EFI, and IEI methods using three sensors.

The same conclusion drawn from the two sensors case applies here: while the correlation between vibration modes improves with three sensors, it still does not reach the accuracy and clarity achieved with four sensors.

Next, the optimal sensor placement was studied using only one sensor to capture a single vibration mode for each method, in order to demonstrate the importance of using a number of sensors at least equal to the number of vibration modes considered.

Firstly, the optimal sensor placements for capturing each vibration mode using the MKE method were studied. The results are shown in the following Fig. 70, Fig. 71, Fig. 72 and Fig. 73.

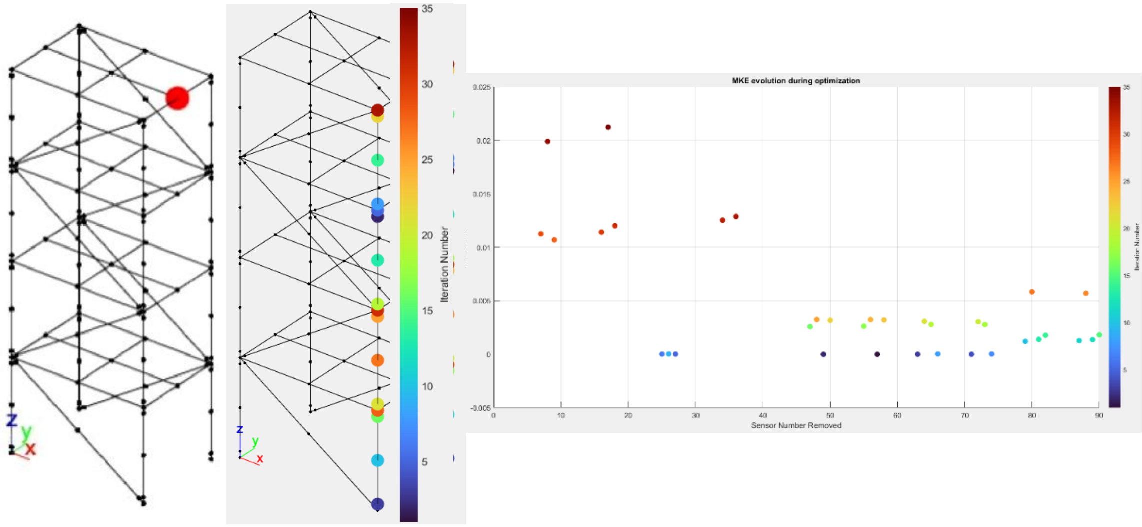

Fig. 70 – Optimal sensor placement for the first vibration mode using the MKE method.

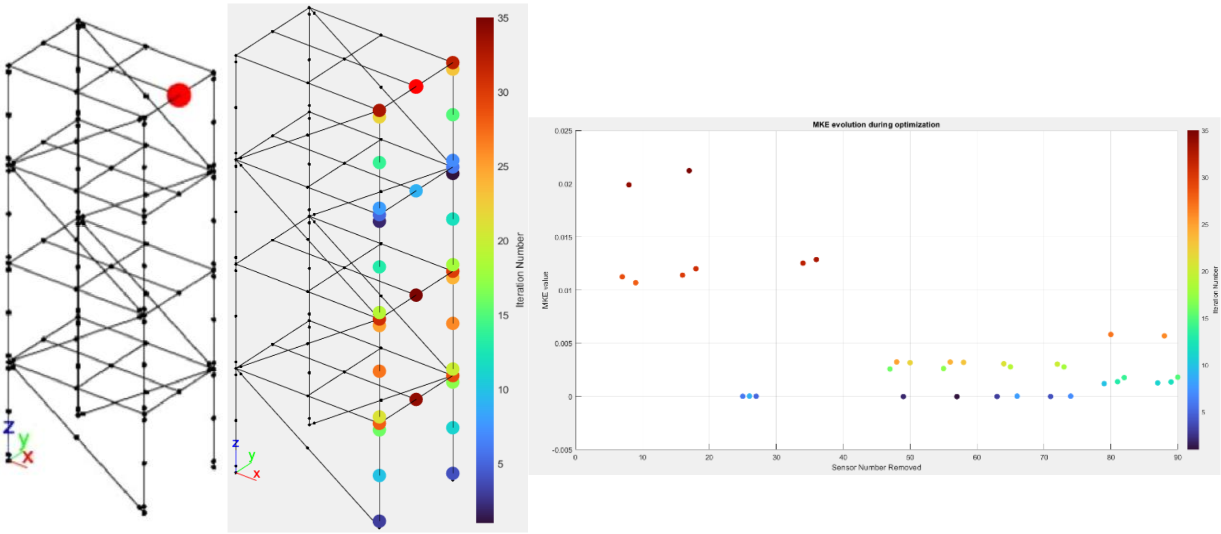

Fig. 71 – Optimal sensor placement for the second vibration mode using the MKE method.

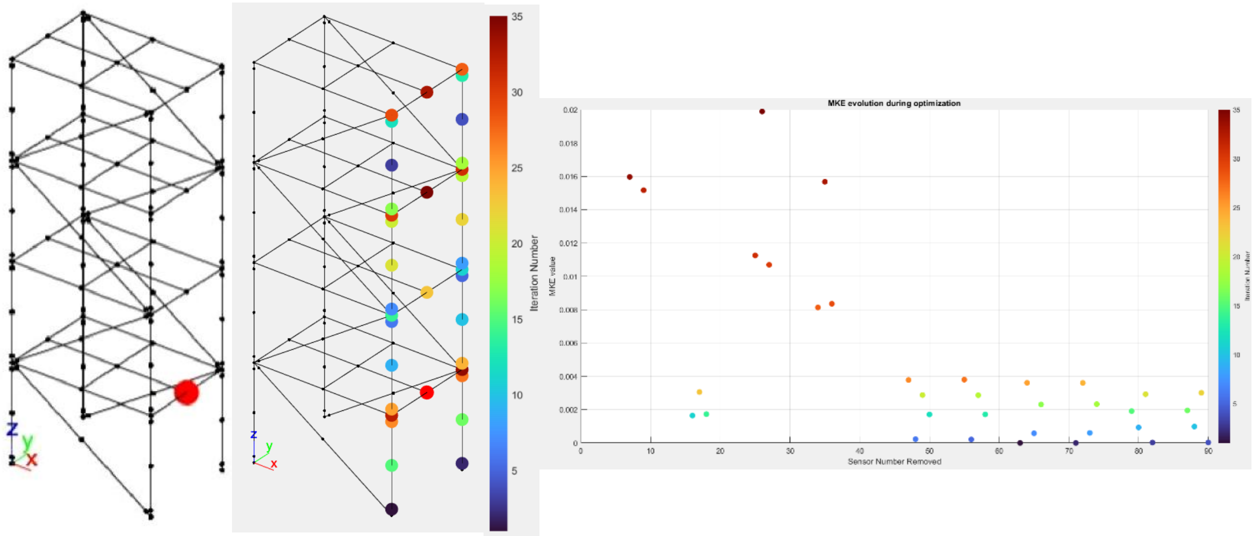

Fig. 72 – Optimal sensor placement for the third vibration mode using the MKE method.

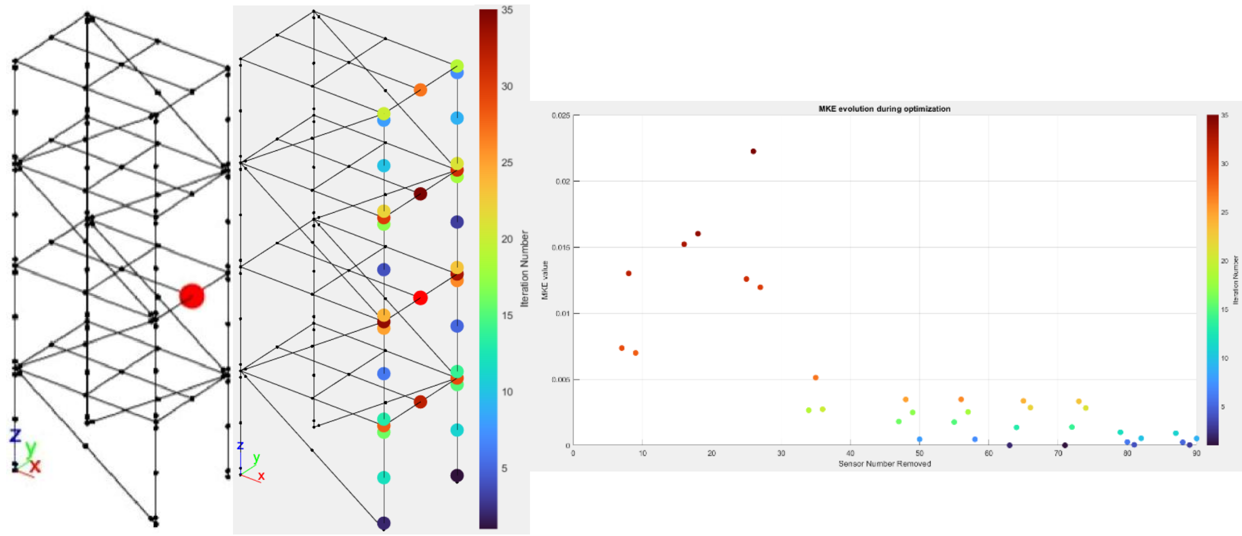

Fig. 73 – Optimal sensor placement for the fourth vibration mode using the MKE method.

With the MKE method optimizations performed for each vibration mode using only one sensor, it is possible to conclude that the optimal sensor placement depends on the specific vibration mode being extracted. For the first and second vibration modes, the sensor positions are the same, as is the sequence of sensor removals, although the iteration values are higher for the second mode. In contrast, the optimal sensor placements and removal sequences differ for the third and fourth vibration modes.

Then, the optimal sensor placements to capture each vibration mode using the EFI method were studied. The results are shown in Fig. 74, Fig. 75, Fig. 76 and Fig. 77.

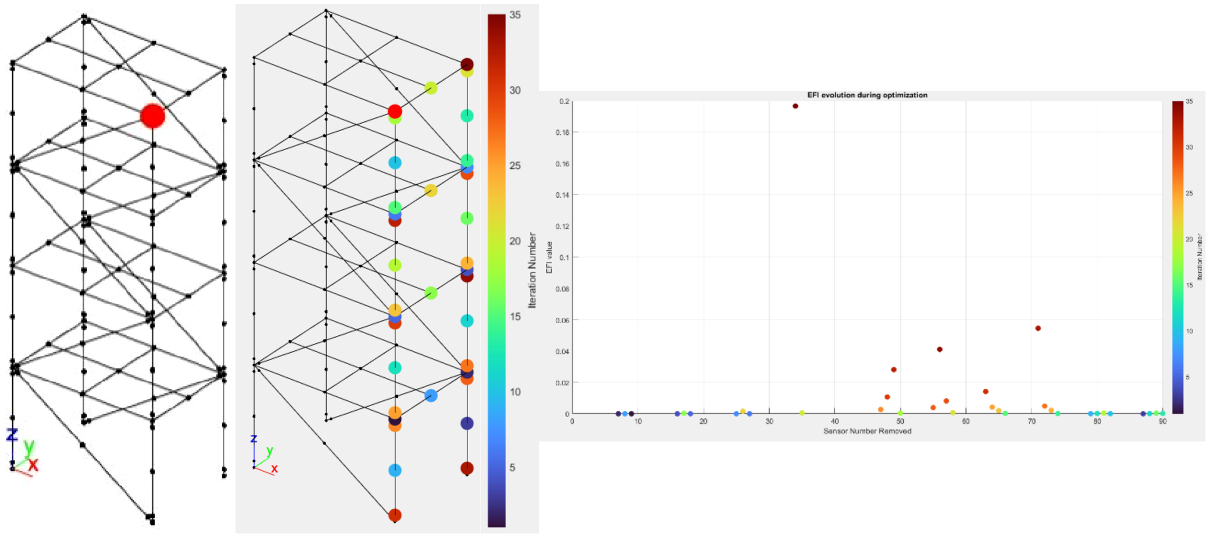

Fig. 74 – Optimal sensor placement for the first vibration mode using the EFI method.

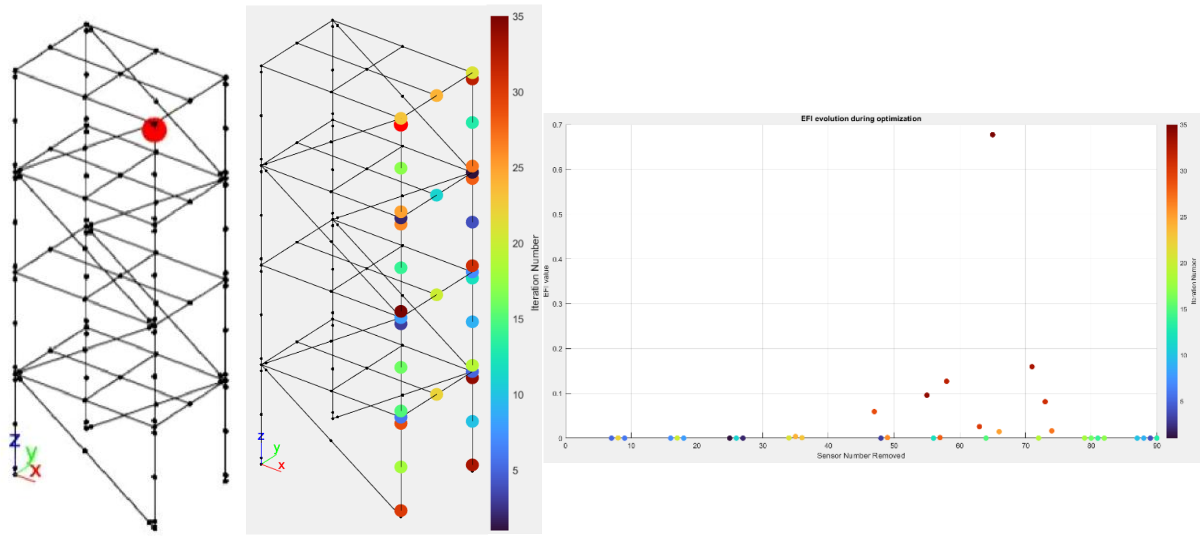

Fig. 75 – Optimal sensor placement for the second vibration mode using the EFI method.

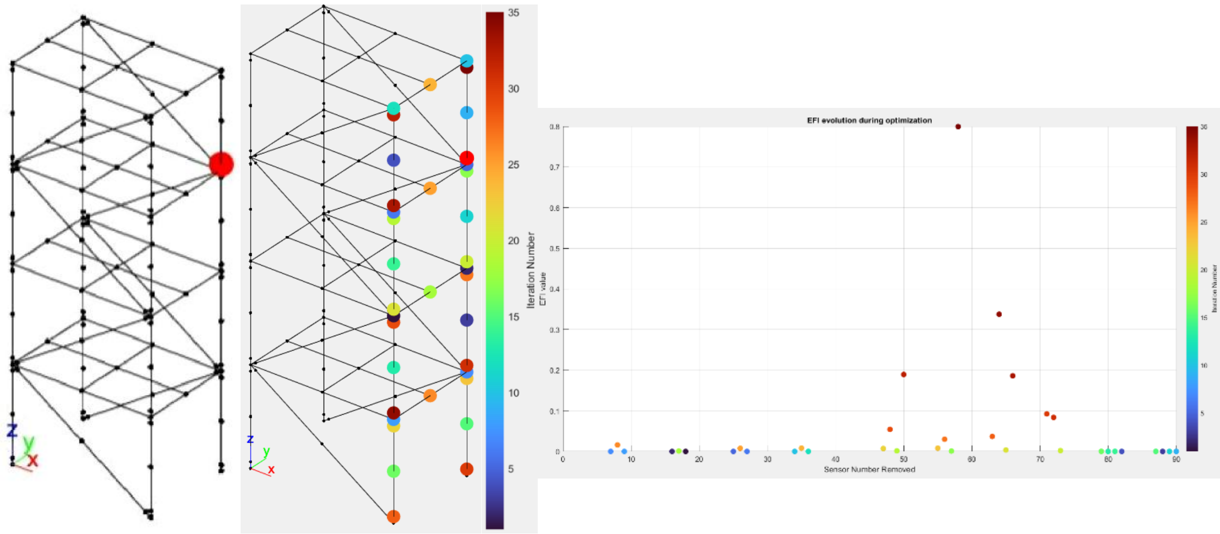

Fig. 76 – Optimal sensor placement for the third vibration mode using the EFI method.

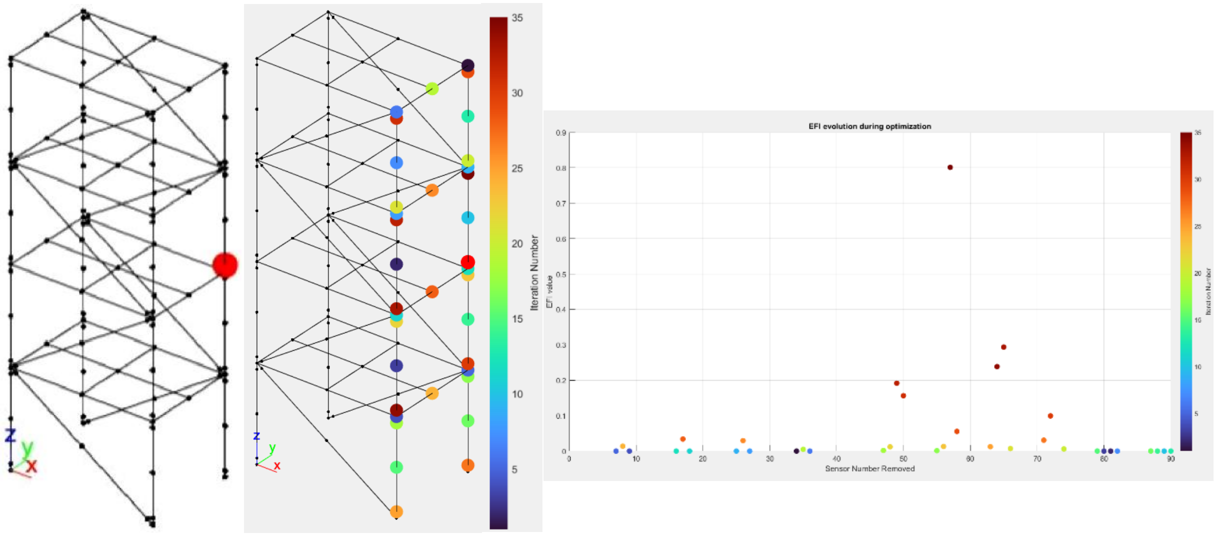

Fig. 77 – Optimal sensor placement for the fourth vibration mode using the EFI method.

With the EFI method optimizations for each vibration mode using just one sensor, it can be concluded that the optimal sensor positions vary for each mode. For the first and second vibration modes, the sensor positions are the same, but the sensor removal process differs. In these cases, it is clear that the last sensor to be removed holds a significantly high method value. For the third and fourth vibration modes, both the optimal sensor placements and the sensor removal sequences differ, again showing a noticeable difference in the value of the last sensor removed.

Next, the optimal sensor placements for capturing each vibration mode using the IEI method were studied, as shown in Fig. 78, Fig. 79, Fig. 80 and Fig. 81.

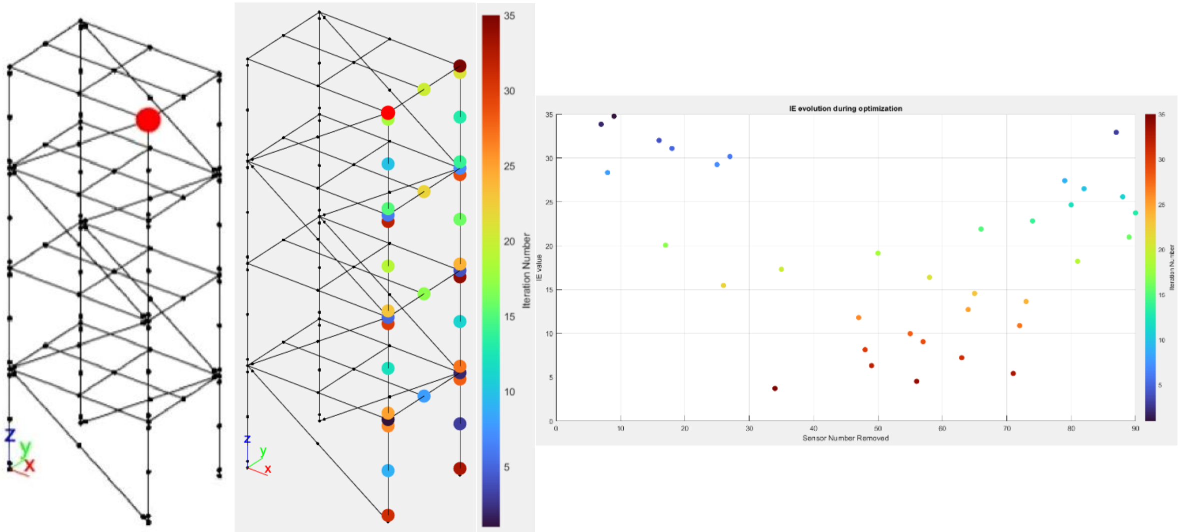

Fig. 78 – Optimal sensor placement for the first vibration mode using the IEI method.

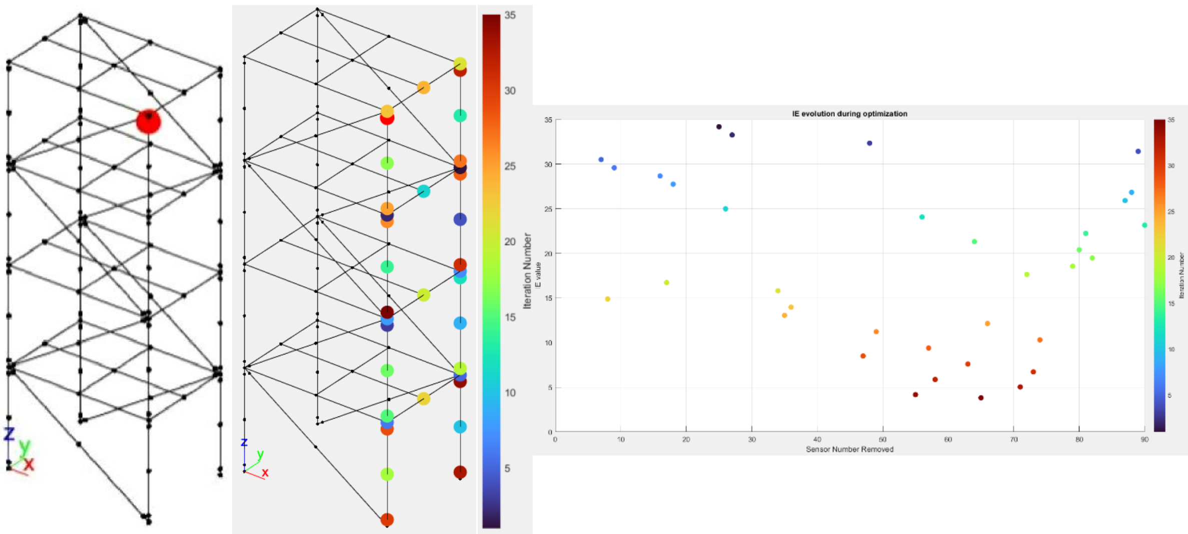

Fig. 79 – Optimal sensor placement for the second vibration mode using the IEI method.

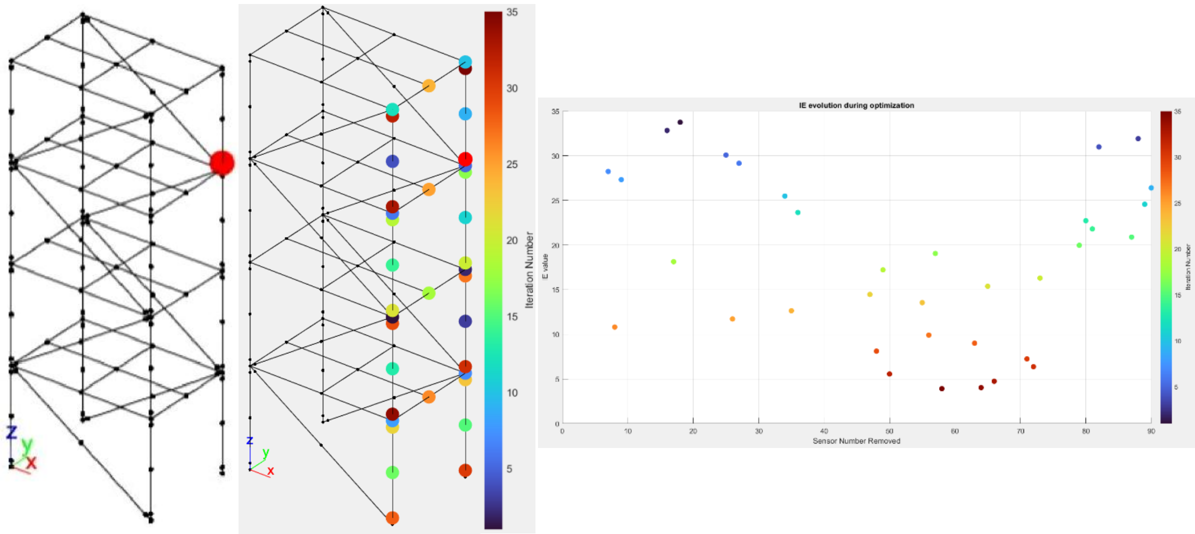

Fig. 80 – Optimal sensor placement for the third vibration mode using the IEI method.

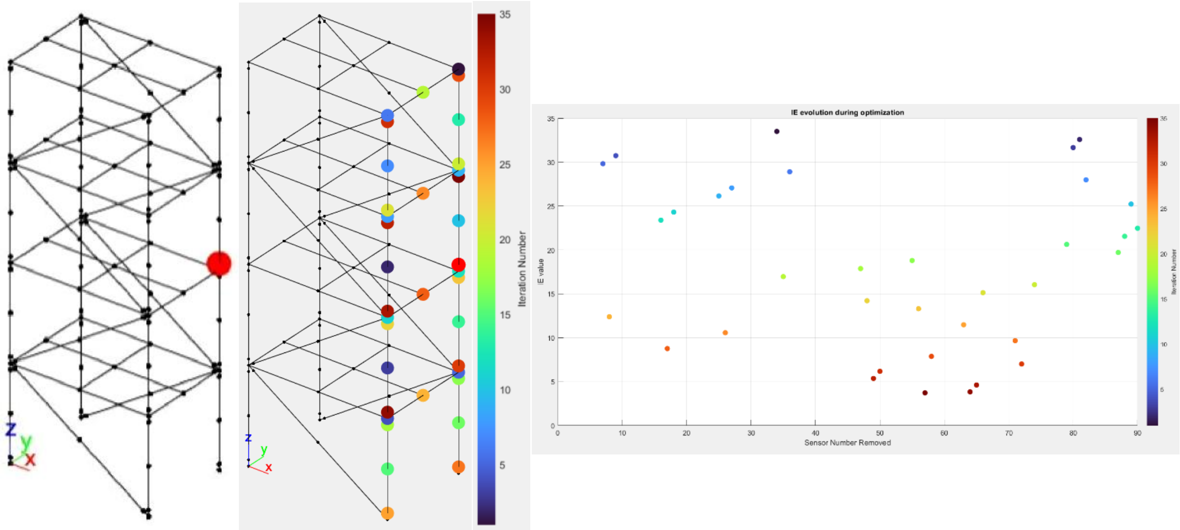

Fig. 81 – Optimal sensor placement for the fourth vibration mode using the IEI method.

With the IEI method optimizations for each vibration mode using just one sensor, it can be concluded that the optimal sensor positions differ depending on the vibration mode. The first and second vibration modes share the same sensor placement, although the sensor removal process differs between them. For the third and fourth vibration modes, both the optimal sensor placements and the sensor removal sequences differ once again.

Now, comparing the optimal sensor placements and the sensor removal processes for EFI and IEI, using colors to indicate the iteration steps, it is evident that the two methods behave very similarly, as observed in previous evaluations where the number of optimized sensors equaled the number of vibration modes. This similarity is due to the correlation of the sensors through the Fisher Information Matrix (FIM) and the Covariance Matrix, showing that these methods are proportional to each other. The differences in the graphs arise because EFI aims to maximize the EFI value, which reflects the importance of each sensor, whereas IEI seeks to minimize the Information Entropy value, thereby reducing uncertainty.

In all the evaluations above, the AutoMAC was plotted with always a value 1, since it compares each vibration mode with itself.

A useful evaluation for this study is to analyze the graph showing the method's value at each sensor removal iteration, observing how the value evolves as sensors are removed down to zero. This demonstrates the importance of having a number of sensors at least equal to the number of vibration modes.

Next, the values of the methods will be evaluated considering one, two, three, and four first vibration modes, with sensor optimization performed down to zero sensors, to observe how the values change and to observe the minimum number of sensors required.

Starting with the MKE method, the required number of sensors for capturing the first one, two, three, and four first vibration modes was evaluated. Fig. 82 presents the graphs illustrating the sensor requirements for each case.

First vibration mode

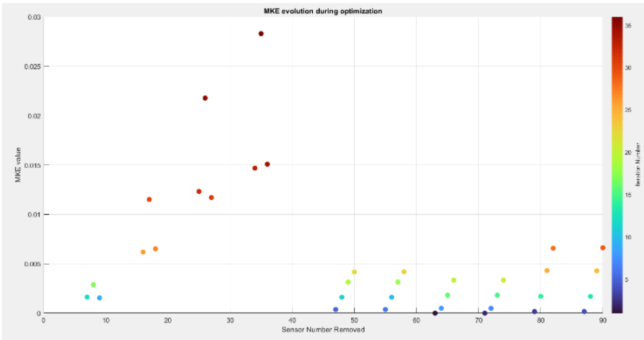

First two vibration modes

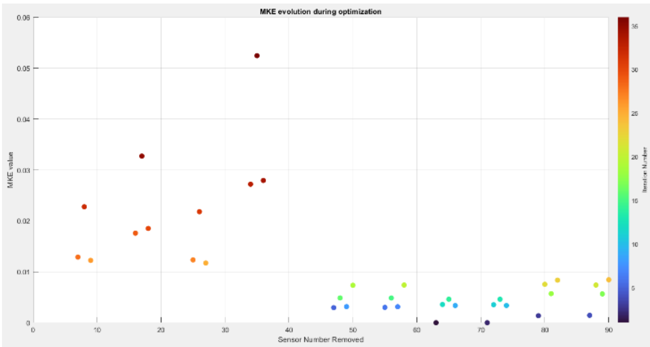

First three vibration modes

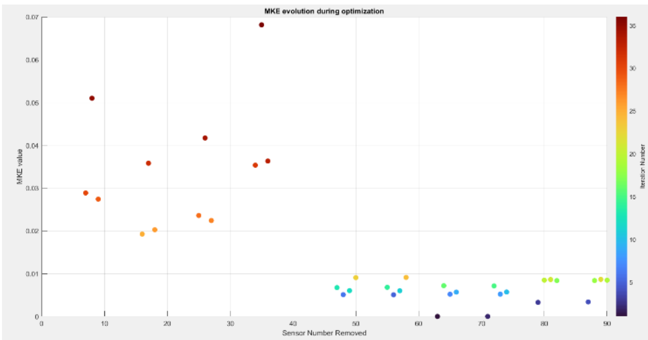

First fourth vibration modes

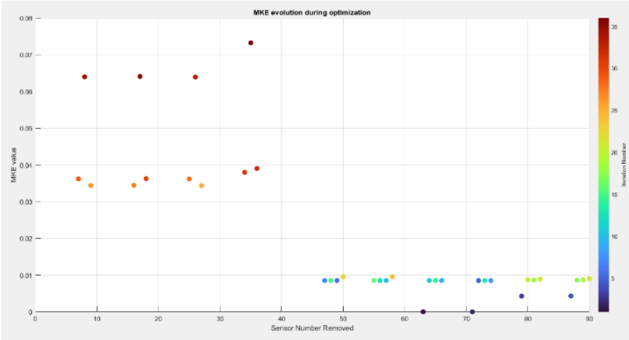

Fig. 82 – Evaluation of MKE values considering the first one, two, three, and four vibration modes.

For the MKE method, it is notable that at least one sensor is necessary. However, the difference in results when considering more vibration modes is not very significant, except when including all four modes. In that case, a noticeable difference appears in the values related to the last four sensors. This outcome is due to the method's strong dependence on the mass of the nodes, which reflects its less satisfactory performance overall.

Now, considering the sensors required by the EFI method for capturing the first one, two, three, and four first vibration modes, Fig. 83 presents the graphs evaluating the necessary number of sensors for each case.

First vibration mode

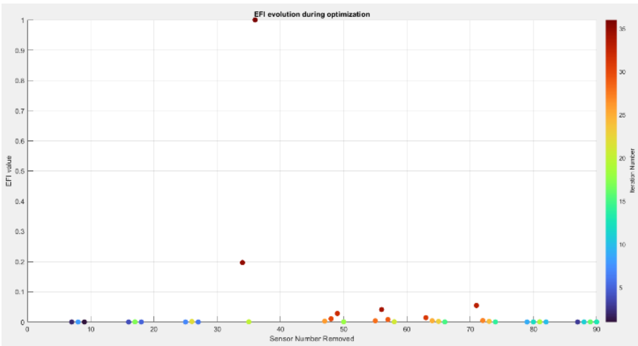

First two vibration modes

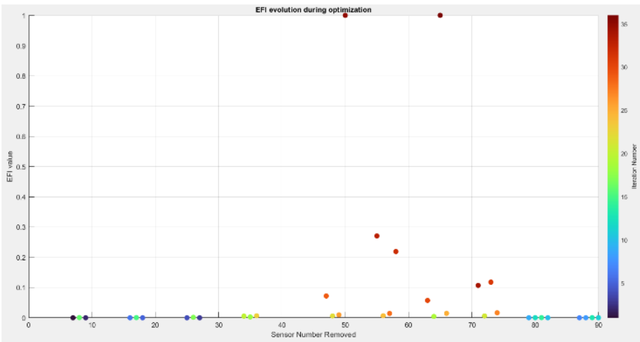

First three vibration modes

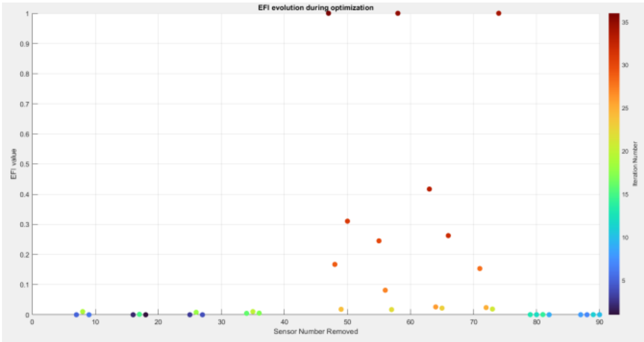

First fourth vibration modes

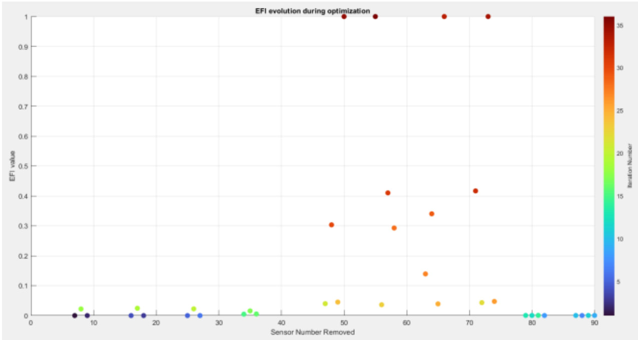

Fig. 83 – Evaluation of EFI values considering the first one, two, three, and four vibration modes.

With the EFI method, it is quite clear that the number of optimized sensors needs to be at least equal to the number of vibration modes. This is evident because the last sensors in these sets show significantly higher values compared to other positions. Once again, the EFI method demonstrates superior insight into the sensor optimization process.

Now, considering the number of sensors required by the IEI method to capture the first one, two, three, and four first vibration modes, Fig. 84 presents the corresponding graphs evaluating the necessary sensor count for each case.

First vibration mode

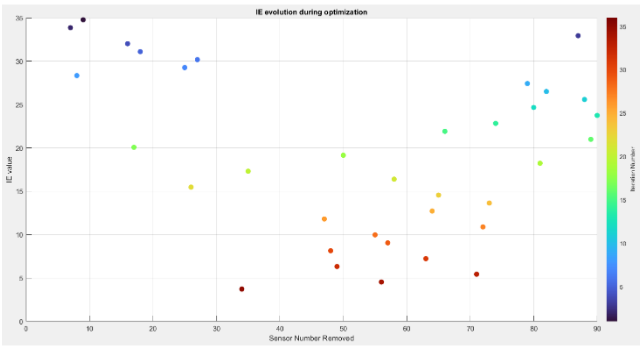

First two vibration modes

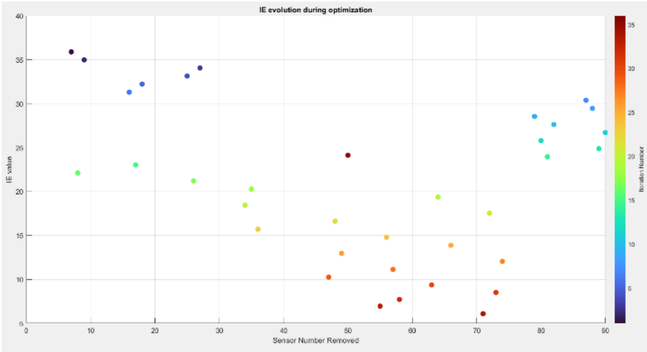

First three vibration modes

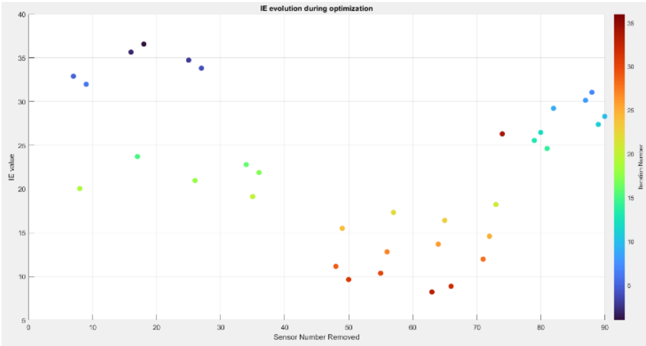

First fourth vibration modes

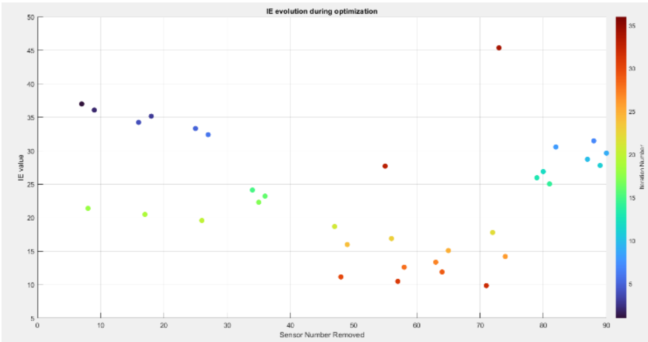

Fig. 84 – Evaluation of IE values considering the first one, two, three, and four vibration modes.

The results for the IEI method are also less intuitive when comparing the influence of the number of sensors considered, because in this method, the optimal sensors are those with the lowest IE values, as the primary goal is to minimize uncertainty.

Therefore, it can be concluded that for optimal performance, especially with the EFI method, the number of optimized sensors should be at least equal to the number of vibration modes under study, as indicated by the results shown in Fig. 83. For the other methods, this premise is also supported by the resulting AutoMAC values when fewer sensors than required are used, presented in Fig. 67, Fig. 68, Fig. 69, Fig. 19, Fig. 23 and Fig. 27.

7
CONCLUSION

The implementation of optimal sensor placement methods in this research was successfully carried out and rigorously evaluated. The study began with a 2D analysis, progressed to comprehensive 3D assessments, and culminated in experimental tests to compare and validate the results. Throughout the process, the Modal Assurance Criterion (MAC) matrix served as a crucial evaluation metric, offering valuable insights into the correlation between numerical models and experimental data.

The optimization of sensor placement was systematically evaluated for each method, revealing different sensor configurations when comparing the Modal Kinetic Energy (MKE) method with the Effective Independence (EFI) and Information Entropy Index (IEI) methods. The MKE method requires relatively low computational effort, whereas the EFI and IEI methods demand higher computational resources but deliver more refined and advanced results.

Two MATLAB toolboxes (Stabil and MACEC) were utilized during this study, both proving highly beneficial. Stabil offered an intuitive and user-friendly environment for constructing the finite element model and obtaining modal results, allowing flexible adaptation to specific research requirements. MACEC, while more complex, was essential for extracting mode shapes from experimental data, though it demanded careful configuration and parameter tuning.

Some limitations in the results can be attributed to imperfections in the finite element model, indicating that future work should focus on refining the model to enhance its accuracy and better align with experimental outcomes.

This work involved the extensive use of MATLAB scripts, requiring significant programming effort. Throughout the process, I developed valuable skills in coding, gained autonomy in problem-solving, and deepened my understanding of the scientific research environment.

7.1. Future Developments

A future research challenge could involve performing both finite element based and experimental optimal sensor placement analyses on larger and more complex structures. This would not only test the robustness of the methodologies developed in this study but also introduce practical challenges, such as managing the structure’s continuous use, dealing with varying weather conditions, and ensuring safety.

A key challenge for further research would be the application of these optimal sensor placement strategies to a real-world, large-scale structure, specifically, the Vierendeel bridge M2.17. Nevertheless, since the methods have been successfully implemented on simpler structures, extending them to a larger, more complex bridge mainly depends on available computational resources, given the significantly increased number of nodes and elements.

Additionally, a promising avenue for high-quality experimental investigations is the use of fiber-optic sensors. This technology provides a cost-effective and reliable solution for experimental testing, as demonstrated in previous research on this bridge (Anastasopoulos e Reynders, 2024).

Finally, a key recommendation for future research is to develop the code to be as automatic and flexible as possible. Over time, unforeseen challenges and new opportunities will emerge, requiring ongoing improvements to the codebase to support alternative approaches and adapt to evolving insights.

BIBLIOGRAPHY REFERENCES

AN, YONGHUI [et al.] (2019) - Recent progress and future trends on damage identification methods for bridge structures. Structural Control and Health Monitoring [Em linha]. 26:10. ISSN 1545-2255

1545-2263.

ANASTASOPOULOS, DIMITRIOS (2020) - Structural health monitoring based on operational modal analysis from long gauge dynamic strain measurements. KU Leuven.

ANASTASOPOULOS, DIMITRIOS; DE ROECK, GUIDO; REYNDERS, EDWIN P. B. (2021) - One-year operational modal analysis of a steel bridge from high-resolution macrostrain monitoring: Influence of temperature vs. retrofitting. Mechanical Systems and Signal Processing [Em linha]. 161: ISSN 08883270.

ANASTASOPOULOS, DIMITRIOS; REYNDERS, EDWIN P. B. (2023) - Modal strain-based SHM of steel railway bridges. [Em linha].

--- (2024) - Dynamic strain-based monitoring of a historical Vierendeel truss bridge under changing environmental and support conditions. Journal of Civil Structural Health Monitoring [Em linha]. ISSN 2190-5452

2190-5479.

ASCE (2021) - 2021 Report Card for America's Infrastructure: Bridges.

AUGUSTYN, ELŻBIETA; KOZIEŃ, MAREK S. (2015) - Possibility of existence of torsional vibrations of beams in low frequency range. Technical Transactions [Em linha].

CARNE, THOMAS G.; DOHRMANN, C.R. (1995) - A modal test design strategy for model correlation. [Em linha].

CASTRO-TRIGUERO, R. [et al.] (2014) - Optimal sensor placement in timber structures by means of a multi-scale approach with material uncertainty. Structural Control and Health Monitoring [Em linha]. 21:12. 1437-1452. ISSN 15452255.

CHERNG, AN-PAN (2003) - Optimal Sensor Placement for Modal Parameter Identification Using Signal Subspace Correlation Techniques. Mechanical Systems and Signal Processing [Em linha]. 17:2. 361-378. ISSN 08883270.

CHIOCCARELLI, EUGENIO [et al.] (2024) - Discussing optimal sensor placement for ambient vibration test of an existing bridge. Engineering Structures [Em linha]. 310: ISSN 01410296.

ESPION, BERNARD (2012) - The Vierendeel bridges over the Albert Canal, Belgium – their significance in the story of brittle failures. Steel Construction [Em linha]. 5:4. 238-243. ISSN 1867-0520

1867-0539.

FARIDI, MD ARIF [et al.] (2024) - Using limited roving sensors to monitor bridge subjected to random traffic load. Journal of Civil Structural Health Monitoring [Em linha]. 14:3. 693-710. ISSN 2190-5452

2190-5479.

FARRAR, C. R., & WORDEN, K. (2013) - Structural Health Monitoring: A Machine Learning Perspective. West Sussex, U.K.:

FRANCE, ES (ES France) - Introduction to Piezoelectric Accelerometers.

GLIŠIĆ, BRANKO; INAUDI, DANIELE (2007) - Fibre Optic Methods for Structural Health Monitoring.

GMBH, HOTTINGER BRÜEL & KJAER (2022) - X60.

HEMEZ, FRANCOIS M.; FARHAT, CHARBEL (1994) - An Energy Based Optimum Sensor Placement Criterion and its Application to Structural Damage Detection. [Em linha].

HEO, G.; WANG, M.L.; SATPATHI, D. (1997) - Optimal transducer placement for health monitoring of long span bridge. [Em linha].

INSTRUMENTS, NATIONAL (2025) - cDAQ-9178.

JUANG, JER-NAN (2002) - Applied System Identification. [Em linha].

KAMMER, D.C.; YAO, L. (1994) - Enhancement of On-Orbit Modal Identification of Large Space Structures Through Sensor Placement. [Em linha].

KAMMER, DANIEL C. (1991) - Sensor placement for on-orbit modal identification and correlation of large space structures. Journal of Guidance, Control, and Dynamics [Em linha]. 14:2. 251-259. ISSN 0731-5090

1533-3884.

--- (1996) - Optimal sensor placement for modal identification using system-realization methods. Journal of Guidance, Control, and Dynamics [Em linha]. 19:3. 729-731. ISSN 0731-5090

1533-3884.

--- (2005) - Sensor set expansion for modal vibration testing. Mechanical Systems and Signal Processing [Em linha]. 19:4. 700-713. ISSN 08883270.

KANG, FEI; LI, JUN-JIE; XU, QING (2008) - Virus coevolution partheno-genetic algorithms for optimal sensor placement. Advanced Engineering Informatics [Em linha]. 22:3. 362-370. ISSN 14740346.

KIM, SEON-HU; CHO, CHUNHEE (2024) - Effective independence in optimal sensor placement associated with general Fisher information involving full error covariance matrix. Mechanical Systems and Signal Processing [Em linha]. 212: ISSN 08883270.

LEYDER, C. [et al.] (2016) - Comparison of optimal sensor placement algorithms via implementation on an innovative timber structure.

LEYDER, CLAUDE [et al.] (2015) - Optimal sensor placement for the modal identification of an innovative timber structure. [Em linha].

LEYDER, CLAUDE [et al.] (2018) - Optimal sensor placement methods and metrics – comparison and implementation on a timber frame structure. Structure and Infrastructure Engineering [Em linha].

LI, D. S.; LI, H. N.; FRITZEN, C. P. (2007) - The connection between effective independence and modal kinetic energy methods for sensor placement. Journal of Sound and Vibration [Em linha]. 305:4-5. 945-955. ISSN 0022460X.

LIU, WEI [et al.] (2008) - Optimal sensor placement for spatial lattice structure based on genetic algorithms. Journal of Sound and Vibration [Em linha]. 317:1-2. 175-189. ISSN 0022460X.

MAGALHÃES, FILIPE; CUNHA, ÁLVARO (2011) - Explaining operational modal analysis with data from an arch bridge. Mechanical Systems and Signal Processing [Em linha]. 25:5. 1431-1450. ISSN 08883270.

MAGALHÃES, FILIPE; CUNHA, ÁLVARO; CAETANO, ELSA (2009) - Online automatic identification of the modal parameters of a long span arch bridge. Mechanical Systems and Signal Processing [Em linha]. 23:2. 316-329. ISSN 08883270.

MAGALHÃES, FILIPE MANUEL RODRIGUES LEITE DE - Identificação Modas Estocástica para Validação Experimental de Modelos Numéricos.

MEO, M.; ZUMPANO, G. (2005) - On the optimal sensor placement techniques for a bridge structure. Engineering Structures [Em linha]. 27:10. 1488-1497. ISSN 01410296.

OMENZETTER, PIOTR [et al.] (2011) - Long-term monitoring and field testing of an innovative multistory timber building. In Nondestructive Characterization for Composite Materials, Aerospace Engineering, Civil Infrastructure, and Homeland Security 2011. 2011.

OSTACHOWICZ, WIESLAW; SOMAN, ROHAN; MALINOWSKI, PAWEL (2019) - Optimization of sensor placement for structural health monitoring: a review. Structural Health Monitoring [Em linha]. 18:3. 963-988. ISSN 1475-9217

1741-3168.

PACHÓN, PABLO [et al.] (2018) - E. Torroja's bridge: Tailored experimental setup for SHM of a historical bridge with a reduced number of sensors. Engineering Structures [Em linha]. 162: 11-21. ISSN 01410296.

PACHÓN, PABLO [et al.] (2020) - Evaluation of optimal sensor placement algorithms for the Structural Health Monitoring of architectural heritage. Application to the Monastery of San Jerónimo de Buenavista (Seville, Spain). Engineering Structures [Em linha]. 202: ISSN 01410296.

PAPADIMITRIOU, C. (2004) - Optimal sensor placement methodology for parametric identification of structural systems. Journal of Sound and Vibration [Em linha]. 278:4-5. 923-947. ISSN 0022460X.

PAPADIMITRIOU, COSTAS; LOMBAERT, GEERT (2012) - The effect of prediction error correlation on optimal sensor placement in structural dynamics. Mechanical Systems and Signal Processing [Em linha]. 28: 105-127. ISSN 08883270.

PEETERS, BART; ROECK, GUIDO DE (1999) - Reference-based stochastic subspace identification for output-only modal analysis. Mechanical Systems and Signal Processing [Em linha].

PROAKIS, JOHN G.; MANOLAKIS, DIMITRIS G. (2006) - Digital Signal Processing: Principles, Algorithms, and Applications

RAINIERI, CARLO; FABBROCINO, GIOVANNI (2015) - Development and validation of an automated operational modal analysis algorithm for vibration-based monitoring and tensile load estimation. Mechanical Systems and Signal Processing [Em linha]. 60-61: 512-534. ISSN 08883270.

REYNDERS, EDWIN (2009) - System identification and modal analysis in structural mechanics. KU Leuven.

REYNDERS, EDWIN; HOUBRECHTS, JEROEN; DE ROECK, GUIDO (2012) - Fully automated (operational) modal analysis. Mechanical Systems and Signal Processing [Em linha]. 29: 228-250. ISSN 08883270.

REYNDERS, EDWIN; PINTELON, RIK; DE ROECK, GUIDO (2008) - Uncertainty bounds on modal parameters obtained from stochastic subspace identification. Mechanical Systems and Signal Processing [Em linha]. 22:4. 948-969. ISSN 08883270.

REYNDERS, EDWIN; SCHEVENELS, MATTIAS; ROECK, GUIDO DE (2021) - MACEC. Disponível em WWW: <https://bwk.kuleuven.be/bwm/macec>.

SECTION, STRUCTURAL MECHANICS; DEPARTMENT OF CIVIL ENGINEERING, KU LEUVEN (2020) - Stabil. Disponível em WWW: <http://bwk.kuleuven.be/bwm/stabil>.

STEPHAN, CYRILLE (2012) - Sensor placement for modal identification. Mechanical Systems and Signal Processing [Em linha]. 27: 461-470. ISSN 08883270.

UBERTINI, FILIPPO; GENTILE, CARMELO; MATERAZZI, ANNIBALE LUIGI (2013) - Automated modal identification in operational conditions and its application to bridges. Engineering Structures [Em linha]. 46: 264-278. ISSN 01410296.

VAN BOGAERT, PHILIPPE; DE PAUW, BART (2023) - Load-carrying capacity of Vierendeel bridges in Mechelen. ce/papers [Em linha]. 6:5. 416-421. ISSN 2509-7075

2509-7075.

WEI, FAN; PIZHONG, QIAO (2010) - Vibration-based Damage Identification Methods: A Review and Comparative Study. Structural Health Monitoring [Em linha]. 10:1. 83-111. ISSN 1475-9217

1741-3168.

WORDEN, K; BURROWS, A.P (2001) - Optimal sensor placement for fault detection. [Em linha].

YI, TING-HUA; LI, HONG-NAN (2012) - Methodology Developments in Sensor Placement for Health Monitoring of Civil Infrastructures. International Journal of Distributed Sensor Networks [Em linha]. 8:8. ISSN 1550-1477

1550-1477.

ZHANG, JIE (2019) - Numerical analysis and experimental assessment of the dynamic characteristics of periodic structures.

ZHANG, JIE [et al.] (2017) - Optimal sensor placement for multi-setup modal analysis of structures. Journal of Sound and Vibration [Em linha]. 401: 214-232. ISSN 0022460X.

ZHOU, ZHENWEI [et al.] (2024) - Optimal sensor placement and Bi-type response reconstruction for structural health monitoring using long-gauge FBG strain sensing network. Structures [Em linha]. 63: ISSN 23520124.